SENSORIMOTOR ENCODING IN PREFRONTAL CORTEX

by

Sanjeev Brice Paul Khanna

B.S., University of Pittsburgh, 2012

Submitted to the Graduate Faculty of

The Swanson School of Engineering in partial fulfillment

of the requirements for the degree of

Doctor of Philosophy

University of Pittsburgh

2018

UNIVERSITY OF PITTSBURGH

SWANSON SCHOOL OF ENGINEERING

This dissertation was presented

by

Sanjeev Brice Paul Khanna

It was defended on

October 29, 2018

and approved by

Aaron Batista, Ph.D., Associate Professor
Department of Bioengineering

Marlene Cohen, Ph.D., Associate Professor
Department of Neuroscience

Carol Colby, Ph.D., Professor
Department of Neuroscience

Neeraj Gandhi, Ph.D., Professor
Department of Bioengineering

Dissertation Director: Matthew Smith, Ph.D., Associate Professor
Department of Ophthalmology

SENSORIMOTOR ENCODING IN PREFRONTAL CORTEX

Sanjeev Brice Paul Khanna, PhD

University of Pittsburgh, 2018

When processing the vast visual world in front of us, eye movements allow us to focus on specific relevant stimuli. To gather information about a stimulus, the brain must determine its location and plan an eye movement to that location. It is not fully understood how populations of neurons store the incoming visual input in a memory signal and then retrieve it to produce a fast and accurate motor output. We sought answers to this question by recording the activity of populations of neurons in cortical regions thought to be involved in the maintenance of working memory and the generation of eye movements.

First, we analyzed how populations of neurons coordinated their activity during the period after a visual stimulus was presented, but before an eye movement was made. Specifically, we were interested in identifying the optimal activity profiles for generating a fast eye movement. We recorded from groups of neurons in the frontal eye fields (FEF), an area known to be important for saccade generation. We found neurons change their activity at both the individual level and by covarying their activity with other neurons to generate fast eye movements.

We then recorded from neurons in prefrontal cortex (PFC) to determine how visual and motor signals are encoded at the single neuron and population level. For single neurons, we observed rich dynamics, including neurons that encoded the entire visual field, and neurons that

shifted their tuning between visual and motor epochs. At the population level, these shifts in tuning created a dynamic population code. These single neuron properties were less likely to be observed in FEF, which resulted in FEF having a more stable population code when compared to PFC.

In summary, the visual and motor representations associated with processing a stimulus and preparing an eye movement manifest in the activity of single neurons and populations, and their dynamics over time. These results lead to a richer view of working memory and eye movement planning at the level of populations of neurons than has previously been appreciated.

TABLE OF CONTENTS

LIST OF FIGURES

PREFACE

Chapter 2 and 3 are in preparation:

Khanna SB, Snyder AC, Smith MA (2018) Distinct sources of variability affect eye movement preparation. *In preparation.*

Khanna SB, Scott JA, Smith MA (2018) Spatial and temporal receptive field structure in prefrontal cortex. *In preparation.*

Acknowledgments

First and foremost, I would like to thank my advisor Matt Smith. In addition to providing a space where rigorous scientific research could be performed, Matt also cultivated a friendly environment that made coming to work every day enjoyable, whether it was Monty Python jokes, bringing in donuts for the lab, or participating in non-research related discussions with other members in the lab (to name a few examples). I am eternally grateful he gave me, a freshly graduated engineer with limited neuroscience knowledge and no experience working with NHPs, the opportunity to conduct research under his tutelage.

I also would like to thank my thesis committee: Aaron Batista, Marlene Cohen, Carol Colby, and Neeraj Gandhi for all their comments, suggestions, and advice in both committee meetings and informal discussions. This also applies to the other members of the Smith Lab for their help throughout my graduate career, from training, to collecting data, to helping analyze/debug code, to sitting through practice defense presentations and giving me feedback., I couldn't have done it without your help.

Finally, I would like to thank all my friends and family for their support and encouragement. A special thank you is warranted to my parents for instilling an eagerness to learn in me, and for the countless meals they sent me home with throughout my graduate experience. The same goes to my brother, Sunil, who was always willing to speak on the phone if I ever needed someone to talk to. To my friends, there are too many of you that have impacted me in a positive way to list individually, but special recognition goes to Tailgate Mobb, the happy hour crew, all Friendship roommates, and other grad students I met within the BioE department and CNBC program. You made graduate school fun and a truly enriching experience.

1.0 GENERAL INTRODUCTION

1.1 THE FRONTAL EYE FIELD

Nearly a century and a half ago, electrical stimulation of the frontal lobe was found to elicit eye movements (Ferrier 1874). Since then, several distinct areas within the frontal lobe have been identified as being central to the generation of eye movements. One of the more well known, the frontal eye field (FEF), lies on the anterior bank of the arcuate sulcus in rhesus macaque monkeys (*M. mulatta)*. Reversible inactivation (Dias et al 1995, Dias & Segraves 1999, Sommer & Tehovnik 1997) or lesions (Schiller & Chou 1998, Schiller et al 1987, Schiller et al 1980) of the FEF impairs the ability to generate saccades (although it can recover over time). Traditionally thought of as an area which controls the initiation of eye movements, recent studies have expanded the role of the FEF, implicating it in attention (Moore & Armstrong 2003), target selection (Schall 2002), visual stability (Sommer & Wurtz 2006, Umeno & Goldberg 1997), inhibition of automatic behavior (Munoz & Everling 2004) and short term memory (Clark et al 2012, Funahashi 2014). The following paragraphs detail 3 reasons why the FEF is a good candidate for mediating sensorimotor transformations in the oculomotor system: 1) connections to other visual and oculomotor areas 2) microstimulation effects and 3) electrophysiological properties of FEF neurons.

Given FEF's involvement in the wide variety of functions stated above, it is no surprise it receives input from a variety of visual cortical areas, inferior parietal cortex, other prefrontal areas (supplementary eye field & dorsolateral prefrontal cortex), and subcortical areas including thalamic nuclei, substantia nigra pars reticulata, and the superior colliculus (Leigh & Zee 2015). Additionally, the FEF projects to contralateral frontal areas (FEF and supplementary eye fields), posterior visual cortical areas, the superior colliculus (both ipsilateral and contralateral) and other midbrain and brainstem nuclei (nucleus reticularis tegmenti pontis & nucleus raphe interpositus). More specifically, FEF is innervated by visual areas from both the dorsal and ventral visual stream (Schall et al 1995b), with neurons projecting to visual areas located in a distinct laminar layer compared to those projecting to the superior colliculus (Pouget et al 2009). In summary, FEF can be considered a "hub" of visual and motor integration, receiving input and projecting outputs to a wide variety of visual and oculomotor areas.

Low intensity electrical microstimulation within the FEF evokes saccades of a fixed vector, with large saccades reported in the dorsomedial portion of FEF and smaller saccades in the ventrolateral portion (Bruce et al 1985, Robinson & Fuchs 1969). Microstimulation in the dorsomedial portion can cause combined eye-head gaze shifts in some circumstances depending on the initial position of the eye in the orbit (Knight & Fuchs 2007). Evidence of increased latencies for ipsilateral saccades shows microstimulation can also suppress saccades in certain conditions (Izawa et al 2005). Even subthreshold stimulation (not evoking a saccade) of the FEF can cause changes in activity in visual cortex mirroring those observed during attentional modulation (Ekstrom et al 2008, Moore & Armstrong 2003, Moore & Fallah 2004). From these studies, it is clear the FEF directly influences saccade generation and other areas in the visual processing hierarchy.

The final aspect which makes the FEF a good candidate to mediate sensorimotor transformations is the physiological properties of the neurons themselves. FEF neurons discharge for purposive saccades much more than spontaneous ones made in complete darkness, even if the target itself was no longer present (Bruce & Goldberg 1985, Umeno & Goldberg 2001). For tasks where two targets are flashed in quick succession, requiring two saccades, most units discharge for the saccade vector needed for the second saccade, not the retinal location of the target itself (Goldberg & Bruce 1990). The traditional separation of subpopulations within the FEF is based on their responses to a visual stimulus relative to a saccade, known as the visuomotor index (VMI). Visual neurons respond predominantly to visual stimuli, motor neurons to saccades, and visuomotor neurons to both visual stimuli and saccades equally (Bruce & Goldberg 1985, Lawrence et al 2005). Lower thresholds for saccade generation via microstimulation were observed for motor neurons compared to visual neurons (Bruce et al 1985), suggesting these subpopulations may sub serve different functions. Like other cortical regions such as the superior colliculus and lateral intraparietal area, some FEF neurons shift their receptive fields in anticipation of a saccade (Crapse & Sommer 2012, Umeno & Goldberg 1997, Zirnsak et al 2014). This evidence demonstrates subpopulations of FEF neurons encode all aspects of the sensorimotor transformation between processing a visual stimulus and generating a saccade.

Because of its many connections with oculomotor and visual areas (such as the superior colliculus and V4), the ability to evoke eye movements upon electrical microstimulation (and influence neural activity in other cortical areas), and the wide variety of visual and motor response properties of its neurons, the FEF is a good candidate to integrate visual information and transform it into a motor command.

1.2 MODELS OF EYE MOVEMENT GENERATION

Some aspects of saccades follow predictable and stereotyped relationships, such as the velocity and duration of a saccade relative to its amplitude, termed the main sequence (Bahill et al 1975). Saccadic reaction time, the time it takes to initiate a saccade, is much more unpredictable. Saccadic reaction time (from now on referred to as reaction time) can vary with target parameters such as the predictability of the location (one possible location for the target versus eight) and luminance (Marino & Munoz 2009), direction of the eye movement (horizontal or vertical) (Thomas 1969), and whether a stimulus is currently being fixated (termed the gap effect) (Saslow 1967). Furthermore, reaction time can also vary with social contexts such as whether eye contact is being made or broken (Ueda et al 2014).

A well-studied model to relate reaction time variability to neural activity has been the accumulator model. In the accumulator model, a signal grows in response to some stimulus and once it has reached some threshold, an eye movement is triggered. Three parameters of the accumulation model that have been studied as sources of reaction time variability are a variable rate of rise of the signal (Figure 1A), a variable threshold the signal must reach (Figure 1B), or a variable baseline level the signal begins at before the target is presented (Figure 1C).

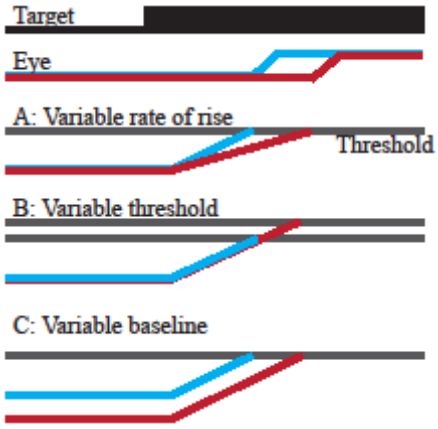

Figure 1: Accumulator models of saccade initiation.

Three parameters of the accumulator model that could cause reaction time variability (blue and red traces represent two eye movements with different reaction times). A: Rate of rise of the signal. B: Variable threshold. C: Variable baseline. Figure adapted from Hall and Moschovakis (2003).

The first neurophysiological recordings aimed at identifying which parameters underlie the variability of reaction times reinforced the rate of rise model. In FEF recordings, the fixed versus variable threshold models were tested by correlating reaction time with the mean and rate of growth of the neural activity in the time preceding the saccade. The mean rate was not correlated with reaction time and rate of growth decreased with increasing reaction time, supporting the fixed threshold/variable rate of rise model (Hanes & Schall 1996). To further relate these single neuron signals to eye movement execution, researchers also studied how these signals varied when a saccade is planned but canceled before movement onset. This was done using a countermanding paradigm, where on a subset of trials in a visually guided task, the subject was required to cancel their eye movement to the peripheral target and maintain fixation instead. In both FEF (Hanes et al 1998) and the superior colliculus (SC) (Pare & Hanes 2003), the activity during canceled trials decayed and never reached the threshold associated with

saccade trials, and this decay occurred within the time epoch the saccade was being canceled. The anti-saccade task was also used to test the fixed threshold model, where in a subset of trials the subject is cued to look away from a visual target instead of towards it. In the fixed threshold model, neural activity preceding saccade initiation should be able to predict whether a correct (successfully looking away from the target) or incorrect (looking at the target instead of away from it) saccade is made. For incorrect trials, it would be predicted that the response to the visual target would exceed the threshold and trigger a saccade. This is the case in FEF (Everling & Munoz 2000) and SC (Everling et al 1998) where activity is suppressed before and after target onset for correct trials, and conversely, when activity was high after target presentation, more errors were observed.

As the accumulator model was fit to different tasks and analyses, however, more parameters than just the rate of accumulation were shown to vary with reaction time. Studies in FEF (Jantz et al 2013) and SC (Dorris et al 1997, Everling & Munoz 2000, Jantz et al 2013) showed firing rate could be correlated depending on the time epoch chosen or whether the task condition was cued or blocked. An additional study emphasized a dynamic initial state (the baseline activity) as already containing internally driven motor plans (Hauser et al 2018). Other SC recordings demonstrated low frequency activity in the epoch leading up to a saccade contained information about the motor command, and that neural activity at both the single neuron and population level does not necessarily have to reach a threshold to initiate a saccade (Jagadisan & Gandhi 2017). Neural data recorded during a speed-accuracy trade-off task contradicted the predictions of a standard accumulator model (lower thresholds when speed is emphasized), with the authors proposing an integrated accumulator model which factored both the magnitude and rate of increase over time (Heitz & Schall 2012). While the accumulator

model is a relatively simple and straightforward explanation for comparing the relationship between variation in neural activity and variation in behavior, it is becoming clear this relationship is more complex than perhaps initially thought. Additionally, many of these accumulator models were implemented at the single neuron level, ignoring how pairwise or population changes in activity may vary with reaction time.

1.3 PREFRONTAL CORTEX

Dorsolateral prefrontal cortex (dlPFC, referred to as PFC from now on) is located anterior to the FEF and includes areas around the principal sulcus. Although microstimulation of PFC can evoke eye movements at high frequencies and durations (Wagman et al 1961), PFC is traditionally functionally separated from the FEF by the inability to evoke saccades via low threshold microstimulation. PFC responds to cue-response associations (Asaad et al 1998) and reward associations (Watanabe 1990), temporal and spatial order of visual stimuli (Barone & Joseph 1989), rule matching (Hoshi et al 1998), visual search (Iba & Sawaguchi 2002), and abstract rules (Wallis et al 2001). PFC can be considered part of the "executive" cortex, where executive control is broadly defined as mechanisms that optimize behavioral performance in situations where cognitive processes are required (for review see Tanji and Hoshi (2008)).

Despite being considered functionally separate, PFC shares many properties with the FEF. One example is patients with lesions in PFC also show deficits in a memory guided saccade task (Pierrot-Deseilligny et al 1991). In a delayed saccade task, PFC neurons responded to both visual stimuli and saccades (Boch & Goldberg 1989, Funahashi et al 1991, Kojima 1980), common properties also observed in the FEF. Additionally, activity is not limited to transient

bursts after the visual stimulus or before the saccade but can persist through the entire memory period (Funahashi et al 1989, Fuster & Alexander 1971). Finally, just as there is a medial-lateral topography in FEF with respect to evoked saccade vector (Bruce et al 1985), there is evidence PFC has similar topography, with larger receptive fields more medial and smaller receptive fields lateral (Figure 2)(Suzuki & Azuma 1983). Despite these similarities, PFC and FEF do have differences in their activity. PFC activity is context dependent, meaning neurons will fire more for purposive saccades compared to spontaneous saccades during the intertrial interval (Funahashi et al 1991). FEF neurons show context dependency only for pre-saccadic activity (Bruce & Goldberg 1985). Furthermore, the presence of ipsilaterally tuned neurons is much greater in PFC (Funahashi et al 1989, Funahashi et al 1991), if not absent in FEF (but see Crapse and Sommer (2009)). Finally, in patients with PFC lesions there is an increased percentage of errors during an antisaccade task (Pierrot-Deseilligny et al 1991, Ploner et al 2005) whereas patients with FEF lesions have a unchanged error rate but at an increased latency (Fukushima et al 1994). These results demonstrate that while PFC is clearly involved in saccade planning, its role may be different than that of the FEF.

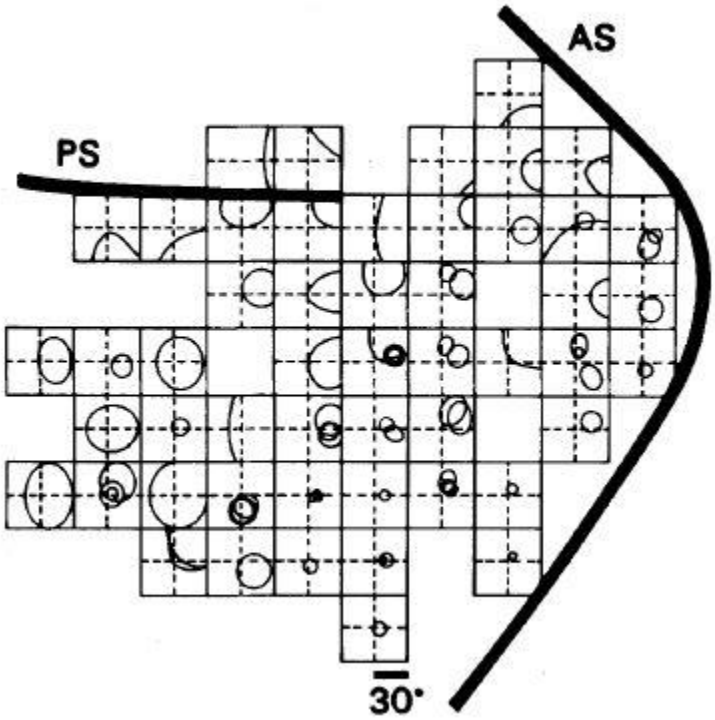

Figure 2: Visual receptive fields in PFC.

Topography of PFC visual receptive fields. The right portion of each square corresponds to the contralateral hemifield. Receptive fields become larger as you move medial within PFC, or as you move anterior. Figure from Suzuki and Azuma (1983).

1.4 MODELS OF WORKING MEMORY

Working memory is the ability to maintain and manipulate information across time, even if the information is not explicitly present. Numerous theories have been put forth proposing a central role for PFC in working memory including representing task contingencies and rules (Miller 2000), biasing other brain structures to guide activity that maps inputs to internal states and outputs (Miller & Cohen 2001), bridging the temporal gap between sensory information and action (Goldman-Rakic 1995), and creating a flexible dynamic coding structure (Stokes 2015). The latter two have opposite predictions of how neural activity in PFC should encode a memory, yet there is no current consensus on which model is a more accurate description. The following paragraphs will outline the evidence supporting each model.

Recordings from single neurons in PFC during a memory guided saccade task revealed a proportion (approximately 30%) of neurons fired after the presentation of a visual stimulus, but also maintained a high level of activity (sometimes for multiple seconds) even after the stimulus was extinguished (Funahashi et al 1989, Fuster & Alexander 1971). This type of activity was labeled “persistent”, and since it was maintained across the entire memory epoch, provided a simple explanation as the neural correlate of working memory. In some instances, activity did not ramp up until many hundreds of milliseconds after stimulus presentation, and would abruptly decrease around saccade initiation, thus tying the activity to memory epoch as opposed to the visual or motor epochs. Persistent activity was also tied to behavioral performance (Funahashi et al 1989, Fuster 1973) in that activity was diminished or absent during error trials and varied in a linear way when task difficulty changed (Constantinidis et al 2001b). Additionally, reversible

inactivation of PFC impaired performance on a working memory task and reduced persistent activity (Chafee & Goldman-Rakic 2000). Proponents of the persistent activity model argue against this activity representing the upcoming movement based on studies where persistent activity after a visual stimulus is observed before the saccade direction is known (Qi et al 2011). Computational models show persistent activity can be maintained through recurrent connections between neurons with similar tuning (Compte et al 2000), and that drifts in the activity explain drifts in behavior (eye endpoint position) using a bump attractor model (Wimmer et al 2014).

More recently, proponents of the persistent activity model have sought to differentiate persistent activity (a stable readout) from stationary activity (not temporally modulated). This clarification was needed given of reports of varying temporal activity during vibrotactile working memory tasks (Romo et al 1999) and direction discrimination tasks (Hussar & Pasternak 2010). A more recent population-based analysis claims that despite heterogeneous and time varying activity at the single neuron level, the population readout during the memory epoch lies in a stable and robust subspace (Figure 3, Murray et al (2017)). The population code resulting from persistent activity is said to have the following properties: The memory is represented at a given time point by spiking activity across the relevant PFC population in a spatial way, is stable across time during the memory epoch, and does not require an overall increase in the population activity as individual neurons may increase or decrease their firing rate.

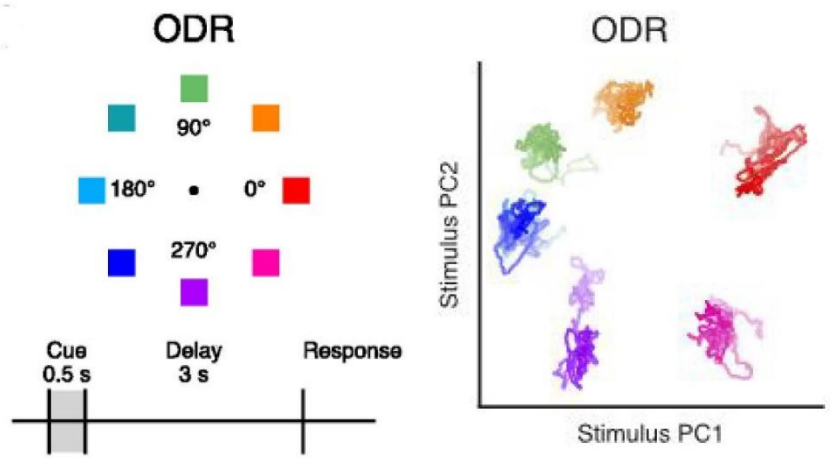

Figure 3: Stable population coding during the memory epoch

Left: Oculomotor delay task (memory guided saccade task) with colors representing target locations. Right: PFC population trajectories for 8 different directions during the memory epoch of a memory guided saccade task. The shading of each color marks time during the memory epoch. From Murray et al (2017).

Opposing the persistent activity model is one which emphasizes dynamic and transient changes in activity as being the main drivers of the working memory signal. Numerous studies have shown that both single neuron and population codes change over time and with task demands (Barak et al 2010, Parthasarathy et al 2017, Spaak et al 2017, Stokes et al 2013). Specifically, some neurons during a working memory task shift their tuning across the memory epoch, sometimes encoding the opposite hemifield (Figure 4, Spaak et al (2017)). These shifts in tuning have been linked to changes in the population code and the ability to decode the working memory signal (Parthasarathy et al 2017, Spaak et al 2017, Stokes et al 2013). The central finding is that decoders trained on population activity from one portion of the memory epoch do not perform well when tested on activity from later time points in the memory epoch, thus the population code has changed. These observations also agree with the previous reports of PFC neurons being tuned for multiple behavioral conditions and stimuli (Rigotti et al 2013, Warden & Miller 2010).

If dynamic selectivity is the model which most accurately describes the neurophysiological data, how is the memory stored if not in sustained activity? One framework suggests the signal is encoded in "activity silent" states which are facilitated by spiking during the encoding phase, maintained through short term plasticity of synaptic weights during the memory phase, and retrieved through context dependent responses in the recall phase (Stokes 2015).

Another theory, not mutually exclusive to the "activity silent" theory, is that narrow band gamma oscillations (40-100 Hz) are responsible for encoding working memory as they have been associated with signals in sensory cortex (Fries et al 2008, Gray & Singer 1989) and the encoding and maintenance of sensory information (Howard et al 2003, Pesaran et al 2002).

These oscillations are thought to reflect coordinated activity at the level of local networks that are transient and sparse. In fact, the averaging over trials of transient, sparse activity could lead to perceived persistent activity (Lundqvist et al 2016).

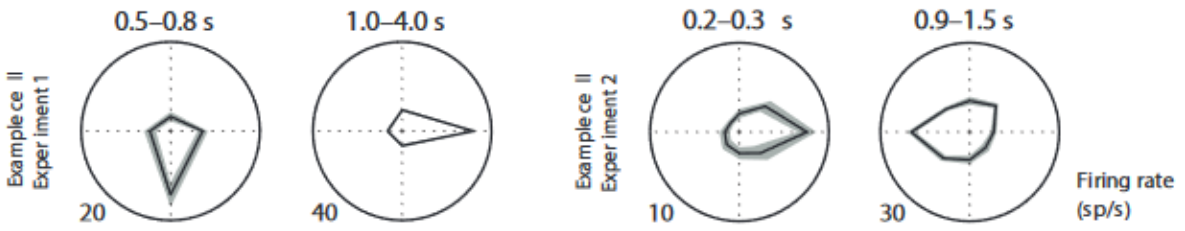

Figure 4: Dynamic tuning changes of single PFC neurons

Two example PFC neurons that change their tuning across the delay epoch. Left) A neuron which rotates its preferred direction. Right) A neuron which inverts its preferred direction. From Spaak et al 2017.

One study that directly compared models with varying levels of dynamic coding with a more traditional line attractor model, found all the models performed comparably, albeit none reproduced all the features of the data (Barak et al 2013). Of the models, an intermediate dynamic model that starts as a random recurrent network but has its recurrent and readout connections tuned through training, most closely approximated the existing physiological data, including the ability of some neurons to lose or change their tuning while others can retain the tuning to specific stimulus attributes for the duration of the memory epoch. It was further suggested that depending on the level of training of the subject, different models maybe more closely approximate the electrophysiological data.

In considering the neural correlate of working memory in PFC, it is clear neural activity needs to be examined at a wide variety of levels. Population averages may obscure relevant dynamics at the single neuron level, while limiting analyses to single neurons does not consider

the “readout” signal. Future analyses which consider working memory signals at the single neuron and population level appear to be the best method moving forward to elucidate the working memory signal in PFC.

1.5 CORRELATED VARIABILITY

Cortical neurons are noisy, meaning their activity varies from trial to trial even when experimental conditions are held constant. If the fluctuations of a subpopulation of neurons tend to be correlated, a simple explanation is all the neurons are receiving a common input, and thus are functionally connected. Correlated spiking has been shown to affect the accuracy of a population code and how information is encoded in both theoretical work (Abbott & Dayan 1999, Averbeck et al 2006, Nirenberg & Latham 2003, Shadlen & Newsome 1998) and experimentally (Adibi et al 2014, Gutnisky & Dragoi 2008, Zohary et al 1994). Correlated variability (r_{sc}, also known as noise correlation or spike count correlation) is calculated as the Pearson correlation of the spike count responses of a pair of neurons to repeats of identical experimental conditions. Correlated variability is known to vary with attention (Cohen & Maunsell 2009, Herrero et al 2013, Mitchell et al 2009, Snyder et al 2015), during visual search task (Cohen et al 2010), during learning (Ni et al 2018), and could be a mechanism by which ensembles of neurons enhance spatial representations (Dehaqani et al 2018) or represent visual-mnemonic space (Leavitt et al 2017).

Signal correlation (r_{signal}) is another measure of correlation frequently used, which is the Pearson correlation between a pair of neuron's mean responses across conditions. Stated differently, correlated variability corresponds to fluctuations in response strength for a given stimulus that are shared across pairs of neurons, while signal correlation is a measure of tuning similarity (Figure 5).

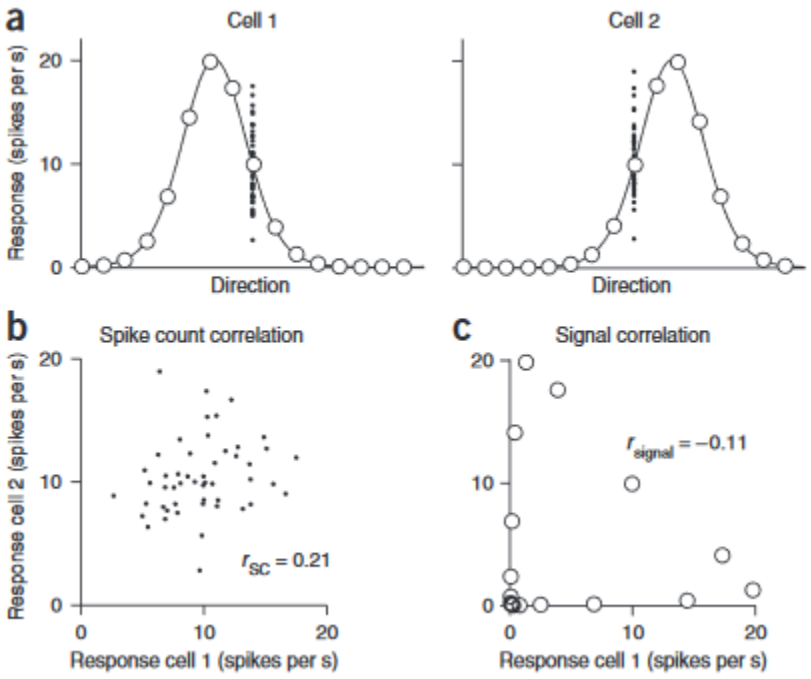

Figure 5: Correlated variability and signal correlation.

A: Tuning curves for two neurons across a wide range of experimental directions. Within a given direction, activity is variable (represented by black dots). B: Correlated variability, or r_{sc}, is calculated from the Pearson correlation of spike counts to a repeated stimulus. C: Signal correlation is the Pearson correlation of the mean responses across experimental conditions. From Cohen and Kohn (2011).

The structure of correlated variability has been well documented, particularly for cortical areas where multielectrode arrays can be chronically implanted such that numerous neurons can be recorded simultaneously. For example, correlated variability decreases with increasing neuronal distance between the pair (Constantinidis et al 2001a, Lee et al 1998, Smith & Kohn 2008), increases with tuning similarity (Averbeck & Lee 2003, Cohen & Maunsell 2009, Ecker et al 2010, Huang & Lisberger 2009, Kohn & Smith 2005, Zohary et al 1994), and the aforementioned attention effects can be dependent on the relative tuning of the pair of neurons (Ruff & Cohen 2014a). More recently, correlated variability has been investigated across cortical areas (Ruff & Cohen 2016a, Ruff & Cohen 2016b) and in the FEF (Astrand et al 2016, Cohen et al 2010, Dehaqani et al 2018) however the fundamental structure of correlated variability in FEF and its influence on saccade generation has been less investigated.

2.0 DISTINCT SOURCES OF VARIABILITY AFFECT EYE MOVEMENT PREPARATION

2.1 ABSTRACT

Preparing an eye movement to a target can begin the moment visual information has reached the brain, well in advance of the eye movement itself. The process by which visual information is encoded and used to generate a motor plan has been the focus of substantial interest partly because of the rapid and reproducible nature of saccadic eye movements, and the key role that they play in primate behavior. Signals related to eye movements are present in much of the primate brain, yet most neurophysiological studies of the transition from vision to eye movements have measured the activity of one neuron at a time. Less is known about how the coordinated action of populations of neurons contribute to the initiation of eye movements. One cortical area of particular interest in this process is the frontal eye fields, a region of prefrontal cortex that has descending projections to oculomotor control centers.

We recorded from populations of frontal eye field neurons in macaque monkeys engaged in a memory-guided saccade task. We found a variety of neurons with visually-evoked responses, saccade-aligned responses, and mixtures of both. We took advantage of the simultaneous nature of the recordings to measure the tendency of pairs of neurons to exhibit trial-to-trial correlated fluctuations in response strength. We found that this correlated variability

was related to behavior as measured by the saccadic reaction times, suggesting that the population-level organization of frontal eye field activity is important for the transition from perception to movement.

2.2 SIGNIFICANCE

The transition from perception to action involves coordination among neurons across the brain. In the case of eye movements, visual and motor signals coexist in individual neurons as well as in neighboring neurons. We used a task designed to compartmentalize the visual and motor aspects of this transition and studied populations of neurons in the frontal eye fields, a key cortical area containing neurons that are implicated in the transition from vision to eye movements. We found that the time required for subjects to produce an eye movement could be predicted from the statistics of the neuronal response of populations of frontal eye field neurons, suggesting that these neurons coordinate their activity to optimize the transition from perception to action.

2.3 INTRODUCTION

The process of identifying salient elements in the world and moving the eyes to foveate them is central to primate behavior. The coordination of visual input and motor output involves neural circuits that are woven throughout the cerebral cortex and subcortical regions (Wurtz 2008). One of the key players in this visuomotor transformation is the frontal eye fields (FEF), located in the

anterior bank of the arcuate sulcus. While FEF's role in both visual processing and saccade generation is well studied at the level of neurons recorded one at a time, there has been relatively less attention paid at the population level to how groups of FEF neurons coordinate from moment to moment during vision and eye movements.

For the brain to produce a fast and accurate eye movement, commands from an oculomotor control area such as FEF would ideally need to be robust. FEF contains neurons that respond exclusively to visual stimuli or eye movements, but most exhibit some degree of response to both (Bruce & Goldberg 1985, Lawrence et al 2005). These responses can take the form of persistent activity after a visual stimulus that remains elevated until an eye movement is made (Bruce & Goldberg 1985). Behaviorally, single-neuron firing rates to target stimuli (versus distractors) is correlated with reaction time (Thompson et al 1996), and eye movements are difficult to cancel once firing rate exceeds a certain threshold (Brown et al 2008). The functional properties of FEF neurons and their relationship to behavior, combined with their anatomical connections to visual cortex (Schall et al 1995b) and the superior colliculus (SC) (Helminski & Segraves 2003, Sommer & Wurtz 1998, Sommer & Wurtz 2000, Stanton et al 1988), make FEF neurons ideal candidates to mediate the visual to motor transformation in an eye-centered coordinate frame (Sajad et al 2015).

To generate consistent, repeatable eye movements, the ideal oculomotor command signal should be reliable. At the single-neuron level, reliability, as measured by Fano factor, is known to decrease after stimulus presentation in a wide variety of visual and motor areas (Churchland et al 2010), including FEF. Fano factor in FEF neurons is lowest before saccade initiation (Purcell et al 2012) and reductions in Fano factor are driven by visual stimulation independent of the saccade plan (Chang et al 2012). Although trial-to-trial correlated variability among pairs of

neurons (also known as "spike count correlation", or r_{sc}) has been widely studied in visual cortex (for a review see Cohen & Kohn 2011) and linked to shifts in visual attention (Cohen & Maunsell 2009, Herrero et al 2013, Mitchell et al 2009, Snyder et al 2016), there has been much less investigation of the role of correlated variability in movement planning and initiation.

The neural code by which FEF neurons signal an eye movement was initially described by relating pre-saccadic activity to saccade reaction time using a fixed rise to threshold model (Hanes & Schall 1996). Yet if saccades are activated directly by activity crossing some threshold within FEF, then how does the oculomotor system avoid generating a saccade reflexively due to the visual activity related to target onset? This question has been recently posed in the SC, where Jagadisan and Gandhi (2018) proposed that stability in the time-varying responses of individual neurons in SC was a key factor in determining whether SC activity leads to an eye movement. In the skeletomotor system, Kaufman et al (2014) posed a similar question, asking why population average delay activity in motor cortex did not appear to appreciably rise or change to signal the onset of a reach. They proposed a "potent" and "null" space for movement generation signals in the population, through which a linear readout could use specific activity patterns, or mixtures of neural responses, to signal movement. Taken together, these results suggest that generating fast movements is not just about having an elevated firing rate at the single neuron level but also can be influenced by interactions at the pairwise (or population) level.

We propose the optimal conditions for executing an eye movement are a function of variability both within and between neurons (i.e. single neuron and correlated variability). The transition from motor preparation to action is associated with a transition in these two sources of variability toward the optimal state for an eye movement. This principal holistically encompasses the FEF neuronal population; it is not constrained to specific neuronal subpopulations or saccade

target locations. We recorded simultaneously from groups of FEF neurons in three rhesus macaque monkeys using linear microelectrode arrays (LMA) while the animals performed a memory-guided saccade task. This task separated the neuronal responses to the visual stimulus from those related to the preparation and execution of a saccade. Once the saccade target appeared, variability changed at the level of single neurons (Fano factor) and the population (trial-to-trial fluctuations in responsivity, or correlated variability), with a prominent decrease after the onset of the saccade target in all FEF neurons for both preferred and anti-preferred saccade directions. Correlated variability in FEF populations was related to behavior, with the lowest values evident on trials with the fastest reaction times. These results suggest FEF population activity is coordinated in a way that contributes to the rapid transition from preparation to execution of an eye movement.

2.4 METHODS

2.4.1 Neuronal recordings

Surgical preparation

Three adult male rhesus macaque monkeys (*Macaca mulatta*; monkeys B, R and W) were surgically implanted with titanium head posts and FEF recording chambers (centered at stereotaxic coordinates: 25 anterior, 20 lateral) using sterile surgical techniques under isoflurane anesthesia. All procedures were approved by the Institutional Animal Care and Use Committee of the University of Pittsburgh and complied with guidelines set forth in the National Institute of Health's *Guide for the Care and Use of Laboratory Animals*.

Electrophysiological methods

Extracellular activity was recorded with a 16-channel linear microelectrode array (U-Probe, Plexon, Dallas, TX), with contacts spaced 150 μm (monkeys R and W) or 200 μm (monkey B), spanning a distance of 2.25 mm or 3.0 mm, respectively. Electrodes were lowered into cortex using a custom-designed mechanical microdrive (Laboratory for Sensorimotor Research, Bethesda, MD), inserted through a plastic grid with 1 mm spacing. The location of FEF within the chamber was identified first by the functional properties of recorded neurons and then confirmed by identifying sites where saccades could reliably (>50%) be evoked using low amplitude microstimulation (≤ 50 μA, 0.25 ms pulse duration, 70 ms pulse train duration, 350 Hz stimulation frequency) (Bruce et al 1985). We mapped out the recording chamber using microstimulation at multiple locations, and then considered successful stimulation sites and their immediate neighbors (1 mm away) as FEF.

Data collection

Stimuli were displayed on a 21" cathode ray tube monitor with a resolution of 1024x768 pixels and a refresh rate of 100 Hz at a viewing distance of 36 cm. Stimuli were generated with custom software written in MATLAB (MathWorks, Natick, MA) using the Psychophysics Toolbox extensions (Brainard 1997, Kleiner et al 2007, Pelli 1997). Eye position was monitored monocularly via infrared tracking at a 1000Hz rate (EyeLink 1000, SR Research, Mississauga, Canada) and neural and behavioral data were recorded with a Grapevine recording system (Ripple, Salt Lake City, UT). For each electrode, waveform segments that exceeded a threshold (set as a multiple of the root mean square noise on each channel) were saved and stored for offline analysis and sorting. Waveforms were automatically sorted using a competitive mixture

decomposition method (Shoham et al 2003) and manually refined based on waveform shape and inter-spike interval using custom time amplitude window discrimination software written in MATLAB (Kelly et al 2007).

Following the offline sorting procedure, the signal-to-noise ratio (SNR) was calculated for each identified unit as the ratio of the average waveform amplitude to the standard deviation (SD) of the waveform noise (Kelly et al 2007). We considered only candidate units with an SNR of 2.5, and then eliminated 162 units whose delay period response was not greater than 1 sp/s for at least one condition. This resulted in a total of 976 units (230, 232 and 514 units in 14, 25, and 36 sessions from monkeys W, B and R), from which we analyzed 7656 pairs of simultaneously recorded neurons (2038 from monkey W, 1199 from monkey B, and 4419 from monkey R, same-channel pairs were excluded).

2.4.2 Experimental design and statistical analysis

Behavioral task

Monkeys performed a conventional memory guided saccade (MGS) task (Figure 6) (Hikosaka & Wurtz 1983). The trial began when the monkey was required to fixate a small blue circle (0.5° diameter). After maintaining fixation within a 1.8° diameter window for 200 ms, a circular peripheral target (0.8° diameter, 11° eccentric) was briefly flashed (50 ms duration) at one of eight locations (cardinal and oblique directions). The animal was required to maintain fixation for 550 or 600 ms (held constant within a session) until the fixation point was extinguished, which signaled the monkey to make a saccade to the remembered location of the stimulus. The monkey had 500 ms to initiate a saccade, as defined by the eye position leaving a window 1.8° in diameter around the fixation point. Once the saccade had been initiated, the monkey's eye

position had to reach the saccade target within 200 ms and maintain gaze within 2.7° of the location for 150 ms in order to receive a liquid reward. Each block consisted of pseudorandomized presentations of all eight directions, with at least 50 blocks gathered per session (mean=132 blocks). On a subset of days, after the fixation point was extinguished and the monkey began its saccade, the target was re-illuminated to aid in saccade completion. The analysis presented here is not affected by this target because it appeared after the analysis window.

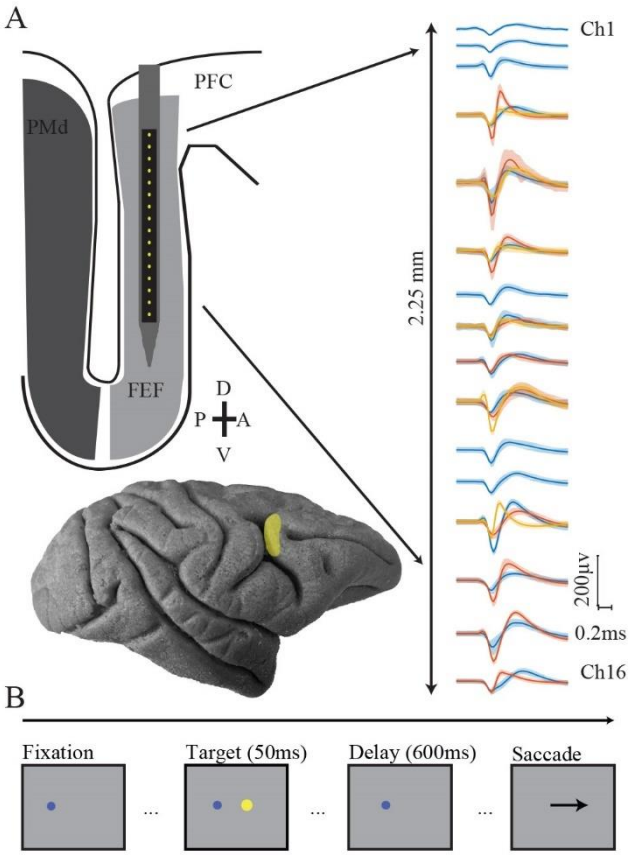

Figure 6: Experimental Methods.

A: Top: Schematic of 16 channel linear microelectrode array, contacts were spaced at either 150 or 200 µm, total length of electrode shank 85mm. Sample waveforms (mean +/- SEM) recorded after manual spike sorting. Bottom: Lateral view of the macaque brain, FEF is highlighted and located along the bank of the arcuate sulcus. B) Memory guided saccade task. Each trial began with the subject fixating on a central dot. After the subject fixated the central dot, a peripheral stimulus briefly appeared at 1 of 8 locations equidistant from fixation and 45 degrees in angle apart. The subject was required to maintain fixation on the central dot while remembering the location of the peripheral stimulus. When the central fixation point was extinguished, this signaled the subject to make a saccade to remember location of the peripheral stimulus.

General statistical analysis

For pairwise analyses (correlated variability & covariance) degrees of freedom were across pairs of neurons (n = 7656 pairs unless stated differently in the results section). For single neuron measurements (firing rate, variance, correlation between firing rate and reaction time) degrees of freedom were across number of single neurons (n = 976 neurons). Detailed information for the specific statistical tests used for each figure can be found in the results.

For statistically testing the time course of variability (Figure 5A-C), a running one sample t-test was computed for each condition after baseline (200ms before target onset) subtraction. To compare conditions to each other, an independent samples t-test was used. Both statistical tests were Bonferroni corrected. For statistical tests on the Fano factor time course, see the section below.

Calculation of preferred direction and tuning selectivity

The preferred direction and selectivity of each FEF neuron, calculated during the delay period, was determined by a vector average similar to that used for preferred orientation (Smith et al 2002). Preferred direction is given by the circular mean angle:

$$\frac{1}{2}\arctan\left(\frac{\sum_{n=1}^{N} R_n \sin(2\theta_n)}{\sum_{n=1}^{N} R_n \cos(2\theta_n)}\right) \qquad (2-1)$$

Where R_n is the response magnitude during the delay period, θ_n is the stimulus location, and n is an index from 1 to the number of points, 8, in the tuning curve.

To measure the selectivity of each neuron's tuning curve, we calculated the complex summed response vector (where $i = \sqrt{-1}$)

$$v = \sum_{n=1}^{N} R_n e^{(i2\theta_n)} \qquad (2-2)$$

And normalized the magnitude by the summed magnitude of all the response vectors:

$$selectivity = \frac{|v|}{\sum_{n=1}^{N} R_n |R_n|} \qquad (2-3)$$

A selectivity of 0 corresponds to a neuron which fires equally for all conditions while a selectivity of 1 would be for a neuron that responds exclusively to one condition. The preferred direction of a pair of neurons was the preferred direction of the neuron with a higher selectivity.

Measurement of correlated variability

The methods used to compute r_{sc} (also known as "spike count correlation" or "noise correlation") have been presented in detail in previous publications (Kohn & Smith 2005, Smith & Kohn 2008). Briefly, correlated variability was measured by calculating spike count correlation (r_{sc}, also known as noise correlation). The r_{sc} of a given pair of neurons is the Pearson correlation coefficient of the evoked spike responses to a repeated stimulus. For most of the results in this paper, r_{sc} was calculated during the memory epoch (550 or 600 ms in duration), and thus does not include the time when the stimulus was on. When a r_{sc} value was calculated across multiple

directions, we normalized each neuron's response for each direction by z-scoring it, and then calculated the r_{sc} by combining responses across directions. For calculating the "preferred" and "anti-preferred" direction of the pair of neurons, we first identified the eye movement direction closest to the preferred direction of the most selective neuron in the pair. That direction, along with the two directions flanking it on either side were combined to yield the "preferred" direction. The three directions 180 degrees opposite the directions used for the preferred direction were combined to yield the "anti-preferred" direction. We combined conditions in this way to increase our statistical power – results using the preferred and anti-preferred directions alone (without the flankers) were qualitatively similar. We also defined the preferred direction of the pair by using the geometric mean of the two neuron's tuning curves instead of the more selective neuron. Instances where these two methods would differ would only result from pairs with disparate tuning, and even for these pairs, results were nearly indistinguishable. We chose to use the method of defining based on the more selective neuron as it guaranteed the direction chosen was in the preferred direction of at least one neuron in the pair (while centering on the geometric mean of the pair can be more likely to identify compromise directions that are not at the peak response of either neuron).

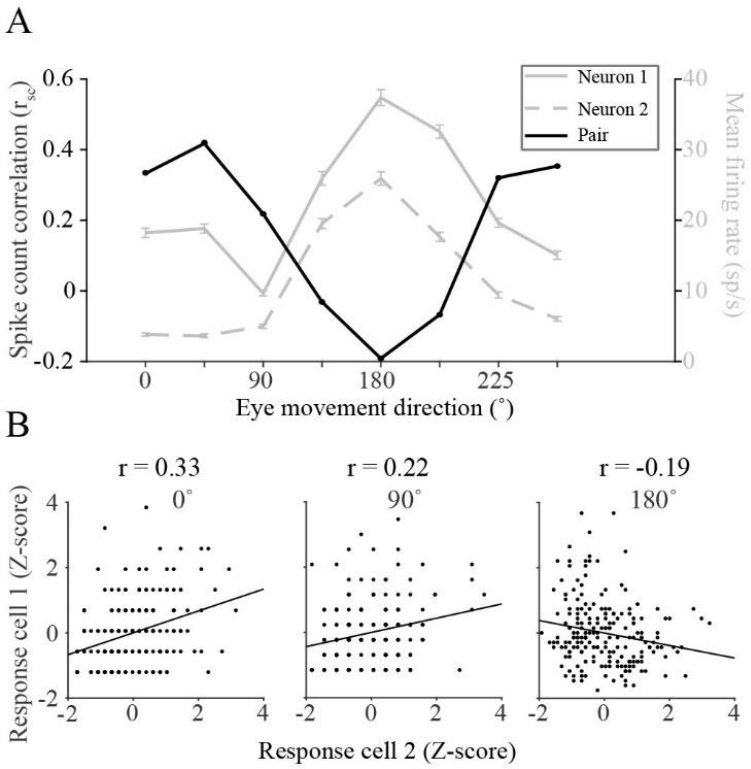

Figure 7: Correlated variability.

A) For a given pair of FEF neurons, firing rates during the delay period (0 - 600ms after target offset) to a repeated stimulus were used to calculate the Pearson's correlation, representing the correlated variability (r_{sc}) of the pair. B) r_{sc} was calculated separately for each of the 8 conditions.

Visual-motor response properties

To classify units as visual, motor, or visuomotor, the relative strength of the response to the visual stimulus was compared to that around the time of the eye movement. The visual response was defined as the spike count from 50 to 150 ms after stimulus onset while the motor response was defined as the spike count from 50 ms before to 50 ms after the onset time of the saccade. We computed a standard *d'* metric for each neuron comparing the distributions of its responses to the visual and motor epochs (differences in the means of the distributions divided by the square root of the product of their variances). We arbitrarily assigned positive *d'* to neurons that responded most in the visual epoch and negative *d'* to those that responded most in the motor epoch. *d'* values that were close to zero represented neurons that had nearly identical visual and motor responses.

r_{sc} and reaction time analysis

To relate r_{sc} to reaction time on a trial by trial basis, r_{sc} was calculated on subsets of trials sorted by their reaction time. For a given recording session, within each saccade direction, trials were sorted according to reaction time. r_{sc} was calculated in a 40-trial sliding window, such that the first bin would correspond to r_{sc} in the 40 trials with the fastest reaction times and the last bin would correspond to r_{sc} in the 40 trials with the slowest reaction times. For a session with 100 repeats, the number of r_{sc} bins would total 60. 3 sessions which did not have sufficient trials for 10 reaction time bins (50 repeats) were omitted. To compare measurements across sessions (as the number of repeats varied day-to-day), the r_{sc} bins, still sorted by reaction time, were then combined into deciles in each session. This ensured each neuronal pair had 10 r_{sc} measurements across a range of reaction times that could be averaged across sessions. The same process was

also used to compare pairwise covariance and single neuron mean firing rate and variance with reaction time bin. For r_{sc}, statistical testing was done by implementing a linear mixed effects model (Matlab function fitlme) with fixed effects for reaction time and summed d' of a pair (and an interaction term), a random effect term for neuron pair, and a correlated random effect term for pair and reaction time. For other measures (covariance, variance, firing rate) the summed d' term was excluded. This model was fit separately for preferred and anti-preferred conditions.

Fano Factor

Fano factor was calculated using methods and code previously published (Churchland et al 2010). Data were aligned on stimulus onset, and Fano factor and mean rate were computed using a 100-ms sliding window. Analysis included only the preferred and anti-preferred directions (flanker directions included for increased statistical power). Fano factor was computed after mean matching the firing rate to rule out any possible changes in Fano factor are trivially due to changes in firing rate. The statistical significance of the Fano factor decrease was assessed by comparing the Fano factor 100ms before target onset to the Fano factor 200ms after stimulus onset. Significance was computed based on sampling distributions from the 95% confidence intervals calculated by the least squares regression used when calculating the Fano factor (see Churchland et al 2010). The decline was significant for both preferred and anti-preferred directions (both $p < .0001$).

Microsaccade detection

Microsaccades were identified using a velocity criterion based on a previously published detection algorithm (Engbert & Kliegl 2003). The criterion, η, was based on a multiple of the

standard deviation of the velocity distribution and calculated separately for the x and y velocity components

$$\eta_{x,y} = \lambda\sigma_{x,y} \qquad (2-4)$$

Where λ is a multiplier and $\sigma_{x,y}$ is a median estimator of the velocity time series defined as

$$\sigma_{x,y} = \langle v_{x,y}^2 \rangle - \langle v_{x,y} \rangle^2 \qquad (2-5)$$

Where ν vrepresents the velocity and $\langle v \rangle \langle \mathrm{v} \rangle$ denotes the median estimator. We used a value of

λ=10 and any potential microsaccades must have had a minimum duration of 6 ms and minimum amplitude of .05 degrees. Trials that contained at least one microsaccade were removed from the r_{sc} calculation. To maximize statistical power in calculating r_{sc} after the microsaccade trial removal, we z-scored both the spike counts and the reaction times for the preferred direction and its two flankers and combined them to calculate one r_{sc} value for the preferred direction (and one for the anti-preferred). On the full set of trials, using this z-scoring procedure did not appreciably change the results from computing the r_{sc} separately for each condition.

2.5 RESULTS

We recorded from 976 neurons (see *Methods*) in FEF across 75 recording sessions in three macaque monkeys. This resulted in 7656 pairs of neurons recorded while the animals performed a memory-guided saccade task (Figure 1). The focus of our analyses was how the population activity structure evolved during the delay period prior to saccade execution.

2.5.1 Trial-to-trial correlated variability

To understand how changes in correlated variability could affect eye movement preparation, we first characterized its overall structure in FEF. Correlated variability (spike count correlation, or r_{sc}), has been extensively studied in visual areas such as V1(Kohn & Smith 2005, Smith & Kohn 2008), V4 (Cohen & Maunsell 2009, Smith & Sommer 2013), and MT (Ruff & Cohen 2014a, Ruff & Cohen 2014b, Zohary et al 1994), but much less in oculomotor areas such as FEF (but see (Astrand et al 2016, Cohen et al 2010, Dehaqani et al 2018, Zirnsak et al 2014)). We calculated r_{sc} for each saccade direction (and combined across directions in some cases, see *Methods*) for each pair of neurons (Figure 7). To understand the structure of r_{sc} with respect to basic functional properties and how that structure compares with findings in other cortical areas, we examined r_{sc} as a function of physical distance, tuning similarity, and visuomotor preference.

We first grouped pairs of neurons by electrode contact distance and calculated r_{sc} during the delay period of the task for all pairs of neurons (Figure 8A). The magnitude of r_{sc} decreased with increasing electrode separation (Pearson's $r = -0.070$, $p < .0001$). This finding is consistent with findings of the distance-dependence of r_{sc} in numerous previous studies (Leavitt et al 2013, Smith & Kohn 2008, Smith & Sommer 2013, Snyder et al 2018, Zirnsak et al 2014).

Tuning similarity between pairs of neurons has also been shown to affect correlated spiking (Bair et al 2001, Cohen et al 2010, Cohen & Maunsell 2009, Smith & Kohn 2008, Smith & Sommer 2013, Zohary et al 1994), with the overarching finding being that similarly tuned neurons exhibit larger levels of correlated variability. As a measure of tuning similarity, we calculated the difference in preferred direction for each neuron in a pair (0 degrees for pairs with identical tuning, to 180 degrees for pairs that have opposite tuning). The firing rate window to determine the preferred direction was the entire memory delay period (from stimulus offset to fixation offset) to incorporate all possible tuning information. Thus, the delay period would include visual responses from the stimulus as well as any preparatory motor activity before the "go" cue. For visual neurons, the preferred direction represents the location of a classical RF of the neuron, while for motor neurons it is often described as a movement field. For r_{sc}, as the difference in preferred direction between the pair increased, the magnitude decreased (Figure 8B; Pearson's $r = -0.115$, $p < 0.0001$; $n = 7656$ pairs).

Finally, given the variety of visual-motor response properties observed in FEF (Bruce & Goldberg 1985), we wanted to determine if similarly tuned visual or motor neurons had higher correlated variability. To perform the memory guided saccade task, a visual stimulus must be processed and transformed into a motor command. The convergence of these response properties in FEF neurons with the demands of the task suggest to us that correlated variability might depend on the role of individual neurons in the visuo-motor transformation. To examine this possibility, we calculated a visual-motor d' for each neuron based on our ability to differentiate between the stimulus-aligned and the saccade-aligned responses in that neuron (see *Methods*). We then divided neurons into quartiles based on this d' measure and focused on interactions between visual-visual (VV), visual-motor (VM), and motor-motor (MM) pairs. VV were pairs of

neurons where both d' measures were positive, MM were pairs of neurons where both were negative, and VM were pairs that had one of each. Given the results above that pairs that are spatially closer and more similarly tuned have higher r_{sc}, if visual and motor tuning similarity followed the same trend, we would expect VM pairs to have the lowest r_{sc} compared to more similarly "tuned" VV and MM pairs. VM pairs did have significantly lower r_{sc} than VV pairs, however, VM pairs were not significantly different from MM pairs (Figure 8C) (two sample t-test, VV to VM p= 0.0025, VV to MM p=0.0002, MM to VM p=0.2602). This result suggests that the level of correlated variability that is beneficial to one subpopulation (for example VV pairs) may not necessarily be beneficial for another (MM pairs).

It has been previously shown that the level of correlated variability is positively correlated with firing rate (de la Rocha et al 2007). This effect cannot underlie our findings, because we observed the highest firing rates in groups with the lowest r_{sc} (VM, MM) Figure 8D). Despite their differences in absolute r_{sc} level, all three groups (VV, VM, MM) had significant trends with respect to electrode distance (Pearson's r = -.129 p<.0001; r = -0.045 p = .007; r = -0.063 p = .003 for VV, VM, & MM respectively) and preferred direction (r = -.119 p<.0001; r = -0.106 p<.0001; r = -0.123 p<.0001 for VV, VM, & MM respectively). To maximize our statistical power, in later analyses in this paper all neuronal pairs are pooled unless stated otherwise. To summarize, correlated variability in FEF is higher in visual populations compared to motor or visuomotor, and the patterns we observed in FEF are largely consistent with other brain regions with respect to the basic properties of distance and receptive field location.

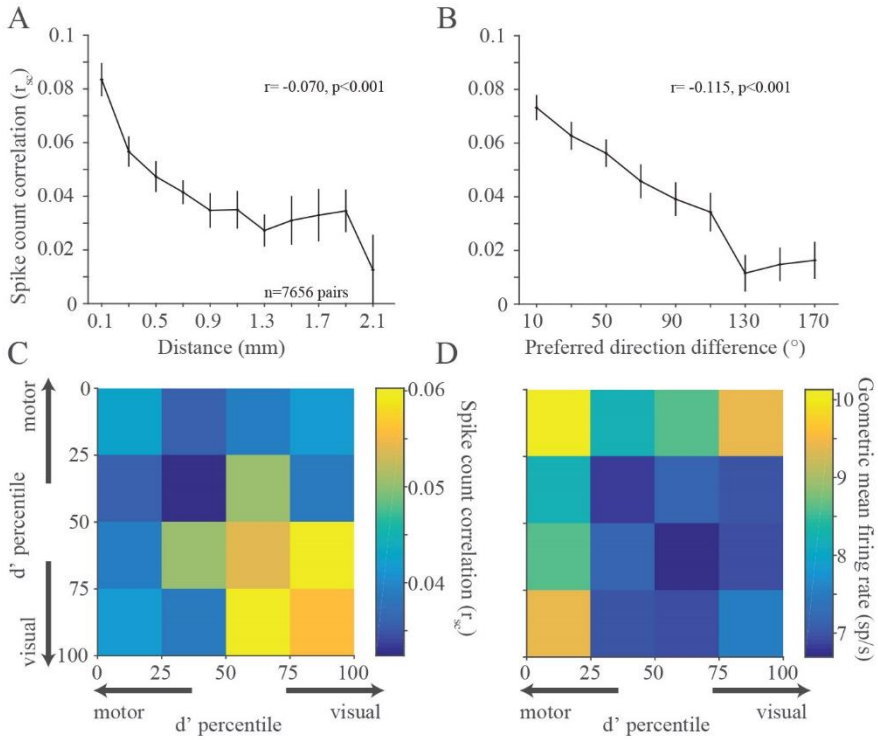

Figure 8: Correlated variability with basic response properties.

A) Mean (+/- SEM) r_{sc} for pairs of neurons as a function of distance. Neuronal pairs were grouped by distance with bin centers starting at 0.100 mm and bin edges spanning ±0.100mm. Bins with < 100 pairs were removed. B) Average r_{sc} for pairs of neurons as a function of preferred direction difference (tuning similarity). Neuronal pairs were grouped in 20° bins starting at 10°. r_{sc} decreases with increasing neuronal distance and tuning dissimilarity. Both panels show binned data, but statistical analyses were performed on 7656 total pairs. C) r_{sc} for pairs based on visual-motor response properties. Each pair was binned based on the visual-motor d' ranking of each neuron in the pair relative to all neurons recorded. D) Same binning in C but geometric mean firing rate during the delay epoch. Visual-visual pairs had significantly higher r_{sc} compared to motor-motor or visual-motor pairs, despite having lower geometric mean firing rate.

2.5.2 Tuning similarity and eye movement direction

In trying to understand how the population of FEF neurons contributes to planning and executing an eye movement, the analyses so far have considered mean r_{sc} across all directions. We were next interested in how r_{sc} changes as animals plan different eye movements. Because the population of FEF neurons contains a range of direction preferences, we aligned the eye movement conditions relative to preferred direction of each pair of neurons. This allowed us to consider the population variability structure in FEF neurons that were presumably involved in an eye movement (when the stimulus aligned well with their preferences) versus neurons that have less involvement (when the stimulus not aligned with their preference).

Correlated variability in the spiking activity of pairs of neurons were lowest when saccades were made towards the pair's preferred direction (chosen as the preference of the more selective of the two neurons) and highest in the anti-preferred direction, particularly for pairs of neurons with similar tuning (Figure 9A and C). The decrease in r_{sc} as a function of proximity to preferred direction was also present, albeit weaker, in pairs with dissimilar tuning. The geometric firing rate computed within the same conditions (Figure 9B and D) demonstrated that the r_{sc} trend was opposite that predicted if the changes in r_{sc} were purely due to an increase in firing rate (de la Rocha et al 2007).

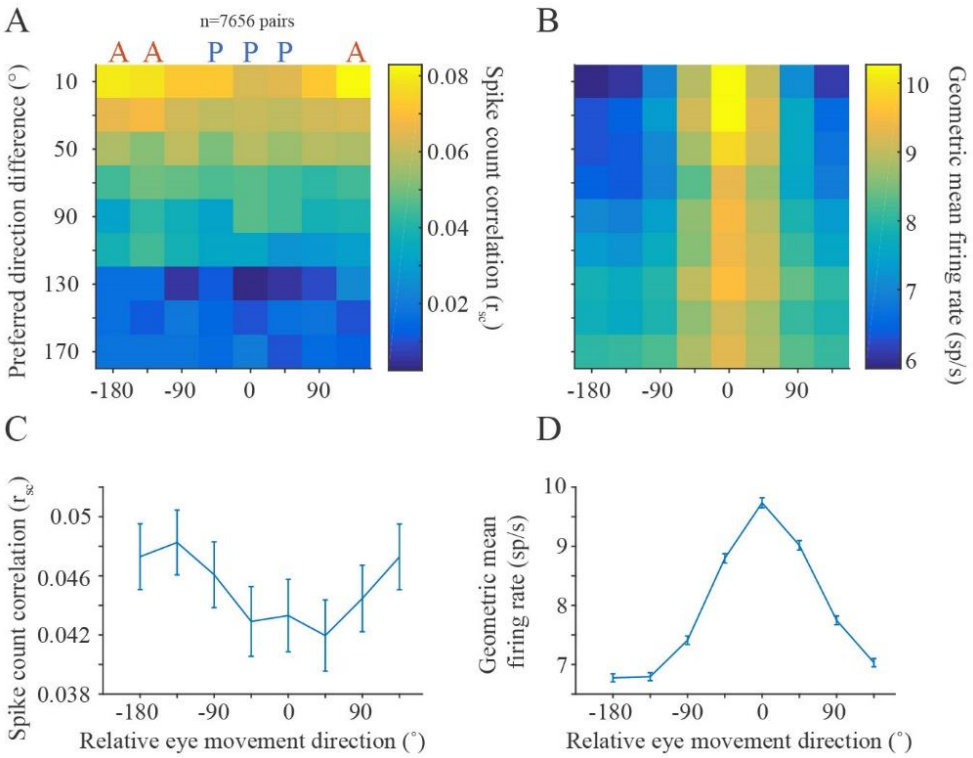

Figure 9: Correlated variability and eye movement direction.

A) Average r_{sc} in each of the 8 conditions binned by preferred direction difference. B) Same binning as in A, but with geometric mean firing rate. Across all preferred direction differences, though more prominent for pairs with similar tuning, r_{sc} is lower in the preferred directions of a pair compared to anti-preferred directions, despite firing rate being higher in the preferred directions. C) Average r_{sc} across all pairs for each of the 8 conditions, relative to the preferred direction of each pair. D) Same as in C, but with geometric mean firing rate.

2.5.3 The time course of correlated variability

If correlated variability in visual target responses in FEF is an important factor in preparing eye movements, then we might expect these effects to manifest shortly after the visual target appears. Our analyses up to this point have considered the delay epoch (550 or 600 ms in duration) in aggregate. Here, we use a sliding analysis window (100ms windows sliding in 10ms increments) to determine the time scale on which the neuronal population structure shifts as a target appears and an eventual saccade takes place. We first considered how r_{sc} and firing rate change over time for different eye movements by grouping the preferred eye movement direction and its flankers with the 180 degree opposite direction and its flankers. It is possible a decrease in r_{sc} observed in a pair's preferred direction could be driven merely by the recent presence of the visual stimulus in or near the RF as observed in previous studies in visual cortex (Smith & Kohn 2008, Smith & Sommer 2013, Snyder et al 2014), with r_{sc} returning to baseline levels as the delay period continues. If a low correlated variability level contributed to a high-fidelity stimulus encoding and reliable motor preparation, we would predict the low level to be persistent across the entire delay epoch. After stimulus onset (time = 0s), mean firing rate increased (Figure 10B) while r_{sc} decreased (Figure 10A) for both preferred and anti-preferred directions, with a sharper decrease in preferred directions. This decrease persisted throughout the entire delay period, consistent with our prediction that FEF population variability could be meaningful for both encoding the stimulus and preparing an eye movement. Towards the end of the delay period, r_{sc} in the preferred and anti-preferred directions overlapped, meaning the variability structure while preparing to make an eye movement is broadly tuned, even for directions in the ipsilateral hemifield.

Because of how r_{sc} is measured (from the covariance of a pair of neurons normalized by the product of the individual variances) it is affected by both the both joint and individual neuronal variability, and both components could drive changes in the overall r_{sc} level. We further investigated the time course of individual neuronal variability and correlated variability through the delay period to determine what components drive the changes observed in r_{sc}. The covariance, like r_{sc}, decreased immediately after stimulus presentation and maintained a low level throughout the delay period (Figure 10C). Contrary to r_{sc}, the covariance was higher in the preferred direction compared to the anti-preferred, and the difference appeared later in the memory period. To measure individual neuron variability, Fano factor was calculated for preferred and anti-preferred directions (Figure 10D). We used a mean matching method to account for changes in firing rate (see *Methods*). Consistent with previously reported findings, Fano factor for both conditions decreased after stimulus onset and remained at a low level (relative to baseline) throughout the memory period (Churchland et al 2010).

In summary, variability at the single neuron and pairwise level decreased relative to baseline when preparing to make an eye movement, even in anti-preferred directions. This implies bilateral populations of neurons are involved in eye movement preparation. We next sought to understand how correlated variability, a measure calculated across groups of trials, could vary with behavior on a trial by trial basis.

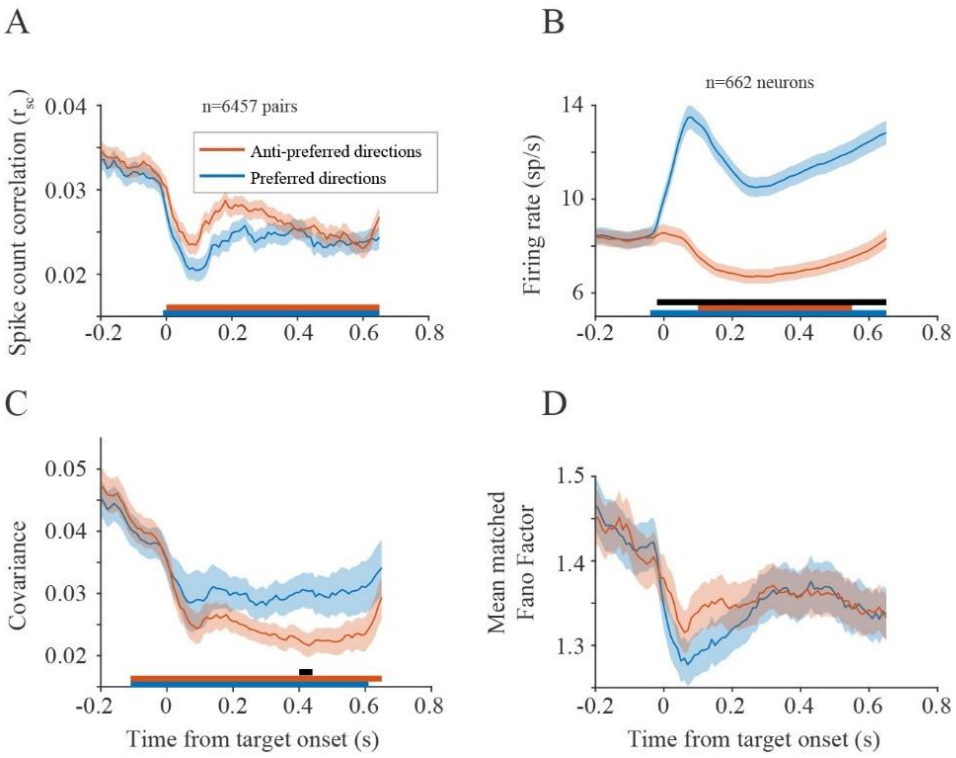

Figure 10: Time course of variability.

Time course of r_{sc} starting at fixation (t= -0.2) through stimulus presentation (t=0.0 to t=.05) until fixation offset (t=.65). r_{sc} was calculated in overlapping 100ms bins, with a sliding window of 10ms. Each time point corresponds to the leftmost point of the bin (t=0 for example corresponds to r_{sc} in a window from 0 to 100ms). All panels use this window analysis. A) r_{sc} time course for preferred and anti-preferred directions. Both conditions show a decrease in r_{sc} after stimulus onset, lower for the preferred direction, that is persistent throughout the delay epoch. B) Same time course as in A, but with individual neuron firing rate. C) Covariance across pairs for preferred and anti-preferred directions. Covariance decreases after stimulus onset and is higher in preferred compared to anti-preferred directions. Statistical data points for A-C are plotted as lines under each subplot. Lines corresponding to the colors in the plot represent each condition relative to baseline, the black line corresponds to differences between the two conditions (see Methods). D) Mean matched Fano Factor follows the same time course as r_{sc}: decrease after stimulus onset (more in the preferred direction) that is persistent throughout the entire period. Pairs from a small number of sessions (n=1199 pairs, 24 sessions), where the time course varied (delay epoch=550ms or stimulus duration= 100ms) were removed from this analysis.

2.5.4 The role of population variability in reaction time

Although the memory-guided saccade task we employed was easy for our subjects, they did vary in their behavior from trial to trial. A primary source of that variation was their reaction time – the difference in time between the 'go cue' (fixation offset) and the onset of their eye movement toward the remembered target location. Comparing a trial to trial measure of variability (r_{sc}) with a single trial measure of behavior presented a problem. To solve this, we grouped the trials to calculate r_{sc} separately based on reaction time. We used a group of 40 trials because smaller numbers of trials produced less reliable estimates of r_{sc}, and larger numbers of trials impaired our ability to measure differences in reaction time. For each condition, r_{sc} was calculated on a sliding group of 40 trials that were ranked based on the reaction time of the subject (Figure 10A and see *Methods*). Our hypothesis was that if the low correlated variability levels observed provide some benefit to eye movement planning, r_{sc} calculated with fast reaction time trials should be lower than that calculated with slow reaction time trials. We found that this was true for saccades in both the preferred and anti-preferred directions (Figure 10B). To statistically test the relationship between r_{sc} and reaction time, we constructed a linear mixed effects model. The model was fit to the reaction times and corresponding r_{sc} bins separately for preferred and anti-preferred directions. We found a significant trend (linear mixed effects model, $p<0.001$) across the population for both directions, indicating that a low r_{sc} value was associated with fast reaction times.

To ensure that our results were not biased due to fluctuations in behavior during the delay period, we performed two additional control analyses. First, we analyzed the first and last 200 ms of the delay epoch and found in both cases the results were qualitatively similar to those reported

here for the entire epoch. This makes it unlikely that simple firing rate effects due to visual or motor transients could account for our results. Second, to ensure the changes in correlation with reaction time were not due to the presence of small eye movements during the delay period, we used a microsaccade detection algorithm (see *Methods*). After removing trials which contained one or more microsaccades, there was still a significant relationship between r_{sc} and reaction time for both preferred and anti-preferred directions (linear mixed effects model, preferred $p = .003$, anti-preferred $p = .001$).

In the same manner, we analyzed single neuron firing rates to determine their association with reaction time (Figure 10C). We found that for saccades in the anti-preferred direction, firing rate was relatively constant (linear mixed effects model, $p=0.036$). However, for saccades in the preferred direction, a high firing rate was associated with faster reaction times (linear mixed effects model, $p<0.001$), consistent with previous findings in FEF (Everling & Munoz 2000) and SC (Dorris et al 1997) . In addition to overall r_{sc}, we broke down this measure of correlated trial-to-trial variability into its constituent statistics – covariance and variance. Covariance (Figure 10D) followed the same trends as r_{sc} in that it was lowest for fast reaction time trials, however the result was not significant in our model for the anti-preferred direction (linear mixed effects model, preferred: $p=.016$, anti-preferred: $p=.204$). Variance (Figure 6E) was also lowest on fast reaction time trials (Figure 6E, linear mixed effects model, preferred: $p<.001$, anti-preferred: $p=.003$). Because a lower variance would tend to increase r_{sc}, we conclude that correlated variability (and not single-neuron variability) is the primary change associated with fast reaction times.

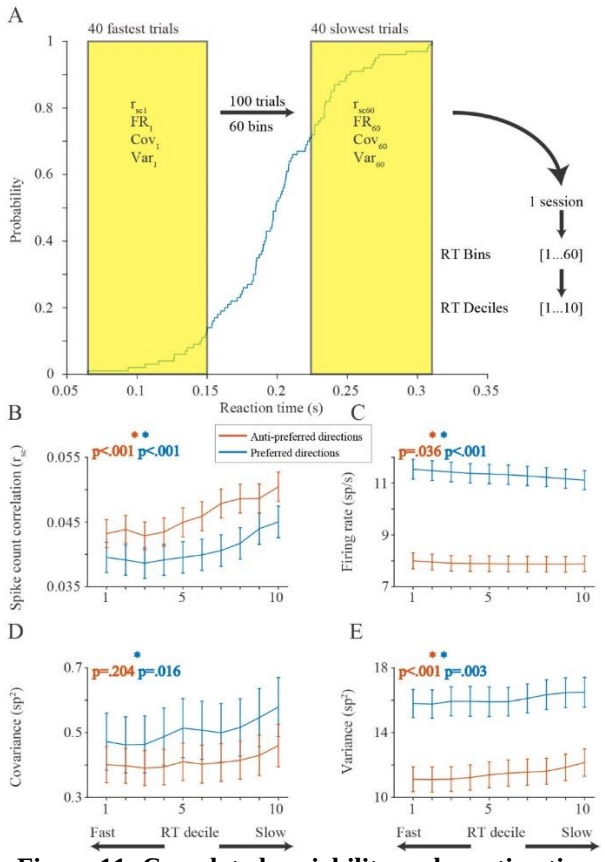

Figure 11: Correlated variability and reaction time.

r_{sc} calculated in subsets of trials based on saccade reaction time rank, for both preferred and anti-preferred directions. A) Blue trace is cdf of reaction time for a given session and saccade direction. For a given saccade direction, trials were sorted from slowest to fastest reaction time. A sliding window 40 trials long was then used to calculate r_{sc} (or firing rate, covariance, and variance) in subsets of trials. For this example session, the result is 60 measures of r_{sc} calculated across fast, slow and intermediate reaction times. To average across sessions that may have different numbers of repeats, r_{sc} measures in each session were divided into deciles. The reaction time decile binning applies to all panels. B) r_{sc} plotted against reaction time decile for preferred and anti-preferred directions. For both directions, r_{sc} is lowest when calculated for fast reaction time trials, compared to slow reaction time trials. C) Firing rate decreases (preferred) or stays the same (anti-preferred) with reaction time decile. D) Covariance follows the same trends as r_{sc} for both preferred and anti-preferred directions (low covariance for fast reaction time bins, high covariance for slow reaction time bins). E) Single neuron variance follows the same trend with reaction time decile as r_{sc} does, when it would be expected to follow the opposite if the r_{sc} trends were being driven by single neuron variability.

2.5.5 Visual and motor subpopulations and reaction time

While the relationship between r_{sc} and saccade reaction time was observed across the entire population, one might suspect differences between visual and motor subgroups. We have already shown r_{sc} for MM pairs is lower than that of VV pairs, but does this persist for the r_{sc} relationship with reaction time? The linear mixed effects model previously used was fit with an additional parameter, the sum of the visual-motor d' of each neuron in a pair. As expected based on the previous d' r_{sc} result, there was a main effect of d' on r_{sc} for both preferred and anti-preferred directions (linear mixed effects model, preferred: p=.011, anti-preferred: p=.002) meaning VV pairs had significantly higher r_{sc} compared to MM pairs. Qualitatively, it appeared the relationship between r_{sc} and reaction time was also stronger in VV pairs compared to MM pairs (Figure 12A-7B), but the interaction term between reaction time and sum d' was not statistically significant (linear mixed effects model, preferred: p=.143, anti-preferred: p=.061). Taken together, our analyses indicate that substantial shifts in correlated trial-to-trial variability in the delay epoch activity accompany eye movement preparation.

While decreases in r_{sc} across the entire population, particularly among visual neurons, may underlie efficient motor preparation, we also observed that increases in firing rate were associated with fast reaction times (Figure 12B). Previous studies have related the firing rate of single neurons to saccade initiation in FEF (Ding & Gold 2012, Hanes & Schall 1996, Hauser et al 2018). While we found a relatively weak (albeit highly statistically significant) relationship over the entire delay epoch, the firing rate signals for saccades would be expected to be more tightly coupled with the timing of the saccade itself.

To relate FEF firing rate to saccade reaction time on an individual neuron basis, we correlated on a trial by trial basis the firing rate of each neuron in its preferred direction for the last 50 ms before the go cue with the reaction time of the animal for that trial. Previous research on firing rate correlations with reaction time have split FEF neurons into motor and visuomotor populations (Jantz et al 2013, Ray et al 2009), however none have divided groups based on the strength of the motor or visuomotor response within these populations. We ranked each neuron based on our visuomotor d' metric (see *Methods*), and then compared the relationship between firing rate and reaction time in each of the deciles transitioning from motor to visuomotor to visual neurons. The 10% of neurons with the relatively strongest motor responses neurons had, on average roughly a -0.08 correlation between their firing rates and the animal's reaction time. That is, higher firing in those neurons led to small (fast) reaction times. As we considered progressively less strong motor neurons, the magnitude of correlation decreased between firing rate and saccade reaction time, such that activity in the strongest visual neurons had nearly zero correlation with reaction time (Figure 12C, Pearson's $r=.205$, $p<.001$). Not only was this firing rate signal strongest in the motor neurons, but it was strongest close to the 'go' cue (Figure 12D), indicating a tight coupling with the eventual saccade. Taken together, our results support a role of both single neuron firing rates and population-level correlated variability in saccade preparation.

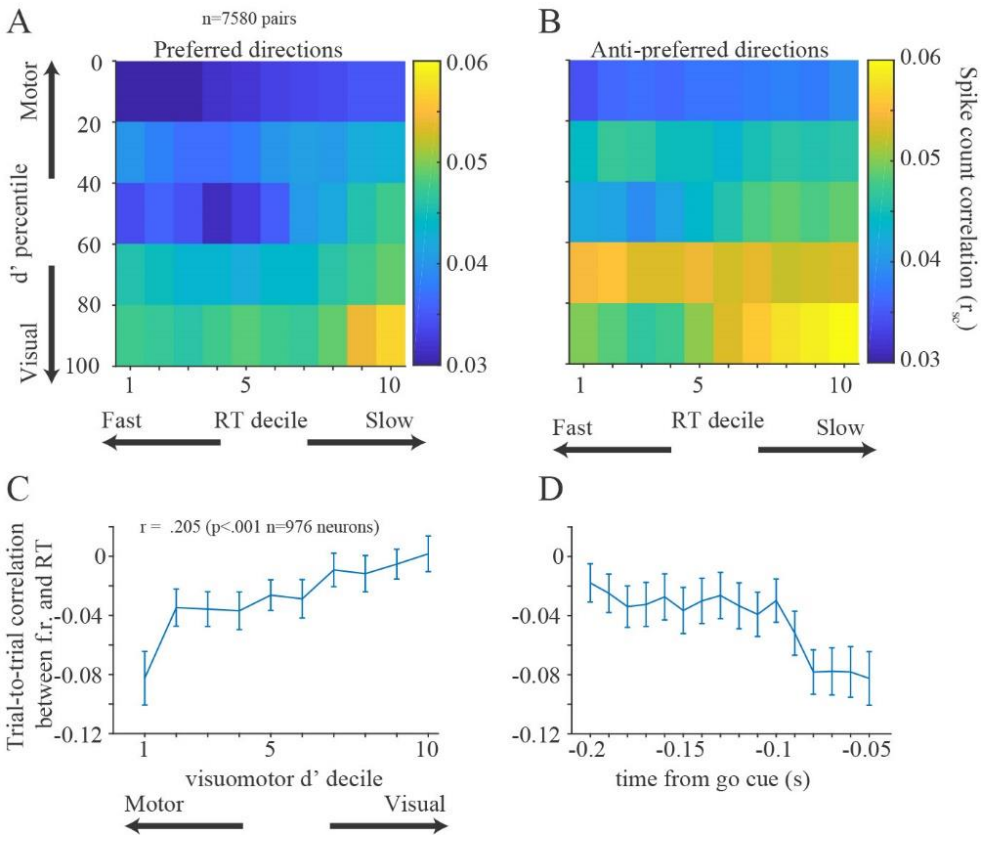

Figure 12: Variability and reaction time in visual and motor subpopulations.

A) r_{sc} with reaction time, grouped by visual-motor d' for preferred and B) anti-preferred directions. r_{sc} is lower for motor-motor pairs, and the relationship between r_{sc} and reaction time decile is weaker, however not significant (preferred: p=.298, anti-preferred: p=.254). C) Trial to trial correlation between firing rate in the last 50ms of the delay period and reaction time. Neurons are divided by visuomotor strength (d' decile). D) Time course of correlation between firing rate and reaction time for neurons with the strongest motor responses (note: 1st decile in C). x axis value marks the beginning of each point's time window (first value is -.2s to -.15s).

2.6 DISCUSSION

Preparation for a saccade involves signals in a diverse population of FEF neurons. We found that two key changes in FEF were associated with efficient oculomotor preparation as measured by a fast-saccadic response. The first was that correlated variability among pairs of neurons decreased immediately after target onset, and that decrease was related to the generation of fast reaction times. This effect was present for saccade in both preferred and anti-preferred directions, was particularly noticeable in pairs of visual neurons because of their higher overall levels of correlation. The second was that, as the end of the delay period approached, a robust spiking response was generated among motor neurons in FEF. Together, these findings point to distinct features in the visual and motor population activity in FEF that lead to the generation of eye movements.

2.6.1 Correlated variability in FEF and other visual areas

Despite being established in many other visual areas (Cohen & Maunsell 2009, Kohn & Smith 2005, Ruff & Cohen 2014a, Smith & Kohn 2008, Smith & Sommer 2013), the structure of correlated variability with respect to basic functional properties has been less investigated in movement-related areas such as FEF and motor cortex (with the exception of (Astrand et al 2016, Cohen et al 2010, Dehaqani et al 2018, Lee et al 1998, Zirnsak et al 2014)). We observed that r_{sc} decreased with interneuronal distance and increased with tuning similarity, traits that match previous findings in visual cortex (Cohen & Maunsell 2009, Kohn & Smith 2005, Leavitt

et al 2013, Ruff & Cohen 2014a, Smith & Kohn 2008, Smith & Sommer 2013, Snyder et al 2018). This is consistent with a conserved structure of correlated variability across multiple cortical regions in the visual hierarchy. It is possible that this conserved computational feature is driven by the similarly conserved anatomical structures across cortex, such as the laminar (Anderson et al 2011, Barbas & Pandya 1989, Felleman & Van Essen 1991) and local structure (Kritzer & Goldman-Rakic 1995, Stanton et al 1989).

We further examined r_{sc} as a function of visuomotor response properties. Motor-motor pairs had lower r_{sc} compared to visual-visual pairs, in agreement with some previous results that demonstrated very low r_{sc} values in motor cortex compared to visual areas (for a review see (Cohen & Kohn 2011)). In a system in which the initiation of movement was in part driven by a large response in a subset of "motor" neurons, the presence of high correlated variability in the trial-to-trial response of that population would be particularly influential in driving trial-to-trial behavioral variability. In the extreme, large correlations among such movement-generating neurons could effectively amplify noisy fluctuations in a few neurons, leading to errant movements. Visual populations, on the other hand, may have higher correlated variability due to fluctuations of internal states (such as attention and motivation) which affect neuronal responses. This comparison hints at potential fundamental differences in the neural code for sensory signals and motor control – the contrast in correlated variability between visual and motor populations may reflect a sort of insulation of the motor signal against fluctuating cognitive signals. Ultimately, the difference in correlated variability between pairs of neurons based on visual-motor response properties adds to the evidence that these subpopulations are separate and play distinct roles in eye movement generation (Gregoriou et al 2012, Sato & Schall 2003, Thompson et al 2005).

2.6.2 Role of variability in planning eye movements across space

FEF neurons encode both visual stimuli and eye movements across the entire visual field. Compared to baseline measures we found that a decrease in both correlated variability of pairs of neurons and in the variability of individual neurons was associated with movement preparation. It occurred rapidly after target onset and was maintained throughout the delay period. This is reminiscent of the decrease in correlated variability in visual neurons that occurs after visual stimulus onset (Smith & Kohn 2008, Smith & Sommer 2013, Snyder et al 2014), as well as the broad finding across cortex of a reduction in variability after stimulus onset (Churchland et al 2010). In FEF, the Fano factor decrease after visual stimulation has been shown to be broadly tuned, occurring for targets inside and outside the response field (Chang et al 2012). In agreement with our time course findings, r_{sc} in FEF drops and remains low after a cue during an attention task (Astrand et al 2016). Similarly, in an attention task in V4, shifts in correlated variability coincide with the time of likely target presentations (Snyder et al 2016). Comparing correlated variability across saccade directions, our result that correlated variability was lowest in the preferred direction differed somewhat from a previous study (Cohen et al 2010). This may be due to their focus on faster time scale interactions using a different (but related) statistical approach, as well as a different experimental paradigm (visual search in their study). Overall, our observation of a link between r_{sc} and the reaction time reinforces the importance of this population-level variability structure in the control of eye movements.

2.6.3 Rapid and efficient coding for eye movements

In oculomotor areas such as FEF, saccade initiation is often linked to increases in activity of oculomotor neurons whose movement fields correspond to the desired saccade. Linear accumulator models have been used to describe how neuronal activity in FEF relates to movement preparation and execution, with initial evidence supporting the presence of a fixed threshold (Hanes & Schall 1996). Recent studies in FEF have modified the accumulator model in a speed-accuracy context (Heitz & Schall 2012) and indicated the mapping between model parameters and neural processes is less clear than initially thought (Heitz & Schall 2013). Reinforcing this idea are studies from FEF showing the baseline rate can contribute to movement initiation timing (Hauser et al 2018) and the role of SC in movement generation incorporates both a preparatory build up to movement and a release from fixation (Dorris et al 1997). In both FEF and SC the movement threshold itself may be variable over time (Jantz et al 2013). Finally, low frequency SC preparatory activity can trigger a movement if inhibitory networks downstream are removed (Jagadisan & Gandhi 2017). All of these studies consider the role of single neurons and the population average in initiating movement, but a further possibility is that movement generation signals involve a weighted population readout that makes use of higher dimensions of neural activity. In FEF, the synergistic activity of ensembles of neurons can represent regions of visual space that are poorly encoded by single neurons (Dehaqani et al 2018). Results in primary motor cortex (M1) have shown that the higher-dimensional activity in preparatory and motor periods are orthogonal but linked (Elsayed et al 2016, Kaufman et al 2014). Our study adds further support for the importance of rich population-level signals for movement control.

Our results extend the existing literature in two key ways. First, we found that a decrease in correlated variability, most strongly among visual neurons, was a key signature of movement preparation. Second, while we found that the generation of an eye movement was influenced by the firing rate of neurons that preferred that movement direction, the correlated variability of the entire population of FEF neurons plays a critical role. That is, to prepare a short-latency rightward eye movement, it is important that (1) rightward-preferring FEF neurons have low correlated variability; (2) rightward-preferring FEF motor neurons fire vigorously prior to the saccade execution; and (3) leftward-preferring FEF neurons have low correlated variability. One way to think about this is that while a group of neurons plans the eye movement, all the others must also be sure to avoid contaminating the planning signal.

An important future direction will be to better link changes in the activity of FEF populations to the signals in their downstream targets in the SC, and in turn to eye movement initiation. While the firing rates of individually recorded neurons clearly can explain some of the variance in behavior given the correlations with reaction time, our study points to the importance of population-level activity structure in generating eye movements. One open question is whether similar approaches are employed to separate movement preparation from execution in the oculomotor and skeletomotor systems. While simultaneous population recordings have been relatively less common in eye movement-related structures because of their relative inaccessibility, new recording approaches can reveal the way populations of neurons give rise to fast and accurate eye movements.

3.0 VISUAL AND MOTOR CODES IN PREFRONTAL CORTEX

3.1 ABSTRACT

Working memory is one of the processes that forms the foundation of higher cognitive actions. The act of storing a visual stimulus in memory and later translating it into an eye movement plan has frequently been used to probe working memory. The neural correlates of the working memory have been studied for many years, however with the recent emergence of new models backed by neurophysiological recordings, no clear consensus has been reached. Dorsolateral prefrontal cortex (dlPFC) has been the subject of many investigations into working memory, due to the presence of heightened activity during the memory period of a task, and its involvement in higher cognitive processes such as reward and rule encoding. Most previous studies examined the neural correlates of working memory in one of two extremes: 1) single neuron recordings where neurons were selected based on certain response properties or 2) population level analyses which can discard the subtleties of single neuron responses. The goal of the current study was to bridge these findings by analyzing PFC single neuron responses in detail, and then consider how these responses might affect the population code. We did this by recording from populations of PFC neurons in macaque monkeys while they performed a memory guided saccade task. We found PFC neurons demonstrated a rich set of activity profiles, both spatially and temporally, that contributed to a dynamic population code when transitioning from processing a visual

stimulus to planning an eye movement. We compared activity in PFC to activity in the frontal eye fields (FEF), another area involved in visual processing and the generation of eye movements, highlighting differences that suggest the areas may play different roles in working memory. Due to the richness in responses and differences from FEF, we conclude activity in PFC contains unique properties that are important to consider when developing future models of working memory.

3.2 INTRODUCTION

Working memory, the act of maintaining information available for processing even when it is absent from the external environment, is an integral process for generating complex behaviors. During active vision, to maintain these memory signals requires a flexible neural structure, as the information to be stored in memory can originate at a wide range of spatial and temporal scales. Lesions in the area around the principal sulcus, part of prefrontal cortex (PFC), are known to cause deficits in working memory (Butters & Pandya 1969) and numerous neurophysiological investigations have identified signals related to working memory in the activity of single neurons (Curtis & D'Esposito 2003, Funahashi 2015, Goldman-Rakic 1995, Riley & Constantinidis 2015). Nonetheless, the exact nature of these mechanisms governing working memory has been hotly debated in recent years.

Some of the first evidence of a working memory signal in PFC, observed in a wide variety of experimental tasks, was persistent firing rate activity during the memory period. This activity, maintained at a relatively constant level even when the stimulus is no longer visible, has been shown in both neurophysiology (Batuev 1994, Chafee & Goldman-Rakic 1998, Funahashi

et al 1989, Fuster & Alexander 1971, Kubota & Niki 1971, Rainer et al 1998, Sawaguchi & Yamane 1999) and modeling (Compte et al 2000, Lim & Goldman 2013, Wimmer et al 2014) studies to effectively encode the identity of a stimulus held in working memory. While this persistent delay activity may form an effective code, the presence of a wide variety of other response properties in PFC leaves open the question as to the true nature of how the memory signal is stored.

Individual PFC neurons can have receptive fields located in either hemifield of space (Funahashi et al 1990, Mikami et al 1982, Suzuki & Azuma 1983), and can exhibit both excitatory and suppressive tuning (Bullock et al 2017). Temporally, during a fixed delay working memory task, individual PFC neurons show rich dynamics, with neurons ramping up and down activity during the delay period (Watanabe & Funahashi 2007) and delay activity varying systematically with time (Brody et al 2003, Romo et al 1999). Thus, in addition to neurons with persistent activity across a delay period, it is clear there are PFC subpopulations with much more complex response dynamics.

Given the wide variety of PFC single neuron responses, it is not surprising that population representations of a remembered stimulus vary across the delay epoch (Barak et al 2010, Rainer & Miller 2002). During the delay period, average population activity can be near baseline yet still maintain the ability to discriminate different (Stokes et al 2013). These changing population patterns, in which different weightings of the neurons are required to read out the memory at different time periods of the delay, have led some to conclude that the code for working memory is tied to these dynamics at the population level, and not the persistent activity of single neurons (Spaak et al 2017). Another dynamic coding model posits that apparent persistent activity could result from trial-averaging sparse, coordinated spiking, and that gamma

oscillations in local populations may instead represent the stored working memory signal (Lundqvist et al 2016), or that other "synaptically silent" mechanisms may be in use (Stokes 2015, Wolff et al 2017).

These two models of PFC's role in working memory, based on either persistent delay activity or a dynamic population code, would seem to be strongly at odds. However, the presence of dynamics and mixed selectivity across the population might not rule out a simple readout if those dynamics can be characterized by simple rules. A recent study demonstrated despite observing heterogenous and temporally shifting single neuron activity, a stable representation of the working memory signal was present at the population level (Murray et al 2017). Given the wide variety of signals encoded in PFC, such as reward (Leon & Shadlen 1999, Watanabe 1996), abstract rules (Wallis et al 2001), time during the delay (Jun et al 2010, Spaak et al 2017), previous trial outcome (Donahue & Lee 2015), and stimulus shape and color (Riley et al 2017), one of the reasons for the dynamic nature of PFC neurons might be the multiplexing of these signals with the visual and saccade codes needed to perform the memory guided saccade task. We set out to systematically characterize the receptive field structure and dynamics of PFC neurons, particularly focusing on the juxtaposition of visual and saccade activity, a known source of changes in response that could be rigorously characterized. Specifically, we hypothesized the dynamic population code is caused in part by the presence of PFC neurons whose receptive fields change between visual and saccade epochs.

We recorded from groups PFC neurons using a multielectrode array while the monkey performed a spatial working memory task. We first characterized the receptive field structure of PFC neurons in visual and saccade epochs. We found a remarkable amount of diversity, both spatially and temporally, in the response field structure of PFC neurons. However, a key pattern

in this diversity was spatial and temporal opponency – many neurons were suppressed at spatial locations opposite their preferred response field to varying spatial extent, and these preferences shifted relative to the saccade, sometimes to the opposite hemifield. Finally, we compared the response field structure observed in PFC and the ability to decode working memory signals at the population level to that of the frontal eye fields (FEF). We found that the diverse response properties observed in PFC are less prominent in FEF, and that the population code in PFC is more dynamic. Taken together, the rich single neuron response field structure, most prominently found in PFC, provides a flexible and dynamic population code where visual and motor signals may be encoded separately for the purpose of storing spatial working memories.

3.3 METHODS

3.3.1 Neuronal recordings

Surgical preparation

A 96-electrode "Utah" Array (Blackrock Microsystems, Salt Lake City, UT) was implanted into two adult, male rhesus macaques (*Macaca mulatta*) in dorsolateral prefrontal cortex (dlPFC) using sterile surgical techniques under isoflurane anesthesia. The array was implanted in right dlPFC for *Monkey Pe* and left dlPFC for *Monkey Wa* (Figure 13A). For FEF recordings, two adult male rhesus macaques (*Macca mulatta*; *Monkeys Ro and Wi*) were surgically implanted with FEF recording chambers (centered at stereotaxic coordinates: 25 anterior, 20 lateral). For FEF recordings, extracellular activity was recorded with a 16-electrode linear microelectrode array (U-Probe, Plexon, Dallas TX) with contacts spaced 150 μm apart. Electrodes were lowered

into FEF daily using a custom designed mechanical Microdrive (Laboratory for Sensorimotor Research, Bethesda, MD) through a plastic grid with 1mm spacing. The location of FEF was first identified by physiological response properties to visual stimuli and saccades, and then confirmed through microstimulation. Recording sites were considered to be in FEF if saccades could be reliably (>50%) evoked using low threshold microstimulation (≤ 50 μA, 0.25 ms pulse duration, 70 ms pulse train duration, 350 Hz stimulation frequency) (Bruce et al 1985) at that location or at an immediately neighboring location (1mm away). Of note, we were not able to induce eye movements by stimulating the electrodes of the PFC arrays, even with microstimulation up to currents of 150 μA. In a separate procedure before the array or chamber implants, a titanium headpost was attached to the skull with titanium screws to immobilize the head during experiments. All procedures were approved by the Institutional Animal Care and Use Committee of the University of Pittsburgh and complied with guidelines set forth in the National Institute of Health's *Guide for the Care and Use of Laboratory Animals*.

Data collection

Stimuli were displayed on a 21" cathode ray tube monitor with a resolution of 1024x768 pixels and a refresh rate of 100 Hz at viewing distance of 36 cm. Stimuli were produced using custom software written in Matlab (MathWorks, Natick, MA) and the Psychophysics Toolbox extensions (Brainard 1997, Kleiner et al 2007, Pelli 1997). Eye position was tracked monocularly using an infrared system at 1000 Hz resolution (EyeLink 1000, SR Research, Mississauga, Canada). Extracellular activity was recorded from the array, band-pass filtered (0.3 – 7,500 Hz), digitized at 30 kHz, and amplified by a Grapevine system (Ripple, Salt Lake City, UT). On each electrode channel, waveforms that exceeded a threshold (a multiple of the root mean squared

noise for that given channel), were saved and stored for offline wave classification. Waveforms were automatically sorted using a competitive mixture decomposition algorithm (Shoham et al 2003) and later refined manually based on waveform shape characteristics and inter-spike interval distributions using custom time amplitude window discrimination software written in MATLAB (Kelly et al 2007).

After the waveforms had been manually refined, the signal-to-noise ratio (SNR) was calculated for each identified unit as the ratio of the average waveform amplitude to the standard deviation of the waveform noise (Kelly et al 2007). We considered only candidate units with an SNR above 2.5 as isolated single neurons for the purpose of further analysis. This resulted in a total of 2511 neurons across 39 recording session in PFC (*Monkey Wa*: 1179 units, 20 sessions; *Monkey Pe*: 1332 units, 19 sessions) and 889 neurons across 50 sessions in FEF (*Monkey Wi:* 305 units, 14 sessions; *Monkey Ro:* 584 units, 36 sessions).

3.3.2 Experimental design and statistical analysis

Behavioral task

Monkeys performed a standard memory guided saccade (MGS) task (Figure 13B) (Hikosaka & Wurtz 1983). The trial commenced when the subject fixated a small blue dot (0.5° diameter) at the center of the screen. For PFC recordings, after fixation was established (200 ms), a target appeared in the periphery at one of eight angular directions (0°, 45°, 90°, 135°, 180°, 225°, 270°, 315°) and one of five eccentricities (5°, 7.5°, 9.9°, 12.3°, 14.7°) (40 total possible locations, Figure 13C) for 50 ms. The animal was required to maintain fixation for 500 ms after the target was extinguished, at which point the central fixation point would disappear, signaling the animal to saccade to the remembered location of the stimulus. The monkey had 500 ms to initiate the

saccade, and once it had been initiated (defined as the monkey's eye position leaving a window 1.8° in diameter around the fixation point) the monkey's eye position had to reach the saccade target within 200 ms and maintain gaze within 2.7° of the location for 150 ms to receive a liquid reward. Each block consisted of pseudorandomized presentations of all 40 conditions, with at least 40 blocks gathered per session (average 58). For a subset of sessions (*Monkey Wa*, n = 4 sessions), the angular directions and target eccentricities were different (angles 26°, 71°, 116°, 161°, 206°, 251°, 296°, 341°; amplitudes 2.6°, 3.9°, 5.2°, 6.5°, 7.8°). This was done for a separate analysis not included in this report, thus when possible, this data is combined with the larger amplitude sessions. For FEF recordings, the same behavioral task (MGS) was used, with stimuli appearing at one of eight angular directions (0°, 45°, 90°, 135°, 180°, 225°, 270°, 315°) but at only one amplitude (10°). The fixation time before target onset (200 ms) and target duration (50 ms) were equal to PFC, however the delay epoch was 600 ms (as opposed to 500ms for PFC). Each block consisted of pseudorandomized presentations of all eight conditions, with at least 50 blocks gathered per session (average 132). On a subset of days, after the fixation point was extinguished and the monkey began its saccade, the target was re-illuminated to aid in saccade completion. The analyses presented here were not affected by this target because all analysis windows were constructed to end prior to any possible visual transient to this target.

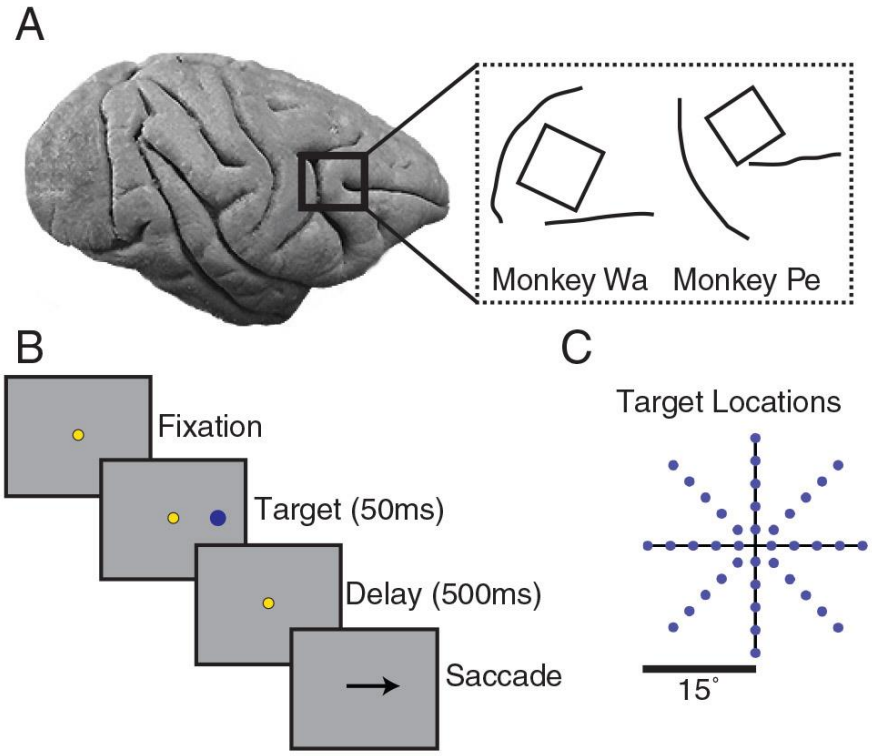

Figure 13: Electrode array locations and task.

A) 96 channel Utah arrays were placed in dorsolateral prefrontal cortex (dlPFC), anterior to the arcuate sulcus and medial to the principal sulcus. The line drawings shown indicate visible sulcal patterns through the durotomy and are not meant to represent the full extent of the arcuate and principal sulci. B) Memory guided saccade task. Each trial began with the subject fixating on a central dot. After 200 ms of fixation, a target appeared in the periphery for 50 ms. Following a delay of 500 ms, the fixation point was extinguished, signaling the subject to saccade to the remembered location of the target. C) Targets could appear at 1 of 40 locations, varying in amplitude and direction.

Neuron selection

All neural firing rates were measured during stimulus presentation, the memory epoch, and the perisaccadic epoch. To determine the ideal response epoch, we used a method described in Smith et al (2005). For our analysis, the variance across the 40 conditions was calculated for each neuron in a sliding window of 50 ms. For a neuron tuned to the spatial location of the visual stimulus or the saccade, the variance is largest when the window is aligned to the latency of the neuron (when it exhibits that tuning in the form of spatially variable responses). We measured the latency of the visual response from 0 ms to 400 ms after stimulus onset in 50ms bins, where the time epoch was determined by visually examining the PSTHs of individual neurons to ensure accurate estimation of the response latency. Similarly, the saccade response was measured 100 ms before to 50 ms after the saccade in 50 ms bins. Once the optimal window had been identified, we determined whether the neuron had significant ($p < .01$) spatial tuning in that response window using a Kruskal-Wallis one-way analysis of variance on the average firing rates with location as the factor.

Response field calculation

The center of each neuron's response field during the visual and saccade epoch was calculated as follows. For each stimulus location, activity during the time epoch desired (visual, saccade, or across the delay as in Figure 18) was subtracted by baseline activity taken 30 ms to 180 ms after fixation was established (170 ms to 20 ms before stimulus onset). Each neuron had a single value estimated for its baseline activity across all trials and all conditions (since they were the same prior to stimulus onset). The resulting baseline subtracted activity was averaged across the trial repeats for each condition, and then linearly interpolated to obtain a map with a resolution of .25°

x .25°. This map was smoothed using a gaussian filter with a standard deviation of 1°. The center of the response field was defined as the center of mass for all locations with responses greater or equal than 75% of the maximum for a given response field map. Only responses above baseline (as opposed to responses suppressed below baseline) were considered for the center of mass calculation. Note that all response field heatmaps are displayed such that contralateral hemifield corresponds to the left hemifield. This only affected *monkey Wa* where recordings were made from an array implanted in left dlPFC, whereas in *monkey Pe*, recordings were made from the right hemisphere.

Visual-motor index calculation

To understand how neurons in each population responded to the visual stimulus relative to the saccade, a visuomotor index (VMI) was calculated using the formula below (Bruce & Goldberg 1985, Lawrence et al 2005, Sato & Schall 2003, Sommer & Wurtz 2000) :

$$VMI = \frac{V - M}{V + M} \qquad (3-1)$$

Where V is the response in the ideal visual window and M is the response in the ideal saccade window (see *Methods)*, with no baseline subtraction. A neuron with VMI of 1 fires exclusively for the visual stimulus, -1 exclusively for the saccade, and 0 fires equally for the visual stimulus and saccade.

For FEF, VMI was calculated individually for the 8 conditions and then averaged over condition to produce 1 VMI value per neuron. For PFC, a subset of conditions (1 amplitude, 8 directions, 8 of the 40 conditions) which most closely approximated the amplitude and direction of the FEF stimuli were selected for ease of comparison between the two areas.

Cross-temporal decoding analysis

A Poisson Naïve Bayesian decoder was implemented to determine the working memory signal readout of PFC and FEF populations. For both regions, a pseudo-population was created by combining neurons across recording sessions. For each neuron, trial repeats were randomly shuffled for each condition to remove any trial to trial correlations between neurons recorded in the same session. Any recording session with less than 40 repeats of each condition (1 session FEF, 4 sessions PFC), and any neurons that did not have an SNR greater than 2.5 or fire at least 1 spike per second during the delay period of at least one condition were omitted (93 FEF neurons, 561 PFC neurons). The instantaneous firing rate of each neuron (100 ms windows with 50 ms of overlap) was used to build a decoder to predict the eight saccade directions in FEF, and the eight saccade directions closest in amplitude to the FEF saccade directions for PFC (8 of the 40 conditions). The training data set contained 80% of the trials, creating a Poisson distribution model for each direction (θ) using the average spike count for each unit (n_{spike}) in the time epoch specified. The remaining 20% of trials were used for testing, at time windows beginning at fixation and ending after the saccade. For a given test trial, the direction with the maximum prediction probability, $P(\theta| n_{spike})$, was defined as the predicted saccade direction. $P(n_{spike}| \theta)$, was calculated using the Poisson distribution model that resulted from the training data. 5-fold cross validation was used, with the average decoding accuracy computed across folds.

$$P(\theta|n_{spike}) = \frac{P(n_{spike}|\theta) * P(\theta)}{P(n_{spike})} \quad (3-2)$$

Comparison of decoding between PFC and FEF

To compare overall decoding accuracy between FEF and PFC, we randomly selected PFC neurons from the total population (1722 neurons) until the number of neurons was equal to that in FEF (770 neurons). When comparing decoding accuracy as a function of other properties (number of neurons, directional selectivity, and reliability) one training and testing time point was used, corresponding to the time bin with the highest accuracy during the delay period (FEF: 50 ms to 150 ms after stimulus offset, PFC: 100 ms to 200 ms after stimulus offset).

Decoding accuracy and reliability

The reliability of a neuron was calculated as the Pearson correlation coefficient of the mean spike count in the bin with the highest decoding accuracy (see *Methods, Comparison of decoding between PFC and FEF*) for even and odd trials of the same condition. A reliability of 1 corresponds to identical tuning curves when calculated for even and odd trials. Each neuron in the pseudo-population was then sorted according to their reliability. Subpopulations of 100 neurons were used to decode eye movement direction, starting with the 100 neurons with the highest reliability, then the next 100 ranked neurons in non-overlapping bins until the remaining population did not have 100 neurons. For the FEF population, this would result in 6 bins (ranked neurons 1-100, 101-200, 201-300, 301-400, 401-500, and 501-600, and 601-700). For the PFC population, each bin contained 100 neurons as well, however the number of bins was more given the larger number of PFC neurons recorded.

Decoding accuracy and tuning selectivity

The selectivity of each PFC and FEF neuron was computed during the time window of maximum decoding accuracy (see *Methods, Comparison of decoding between PFC and FEF*) using a vector average previously used for calculating orientation selectivity (Smith et al 2002). To measure the selectivity of each neuron's tuning curve, we calculated the complex summed response vector (where $i = \sqrt{-1}$).

$$v = \sum_{n=1}^{N} R_n e^{(i2\theta_n)} \qquad (3-3)$$

R_n is the response magnitude during the delay period, θ_n is the stimulus location, and n is an index from 1 to the number of points, 8, in the tuning curve. This was then normalized by the summed magnitude of all the response vectors:

$$selectivity = \frac{|v|}{\sum_{n=1}^{N} R_n |R_n|} \qquad (3-4)$$

A selectivity of 0 corresponded to a neuron that fires for all conditions equally while a value of 1 is a neuron that responds exclusively to one condition. Decoding was grouped into bins as in the reliability analysis (see *Methods, decoding accuracy and tuning selectivity*) but each neuron was sorted based on the directional selectivity.

3.4 RESULTS

We recorded from 2511 PFC neurons across 39 sessions and 889 FEF neurons across 50 sessions (see *Methods*) in four macaque monkeys while the animals performed a memory guided saccade task (Figure 13B). The focus of our analysis was on understanding how visual and motor signals are represented during spatial working memory in PFC, and what similarities and differences exist with FEF.

3.4.1 Spatial constancy in PFC single neurons

To understand how visual and motor signals are processed at the population level in PFC, we first wanted to ensure robust responses were observed at the single neuron level. Previous studies examined visual (Funahashi et al 1989) and motor (Funahashi et al 1991) responses in PFC during an oculomotor task, reporting a wide variety of response properties including significant tuning for the visual, delay, and/or saccade epochs, ipsilateral and contralateral tuning, and suppression in delay period activity (appearing opposite the preferred stimulus location). Having visual stimuli and saccades of numerous amplitudes and directions allowed us to create detailed response fields in the visual and saccade epochs for all neurons recorded. Figure 14 demonstrates two example neurons with large responses during the visual and saccade epochs. Of note, each neuron has a spatially defined area of high firing rate that did not change between visual and saccade epoch, that could be contralaterally tuned (Figure 14A) or ipsilaterally tuned (Figure 14B). Additionally, both neurons exhibited varying levels of suppression below baseline (more strongly in Figure 14B), coinciding with the stimulus and saccade onset. This suppression also tended to appear in the hemifield opposite the neuron's response field.

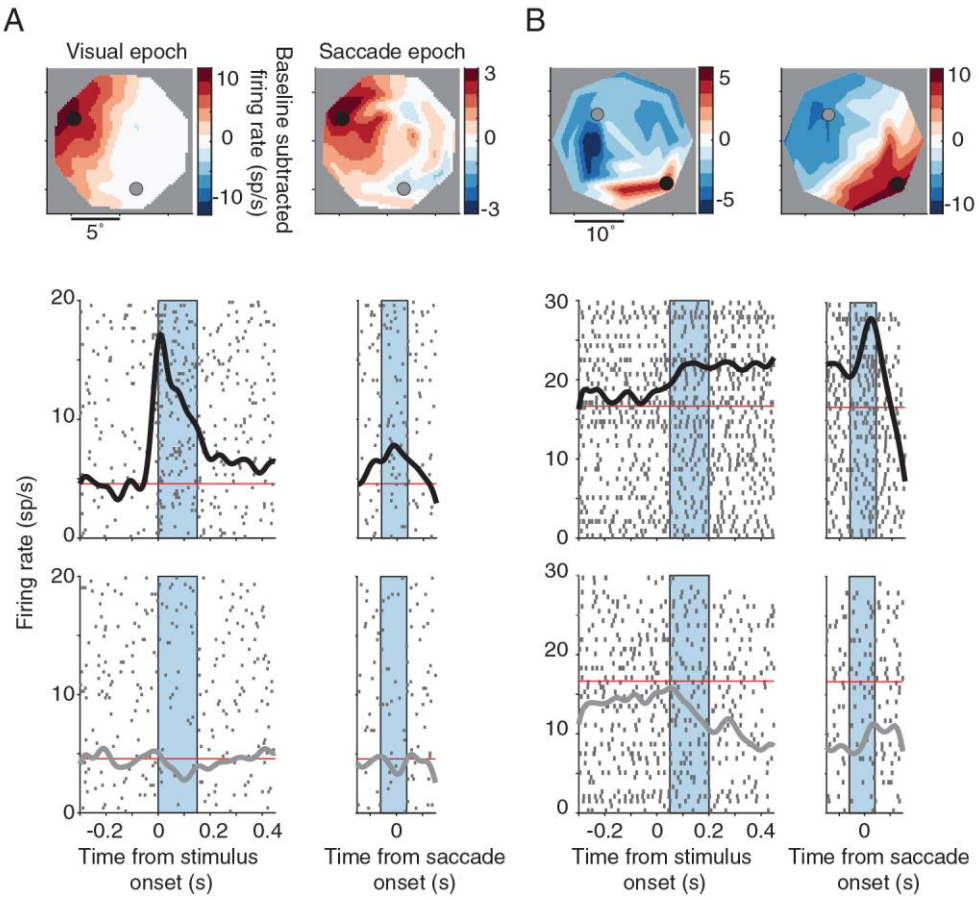

Figure 14: Spatial constancy in PFC neurons.

A) Top: Response field heatmap for an example neuron during the visual and saccade epoch. Firing rate was baseline subtracted (170 ms to 20 ms before stimulus onset) such that red colors represent activity above baseline, blue colors suppression below baseline, and white near baseline. Middle: PSTHs aligned to stimulus onset and saccade onset for a condition close to the center of the response field. Bottom: PSTHs aligned to stimulus onset and saccade onset for a condition in the opposite hemifield of the center of the response field. This neuron showed a robust visual and saccadic response that is localized to the contralateral hemifield and is spatially congruent between the visual and saccade epoch. B) An example neuron with a robust and spatially congruent visual and saccadic response localized to the lower portion of the ipsilateral hemifield. Spatial locations opposite the center of the response field were suppressed below baseline. Note: heatmaps were flipped when necessary such that the left hemifield always represented the contralateral hemifield. Example A is from *monkey Wa* and example B is from *monkey Pe*.

3.4.2 Response latency in PFC and FEF

Having confirmed the PFC neurons being recorded had distinct and spatially localized response fields in both visual and saccade epochs, we next wanted to identify the ideal time window to accurately capture the visual and saccadic responses. Previous studies have demonstrated PFC visual responses can have a variety of time courses (Mikami et al 1982, Suzuki & Azuma 1983): transient bursts after stimulus onset, sustained activation throughout the entire delay period, a transient superimposed on sustained activation, and transient or sustained suppression. We first examined the population PSTH aligned to the visual stimulus or saccade, to get a general idea of the time course of PFC activity. The PFC population showed a small visual transient with a longer sustained period of activity during the delay period and rising perisaccadic activity that peaked after saccade onset (Figure 15A). This contrasted with the FEF population PSTH, which had a larger, earlier onset, and more phasic visual transient, as well as perisaccadic activity that peaked closer to saccade onset (Figure 15B). To determine the latency and window of analysis (visual or saccade epoch) for each neuron, the 50 ms window in the visual (or saccade) epoch that had the highest variance across the 40 conditions was selected (see *Methods*). To ensure a fair comparison between PFC and FEF latencies, the same window width and epoch times were used. Across the FEF and PFC distributions of neurons with significant visual responses ($p < .01$, Kruskal-Wallis test), the PFC distribution had a significantly longer latency (PFC mean = 189 ms, FEF mean = 154 ms; two sample t-test $p < .001$). In summary, PFC neurons had longer and more uniformly distributed latencies in the visual and saccade epochs as evidenced by both the population PSTH and individual neuron distributions.

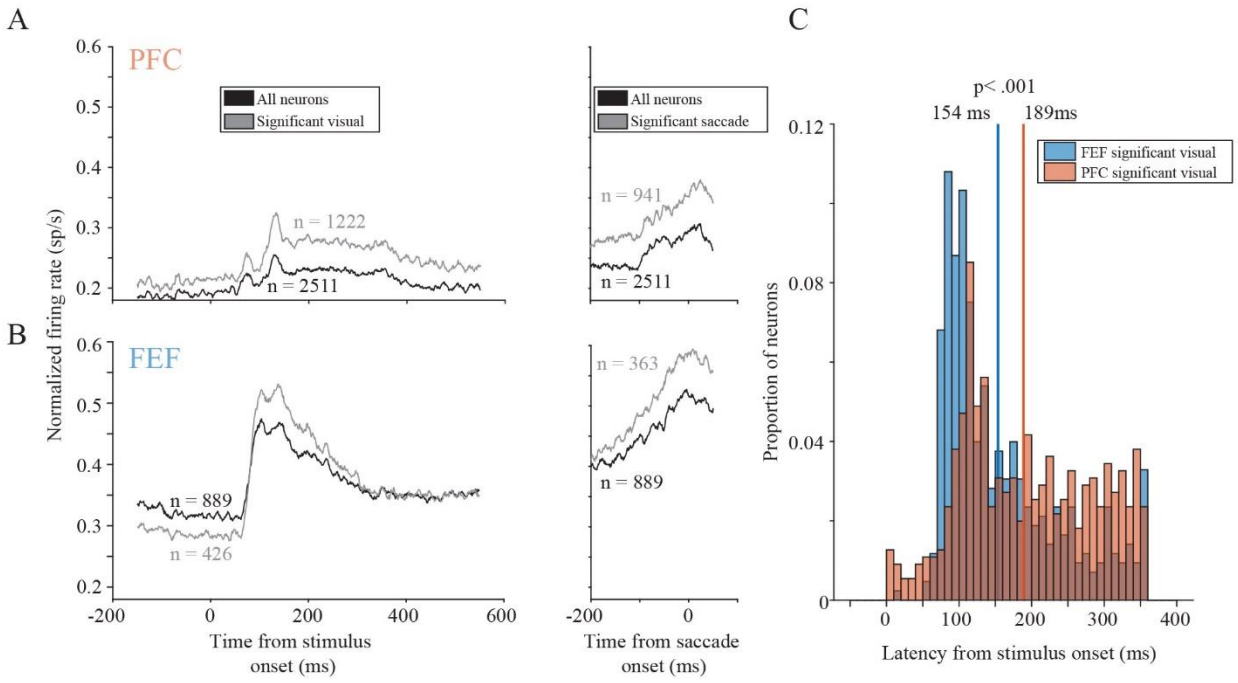

Figure 15: Latency in PFC and FEF.

A) Population PSTH for all PFC neurons (black line, n = 2511 neurons) and significantly tuned PFC neurons (grey line; $p < .001$ Kruskal Wallis test) in the visual (left) or saccade (right) epoch. Significant visual neurons (n = 1222 neurons) passed the significance test in the visual epoch while significant saccade neurons (n = 941 neurons) passed the test in the saccade epoch. Each neuron's PSTH was normalized by the maximum firing rate in either the visual/delay epoch (0 ms to 550 ms after stimulus onset) or the saccade epoch (-200 ms to 50 ms before saccade onset). B) Same convention as in A, but with all FEF neurons (black line; n = 889 neurons) and significantly tuned neurons (grey line) in the visual (n = 426 neurons) or saccade (n = 363 neurons) epoch. The PFC population PSTH had less modulation with respect to baseline and a longer latency compared to FEF in the visual and saccade epochs. C) Distribution of single neuron latencies for FEF (blue) and PFC (orange) during the visual epoch. Only neurons with significant visual responses were included (PFC = 1222 neurons; FEF = 426 neurons). The PFC distribution had a significantly longer visual latency compared to FEF ($p < .001$; two sample t-test).

3.4.3 Hemifield tuning differences in PFC

Having identified the appropriate windows for the visual and saccade epochs for each neuron, we returned to more closely examining the response properties of PFC single neurons, specifically differences between contralateral and ipsilateral tuned neurons. PFC has been previously reported to contain neurons tuned to stimuli in the ipsilateral visual field (Funahashi et al 1989, Funahashi et al 1991), unlike earlier visual areas (Gattass et al 1981, Gattass et al 1988). We hypothesized ipsilateral tuned neurons would have a longer visual latency compared to contralateral tuned neurons, given that at some point during the visual processing stream the information must be supplied by the opposite hemisphere. Leveraging the large number of visual and saccadic neurons we recorded, we examined differences in latencies and suppression, between contralaterally and ipsilaterally tuned neurons during the visual and saccade epoch.

To examine the degree of suppression in ipsilateral and contralateral tuned neurons, we first wanted to combine all neurons in each group into a population measure. For each group (ipsilateral and contralateral), we rotated the response field heatmap of each neuron such that its center of mass was on the horizontal meridian. Ipsilateral and contralateral tuned neurons were then combined separately to form a population response field heatmap for the visual epoch and then the saccade epoch. For the visual epoch, in agreement with previous findings (Bullock et al 2017), the ipsilateral population showed more suppression in the opposite hemifield than the contralateral population (Figure 16A). During the saccade epoch, however, both populations qualitatively looked the same in that suppression appeared in both (Figure 16B).

We then investigated the contralaterally and ipsilaterally tuned population PSTHs aligned to stimulus and saccade onset. For the visual epoch, the ipsilateral tuned population had a later and weaker visual transient, coupled with a stronger sustained level of activity in the delay period after the visual transient (Figure 16C). During the saccade epoch this trend was flipped, as the ipsilateral population began at a lower level of activity and increased more sharply perisaccadically. Comparing the visual latency distributions, ipsilateral neurons had significantly longer visual latencies ($p < .001$, two sample t-test) and had a more uniform distribution of latencies compared to the contralateral distribution, which had a clear peak around 120 ms (Figure 16D).

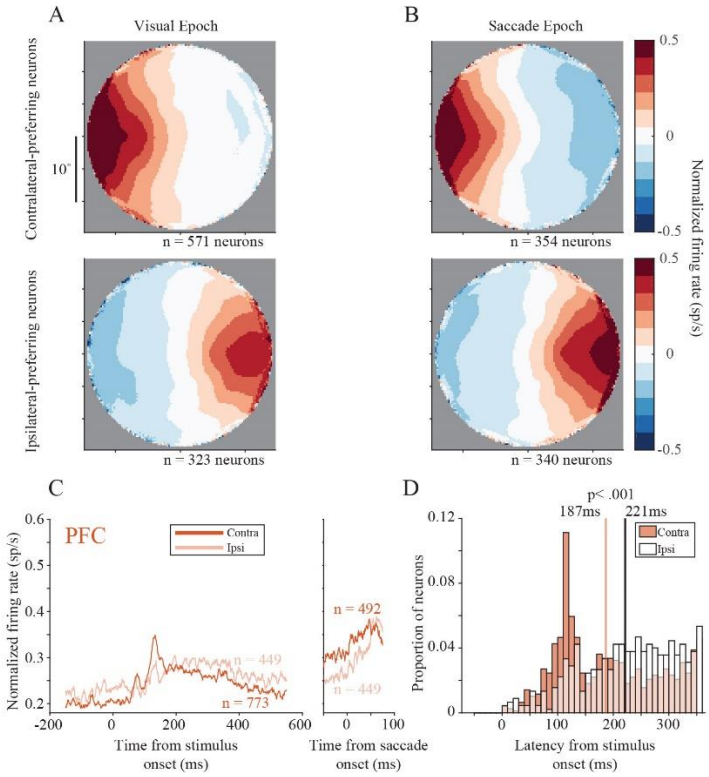

Figure 16: Hemifield tuning differences in PFC.

A) Population response field heatmaps for contralateral (top) and ipsilateral (bottom) tuned neurons during the visual epoch. Each neuron's response field heatmap was normalized by the maximum response in the heatmap and rotated to the horizontal meridian. All normalized and rotated heatmaps were then averaged across neurons to yield the population heatmap. During visual epoch, the ipsilateral population showed a stronger suppression in the opposite hemifield of the center of the response field when compared to the contralateral population. B) same convention as in A but for the saccade epoch. The ipsilateral and contralateral populations had similar suppression during the saccade epoch. Population PSTHs for contralateral (dark orange) and ipsilateral (light orange) neurons aligned to stimulus onset or saccade onset. During the visual epoch, the ipsilateral population PSTH had less modulation relative to baseline and a later latency than the contralateral population. During the saccade epoch, the ipsilateral population PSTH had more modulation relative to baseline but still had a later latency. D) Distribution of latencies for contralateral (filled) and ipsilateral (open) neurons during the visual epoch. Only neurons with significant visual responses were included (contralateral = 773 neurons; ipsilateral = 449 neurons). The ipsilateral distribution had a significantly longer visual latency compared to the contralateral distribution ($p < .001$; two sample t-test).

3.4.4 Dynamic selectivity in PFC

So far, we have demonstrated PFC neurons show a wide variety of spatial tuning and latencies across the visual and saccade epochs. Given this variety, we sought to understand how these visual and motor signals coexist within PFC. One particularly intriguing aspect of dynamic selectivity in PFC at the single neuron level is the spatial shifting of the response field during the delay period of a working memory task, often referred to as mixed selectivity (Parthasarathy et al 2017, Spaak et al 2017). However, these studies employed a limited set of conditions, displaying stimuli at only one eccentricity. Our experimental paradigm, on the other hand, tiled a substantially larger portion of visual space, resulting in a more accurate estimate of each neurons visual and saccadic response field. With a more accurate representation, we set out to confirm the presence of dynamic selectivity in PFC neurons and understand how this selectivity evolved over the time period between the visual stimulus and the saccade.

Mixed selectivity existed in a subset of PFC neurons, and comparing single neuron examples illuminated subtle differences in how individual neurons changed their tuning. For some neurons, the selectivity changes between the visual and saccade epoch shifted the center of the response field to the opposite hemifield, resulting in a 90-degree rotation (Figure 17A). For other neurons, the response field during the visual epoch broadened during the saccade epoch, such that stimuli that were suppressed during the visual epoch became regions of peak activity during the saccade epoch (Figure 17B). Finally, some neurons shifted the center of their response field 180-degrees, where the area of maximum activity during the visual epoch was suppressed below baseline during the saccade epoch (Figure 17C). These results provide clear examples of single neurons shifting their tuning preferences between the visual and saccade epochs and highlight the diversity of spatial shifts observed across individual neurons.

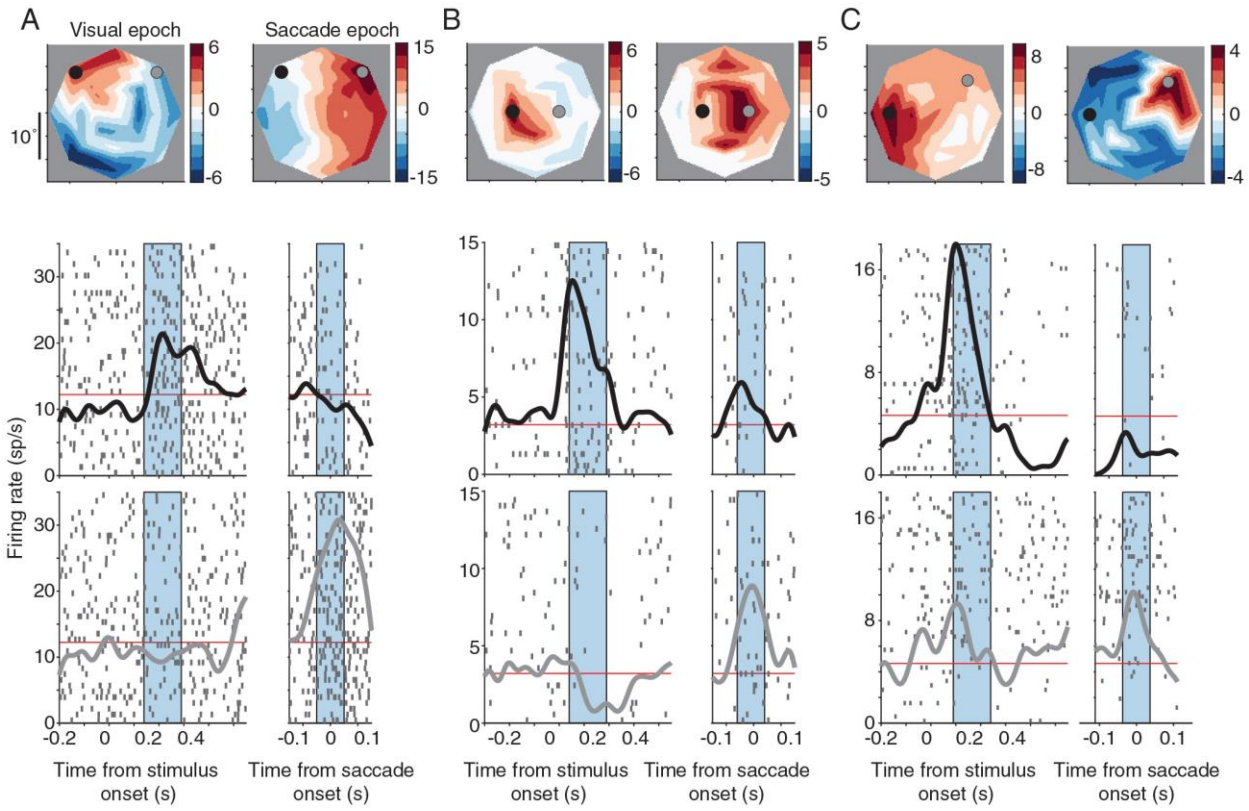

Figure 17: Dynamic selectivity in single neurons.

A) Top: response field heatmap of the baseline subtracted firing rate for an example neuron. Bottom: Average PSTH for a condition close to the center of the visual response field (black) and close to the center of the saccade response field (grey). This example neuron was contralaterally tuned during the visual epoch but rotated its response field 90-degrees to the ipsilateral hemifield during the saccade epoch. B) Example neuron with contralateral tuning during the visual epoch, with the ipsilateral hemifield suppressed. During the saccade epoch, the response field broadens such that the neuron fires above baseline for the condition that was previously suppressed. C) Example neuron with a robust visual response in the contralateral hemifield that is suppressed during the saccade epoch. The response field shifts nearly 180-degrees between the visual and saccade epochs. Note: examples A and B are from *monkey Pe*, example C from *monkey Wa*.

The previous examples of mixed selectivity compared the tuning of individual neurons in specific windows during the visual and saccade epochs. If the visual stimulus and saccade signals are indeed separately coded in PFC, and the switch from a visual to a saccadic code accounts for much of the diversity seen in PFC neuronal response, we hypothesized the maximum difference in the response field of the visual and saccade epochs should occur between the peak of the visual response and the onset of the saccade. To answer this, we calculated the center of the response field in 50 ms windows throughout the entire trial (fixation onset to saccade onset). To understand how the center of the response field shifted over the course of the trial, we subtracted the center of the response field in the ideal visual epoch window (see *Methods*) from the center of the response field calculated throughout the trial. If a neuron maintained the spatial location of its visual response field throughout the entire trial, subtracting by the preferred location would yield an angular difference of 0 throughout the trial. Conversely, if a neuron shifted its tuning during the saccade epoch, we would predict the angular difference to be low in the visual epoch (as it is close to the ideal visual time window) but increase as the time window approached the saccade. The same process was repeated for the ideal saccade window, where the center of the response field throughout the trial was subtracted by the ideal saccade window. The angular difference between the center of the response field throughout the trial and the ideal visual or saccade window was calculated for each neuron and then averaged across neurons to yield a population response. Across the PFC population, the maximum angular difference between the center of mass at a given time in the trial and the ideal visual window corresponded to saccade onset, while the minimum angular difference was observed around the mean visual latency of the population (180ms after stimulus onset) (Figure 18A, left).

Conversely, the maximum angular difference for the ideal saccade window was after stimulus onset (~200 ms), and the minimum angular difference was at saccade onset (Figure 18A, right).

However, large shifts in the center of the response field could be confounded by neurons that did not fire in the other epoch, thus creating a noisy estimate of the center of the response field. To address this, we selected PFC neurons which were tuned both to the location of the visual stimulus as well as the saccade. We found those neurons in the population which had significant tuning (Kruskal Wallis test, $p < .001$) in at least 50% of the time points following the visual stimulus (50 ms to 350 ms after stimulus onset) and preceding the saccade (-100 ms to 0 ms before saccade onset). The rationale was these neurons maintained their tuning in the visual and saccade epochs, and thus any shifts in tuning were not due to neurons that encoded one epoch but not the other. Within this subpopulation, the same angular difference trends were maintained (Figure 18B). In summary, the maximum shift in response fields occurred between the visual and saccade epochs and this shift was not confounded by neurons that were untuned in either of the epochs.

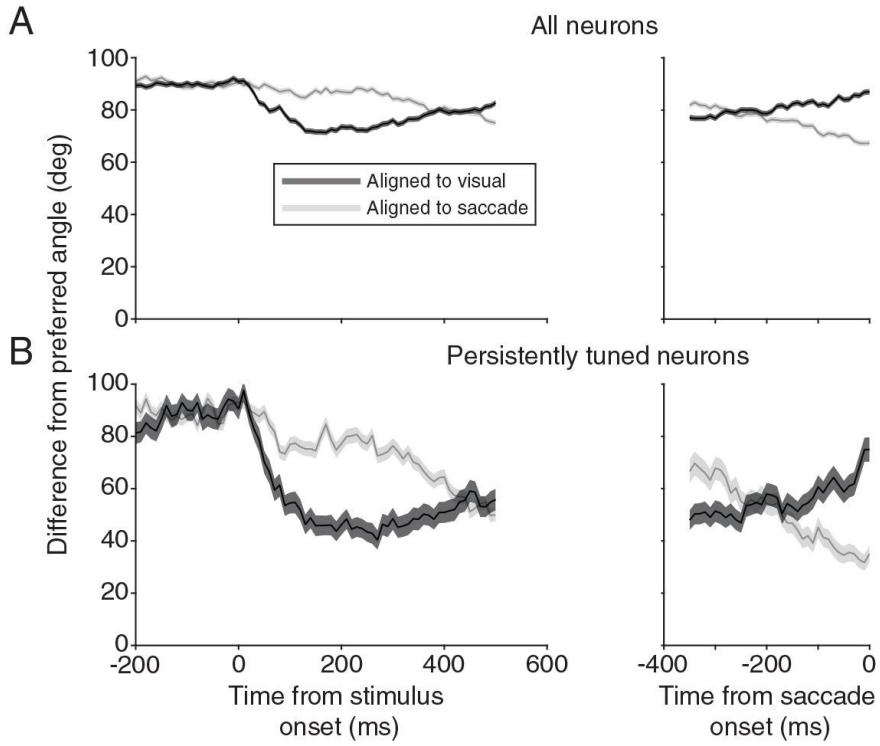

Figure 18:Time course visual and motor selectivity.

A) Angular difference for all PFC neurons (n = 2511 neurons) between the center of the response field at a specific time during the trial and the center of the response field for the ideal latency in the visual (black) or saccade (grey) epoch aligned to stimulus (left) or saccade (right) onset. B) same convention as in A however only for a subpopulation of neurons that had persistent significant tuning during the visual and saccade epochs (n = 158 neurons). The time during the trial at which the response field center was furthest from the response field calculated during the ideal visual latency was saccade onset. Conversely, the time during the trial at which the response field center was furthest from the response field calculated during the ideal saccade latency was in the 200ms following stimulus onset.

3.4.5 Dynamic selectivity in PFC and FEF subpopulations

Based on the results presented up to this point, it is clear a subpopulation of PFC neurons alters their tuning between the visual and saccade epochs even when the visual stimulus and saccade endpoint are at the same spatial location. Furthermore, this is not simply due to a loss of tuning during one of the epochs. If mixed selectivity occurs in PFC, a natural step would be to determine whether this is a unique property to a subpopulation of PFC neurons and whether other cortical regions exhibit similar changes in tuning. Our previous findings indicate ipsilateral and contralateral tuned neurons differ in their response latencies and in the degree of suppression opposite the response field. Given ipsilateral neurons show more suppression which could serve as a spatial code, perhaps it is these neurons that shift their tuning. With respect to other cortical areas, in motor and premotor cortex the preferred direction of single neurons frequently varied across time, reach speed, and/or reach distance (Churchland & Shenoy 2007), suggesting mixed selectivity may not be unique to PFC. Within the oculomotor system, a cortical area that resembles primary motor cortex is FEF. Given FEF is more directly involved in the saccade generation network, mixed selectivity could be problematic for relating visual inputs to saccadic outputs, so we hypothesized more FEF neurons would have a congruent alignment of their visual and motor signals compared to PFC. Furthermore, given ipsilateral neurons encode both hemifields when suppression is present, we predicted these neurons would be more likely to shift their tuning to the opposite hemifield.

To compare shifts in tuning in ipsilateral and contralateral populations, we computed the angular difference between the center of the response field in the ideal visual and saccade epoch. Neurons included in this analysis had to be selective for both the visual and saccade epoch ($p <$

.001; Kruskal Wallis Test; Contra: n = 412 neurons; Ipsi: n = 217 neurons). The ideal visual/saccade window, response field center, and significance test were computed across all 40 conditions. To calculate the shifts in tuning expected by chance, neuron indices for the entire population in the saccade epoch were randomly shuffled with respect to the visual epoch. This process was done 1000 times to obtain the 5^{th} and 95^{th} confidence intervals. No substantial difference was observed across the contralateral and ipsilateral populations, with both groups having significantly higher aligned neurons (angular difference less than 60 degrees) and significantly lower rotated neurons (angular difference between 60 and 120 degrees) (Figure 19A). These findings demonstrate PFC neurons, regardless of spatial tuning preference, are likely to have aligned (< 60 degrees) or inverted (> 120 degrees) tuning shifts when compared to intermediate rotations.

To compare the angular difference of the response field between the visual and motor epochs in FEF and PFC, sessions were matched across conditions and trial repeats (see *Methods)*. This meant a subset of the PFC conditions were used (1 target amplitude, 8 directions), and all FEF and PFC sessions were randomly subsampled to 40 trial repeats per condition. The same method for calculating latency was used for calculating the ideal visual and saccade response window and to identify significantly tuned neurons ($p < .01$; Kruskal Wallis test). To ensure that any angular differences we observed were due to a shift in tuning and not a loss of tuning resulting in a noisy estimate of the response field center, we only included neurons that had significant tuning in both the visual and saccade epochs (FEF n = 251 neurons, PFC n = 152 neurons, $p < .01$; Kruskal Wallis test). From the distribution of angular differences between the visual and saccade epoch, FEF was clearly more aligned, although FEF had a similar number of neurons that strongly inverted their tuning (>150 degrees) (Figure 19B). In summary, both

contralateral and ipsilateral neurons shift their tuning in similar ways: a large portion maintain a visual/saccade alignment and the neurons that do shift are more likely to invert their tuning (>120 degrees). FEF also contains neurons that change their selectivity between the visual and motor epoch, however, a much larger proportion of FEF neurons have congruent tuning, particularly when compared to the PFC population.

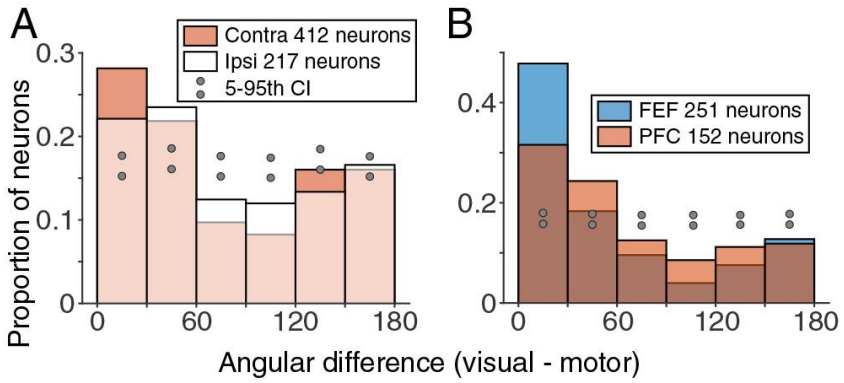

Figure 19: Tuning shifts in PFC subpopulations and FEF.

A) Shifts in response field centers between the visual and saccade epoch as measured by angular difference for contralateral (filled) and ipsilateral (open) tuned neurons. Only neurons with significant visual and saccade responses were analyzed ($p<.01$, Kruskal Wallis Test; Contra n = 412; Ipsi n = 217). 5^{th} and 95^{th} percent confidence intervals show the proportion of neurons expected for a given angular difference by chance (upper and lower grey dots). Contralateral and ipsilateral populations had similar distributions with respect to angular difference. Many neurons had consistent visual and saccade alignment, however a substantial portion also inverted their tuning. B) same conventions as in A but comparing the FEF population to the PFC population. Some FEF neurons had substantial shifts in tuning, equivalent to the PFC population, however FEF also had more neurons with congruent visual and motor response fields.

3.4.6 Visual and motor response properties in PFC and FEF

One explanation for the observed differences in tuning could be due to visual/motor response properties or spatial tuning differences between FEF and PFC. FEF is known to primarily possess contralateral tuning (Bruce & Goldberg 1985) yet there is evidence of ipsilateral tuning in a subpopulation of FEF neurons (Crapse & Sommer 2009). This contrasts with PFC, where previous studies have reported a quarter to nearly a half of neurons may have ipsilateral tuning (Bullock et al 2017, Funahashi et al 1989, Funahashi et al 1991, Lennert & Martinez-Trujillo 2013). If an area mainly encoded information from the contralateral hemifield, shifts in tuning would be limited to a maximum of 90 degrees (i.e. within the contralateral hemifield), while areas with information from both hemifields would be able to shift their tuning across the hemifield, which could be the case for FEF and PFC respectively.

To understand how a neuron fires for the visual stimulus relative to the saccade, we computed the average VMI (see *Methods*) across conditions for the entire FEF and PFC population. Relative to the FEF distribution, PFC was significantly ($p = .003$; two sample t-test) shifted towards 1 meaning PFC neurons were more likely to have a stronger visual response compared to a saccade response (Figure 20A). Overall, FEF had a significantly larger proportion of tuned ($p < .01$ in the visual, motor, or both epochs; Kruskal Wallis test) visual, visuomotor, and motor neurons (chi squared test; visual: $p = .01$; motor: $p = .007$; visuomotor: $p < .001$) (Figure 20B). When combining the three groups (tuned visual, motor, and visuomotor) FEF also had a significantly higher proportion of contralaterally tuned neurons (chi squared test; FEF 68% contra, PFC 59% contra, $p = .002$). The bias towards ipsilateral tuning in PFC was even more striking when considering only the most directionally selective (see *Methods*) neurons in each

population (Figure 20C). To obtain these selective neurons for a given visual/motor/visuomotor group, a neuron had to be significantly tuned ($P < .01$; Kruskal Wallis test, visual, saccade, or both for visuomotor) as well as have a directional selectivity (see Methods) that was in the top 90^{th} percentile for the epoch. For most of the groups in both PFC and FEF, selective neurons had a strong contralateral bias (FEF contralateral: visual 82%, motor 71%, visuomotor 79%; PFC contralateral: visual 79%, motor 30%, visuomotor 71%). Unexpectedly, when considering only these selective neurons, the PFC motor population had more ipsilateral tuned neurons than contralateral tuned neurons. Two observations that provide an explanation for the propensity of ipsilateral tuned motor neurons are the existence of large shifts in tuning that cause response fields to shift into the opposite hemifield, and that visual neurons were predominantly contralaterally tuned. Indeed, upon visual inspection of the visual and saccade response fields for the selective ipsilateral tuned motor neurons, a subset of the population had shifts in tuning across the hemifield. In summary, FEF contains more tuned visual, motor, and visuomotor neurons in addition to having a larger percentage of contralateral tuned neurons. When considering only the most directionally selective neurons of each area, FEF is even further biased towards contralateral tuning and an interesting pattern in PFC motor neurons appears, suggesting our estimate of the number of neurons who shift their tuning might be conservative. These differences in visual/motor response properties and spatial tuning hint that FEF and PFC may be encoding information about the trial in separate ways.

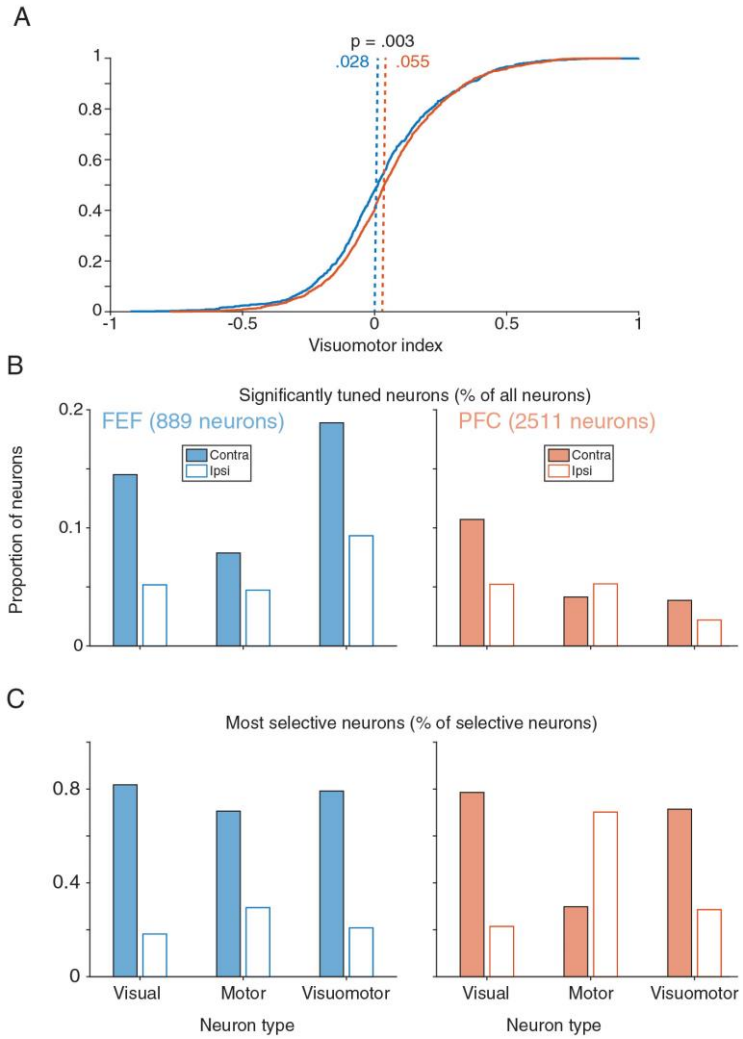

Figure 20: Visual/motor tuning in FEF and PFC.

A) Cumulative distribution of visuomotor index for PFC and FEF populations, all neurons included (FEF n = 889 neurons; PFC n = 2511 neurons). PFC neurons had a stronger visual response when compared to the saccadic response. B) Distribution of visual, motor, and visuomotor neurons within FEF (left) and PFC (right), normalized to the total number of neurons recorded. Groups are divided by spatial tuning (contralateral: filled, ipsilateral: open). To be included, a neuron needed to have significant tuning in at least one epoch or both (visuomotor group). FEF had more tuned neurons for all groups (visual, motor, visuomotor). C) Same convention as in B, but with the additional criterion that each neuron had to be in the 90th percentile or above ranked by directional selectivity (FEF: visual = 22, motor = 17, visuomotor = 24; PFC: visual = 70, motor = 57, visuomotor =12). A majority of the most selective FEF neurons had contralateral tuning, while in PFC, highly selective motor neurons were more likely to be ipsilateral tuned.

3.4.7 Decoding from PFC and FEF populations

Numerous studies have used population level analyses to understand the effects dynamic selectivity might have during working memory tasks (Barak et al 2010, Parthasarathy et al 2017, Spaak et al 2017, Stokes et al 2013). If the working memory population signal is made up of single neurons whose tuning shifts, using information in one part of the trial, for example the visual epoch, to predict the activity in other part of the trial, for example the saccade epoch, could result in classification errors. Given that we observed the FEF population to be more congruent between epochs compared to the PFC population, we hypothesized the population signal in FEF would be more generalizable when predicting activity from different time epochs. To understand how PFC and FEF encode trial information, we trained a population decoder for each area and measured its accuracy throughout the trial.

We used a Poisson Naïve Bayes decoder, trained on neural activity from one time window in the trial, and tested on all other time points during the trial (see *Methods*). To increase decoder accuracy, neurons were combined (separately in FEF and PFC) across recording sessions to create a pseudo-population. 8 conditions were decoded (1 amplitude, 8 directions) and to normalize across sessions, 40 trial repeats were randomly selected from each condition. All decoding accuracies reported are the average across the eight conditions, and standard errors are computed across cross-validation folds. For comparisons between FEF and PFC, the PFC pseudo-population was randomly subsampled to match the number of neurons in the FEF pseudo-population unless stated otherwise.

Overall decoding performance, as well as generalizability across time, was higher in the FEF pseudo-population compared to PFC. For FEF, decoding was highest shortly after visual onset and around the time of the saccade, but also maintained a high accuracy throughout the

delay period (Figure 21A). The generalizability of the FEF population code can be seen by examining bins on the off-diagonal, where the training and testing epochs were temporally separated. The decoder trained using PFC activity also showed peaks in accuracy after stimulus onset and around the time of the saccade but had a lower overall decoding accuracy and was less generalizable when compared to FEF (Figure 21B). This suggests the FEF population code has a more accurate readout, and that the code is more generalizable throughout the trial.

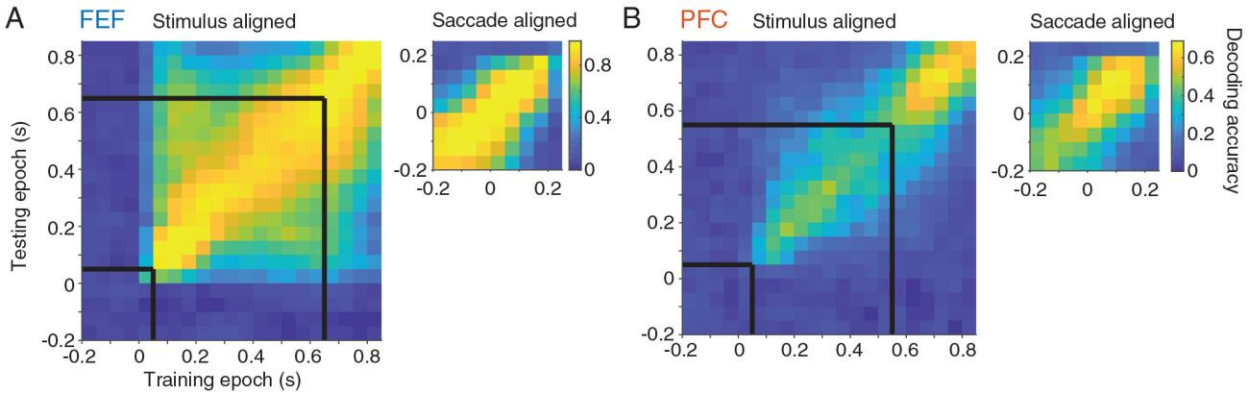

Figure 21: Decoding in FEF and PFC.

A) Decoding performance of the FEF pseudo-population (n = 770 neurons) for various training and testing points throughout the trial, aligned to stimulus onset or saccade onset (inset). Black lines denote the beginning and end of the delay epoch. B) same convention as in A, but with a PFC pseudo-population randomly subsampled to have the same size as the FEF pseudo-population (n = 770 neurons of 1722 neurons). Decoding accuracy was highest for training and testing points that were temporally in the same bin, particularly after stimulus onset and around the time of the saccade. FEF had a higher overall decoding accuracy and a higher accuracy for training and testing points that were temporally separated.

To understand why the FEF decoder performed better than the PFC decoder, we related decoding accuracy to three basic properties of the pseudo-population: the number of neurons in the population, the direction selectivity of the neurons, and their reliability (see *Methods*). For this analysis, one time point was selected to test and train on, based on the time point with the highest decoding accuracy after stimulus onset (FEF: 100 ms after stimulus onset, PFC 150 ms after stimulus onset). We first examined decoding accuracy as a function of the number of neurons in the pseudo-population. Across all pseudo-population sizes, the FEF decoder performed better than the PFC decoder (Figure 22A). Starting with a population of 100 neurons, the FEF decoder increased in accuracy as more neurons were added and began to asymptote at 100% accuracy for populations over 500 neurons. The PFC population started at an overall lower accuracy level and monotonically increased as more neurons were added, but the decoder never reached the accuracy of the FEF population, even compared to FEF population of 100 neurons (FEF accuracy, 100 neurons 71.5%; PFC accuracy 1722 neurons 63.5%).

Knowing that a decoder trained on activity from a small population of FEF neurons (100 neurons) could outperform one trained on the entire PFC population (1722 neurons) we examined what individual response properties could lead to such a wide margin in decoding. We first examined the direction selectivity, a measure of how tuned a neuron is across the 8 conditions (see *Methods*). For each pseudo-population (FEF and PFC separately), each neuron was ranked by their selectivity. Then, nonoverlapping groups of 100 neurons were chosen starting with the most selective. Decoding accuracy increased with the directional selectivity of the neurons for both FEF and PFC, however even for subpopulations where the average selectivity of the 100 neurons was the same, FEF decoding accuracy was still larger (Figure 22B). Comparing the top 100 ranked neurons by directional selectivity in FEF and PFC, the FEF

subpopulation had a higher selectivity and near perfect decoding accuracy. The same process was used for neuron reliability, except ranking by reliability instead of selectivity. Reliability was defined as the Pearson correlation coefficient between even and odd trials for a given condition, averaged across the 8 conditions (see *Methods*). As with selectivity, decoding accuracy increased with reliability for both FEF and PFC populations, yet FEF performance was still higher for reliability matched neurons (Figure 22C). Again, examining the top 100 ranked neurons in each area, the FEF population had a near perfect accuracy and was more reliable. In summary, the FEF population code is more accurate and generalizable when compared to PFC. The results evaluating decoding accuracy with respect to single neuron properties highlight a subpopulation of FEF neurons that are very selective and reliable that could contribute to decoding accuracy being higher in FEF.

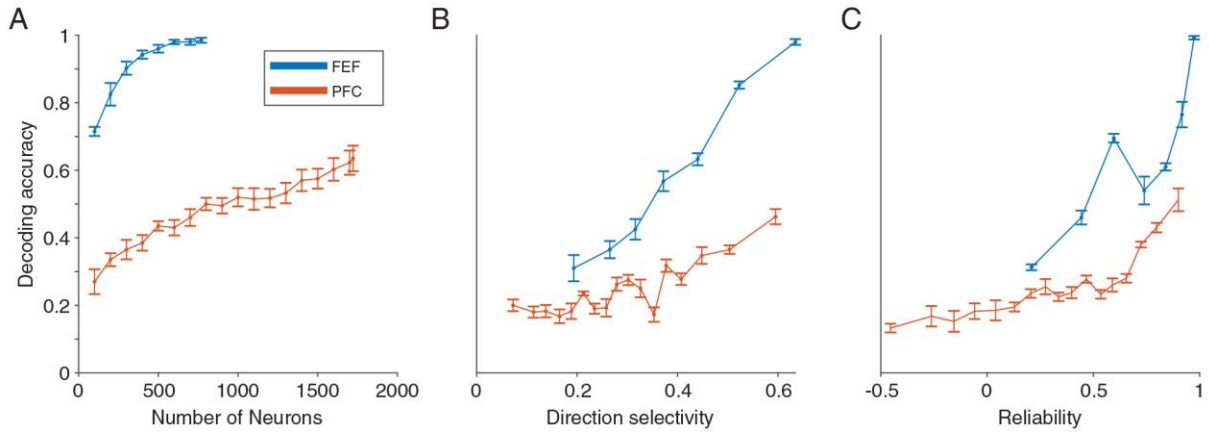

Figure 22: Decoding accuracy with single neuron properties.

A) Decoding accuracy in FEF (blue) and PFC (red) as a function of the size of the pseudo-population. Decoding accuracy increases for both populations as more neurons are added, however FEF begins at a higher accuracy and asymptotes around 500 neurons. PFC decoding accuracy increases but even with the full population (1722 neurons) it does not reach the accuracy of the 100 neuron FEF population. B) Decoding accuracy for subpopulations of 100 neurons ranked by direction selectivity. For each line, the rightwards most point corresponds to the 100 most selective neurons. FEF has higher accuracy for direction selectivity matched bins, but also has a higher overall selectivity, with the 100 most selective neurons performing at nearly 100%. C) Same conventions as in B but ranked by reliability. For reliability matched bins, FEF had a higher accuracy but also FEF neurons had larger overall accuracy.

3.5 DISCUSSION

The primary signals that need to be processed and relayed during a memory guided saccade task are a visual signal, which identifies the location of the visual stimulus, and a motor signal which encodes the impending saccade vector. Comparing single neuron response properties between PFC and FEF, PFC neurons had later latencies and were more likely to be ipsilaterally tuned. Across the population, FEF had more significantly tuned neurons, particularly for the visual and motor epoch (visuomotor neurons). We found a subpopulation of PFC neurons which shift their tuning between the visual and saccade epochs. These shifts can be of varying degrees, but frequently resulted in the center of the response field in the visual and saccade epochs being in opposite hemifields, with the location opposite the center being suppressed below baseline. Considering the time course of the entire trial, tuning disparity was largest when evaluated around the visual latency of the PFC population relative to saccade onset. Comparably, FEF neurons had more congruent tuning between the epochs, which combined with more selective tuning and reliability, were able to decode more accurately across all portions of the trial. Together, these findings provide evidence that visual and motor signals may be processed differently between the two prefrontal areas and that PFC may be encoding more than just the target location and impending saccade.

3.5.1 Spatial representation

For many visual and oculomotor areas, neurons primarily represent the contralateral hemifield. This includes the FEF (Bruce & Goldberg 1985), LIP (Ben Hamed et al 2001, Blatt et al 1990, Patel et al 2010), SC (Cynader & Berman 1972, Goldberg & Wurtz 1972, Schiller & Koerner 1971), and SEF (Schlag & Schlag-Rey 1987). Some areas show evidence of ipsilateral tuning, such as MT (Gattass & Gross 1981, Van Essen et al 1981), FST (Desimone & Ungerleider 1986), and IT (Ungerleider 1983), although these are typically confined to regions of space that are just across the vertical meridian. Additionally, various PFC recordings have demonstrated ipsilateral tuning throughout the visual, delay, and saccade epochs of oculomotor tasks (Funahashi et al 1989, Funahashi et al 1990, Funahashi et al 1991, Mikami et al 1982, Suzuki & Azuma 1983). With many of these studies however, the ipsilateral tuning is more a reflection of a wide response field encompassing a portion of the ipsilateral hemifield.

The present findings differ from these previous studies by identifying spatially localized ipsilateral response fields across over 15 degrees of visual ipsilateral space. When considering all conditions (not subsampled to match FEF), the percentage of significantly tuned PFC neurons across all epochs (n = 1534 neurons) that were contralateral (61%) is in line with two previous studies reporting 76% (Bullock et al 2017) and 58% (Lennert & Martinez-Trujillo 2013).

The topographical organization of PFC is still unclear, however some evidence suggests a rostral-caudal gradient of tuning, where posterior areas have spatial, shape, and color specificity (basic stimulus properties) with anterior areas engaged in more abstract operations (Riley et al 2017). An earlier study proposed a medial-lateral axis in PFC, with smaller receptive fields lateral and larger and more eccentric receptive fields medial (Suzuki & Azuma 1983), similar to the topography observed when microstimulating in FEF (Bruce et al 1985). Some have reported

clustering of neurons with similar tuning properties (Bullock et al 2017, Leavitt et al 2017), however others saw no systematic pattern with receptive field direction (Suzuki & Azuma 1983). Any kind of rostral-caudal or medial-lateral comparison is difficult due to the limited spatial extent of the array (the entire array would be in the posterior prefrontal region according to Riley et al (2017), for example). However, we can compare evidence of clustering, as these studies also recorded from arrays of similar size. Based on the response fields of neurons in the visual and saccade epoch, as a function of their location on the recording array, it would be difficult to conclude any kind of distinct topography (Figure 23). It should be noted, however, this is based only on visual inspection of the array maps. A more systematic analysis should be performed in the future, such as the spatial autocorrelation analysis used by Leavitt et al (2017). There are clear examples of clustering of neurons with similar response fields, but also plenty of examples of neurons close by with disparate tuning. Examples of neurons who shift their tuning between visual and saccade epochs are also shown, although no conclusion can be made with respect to their topography at this point.

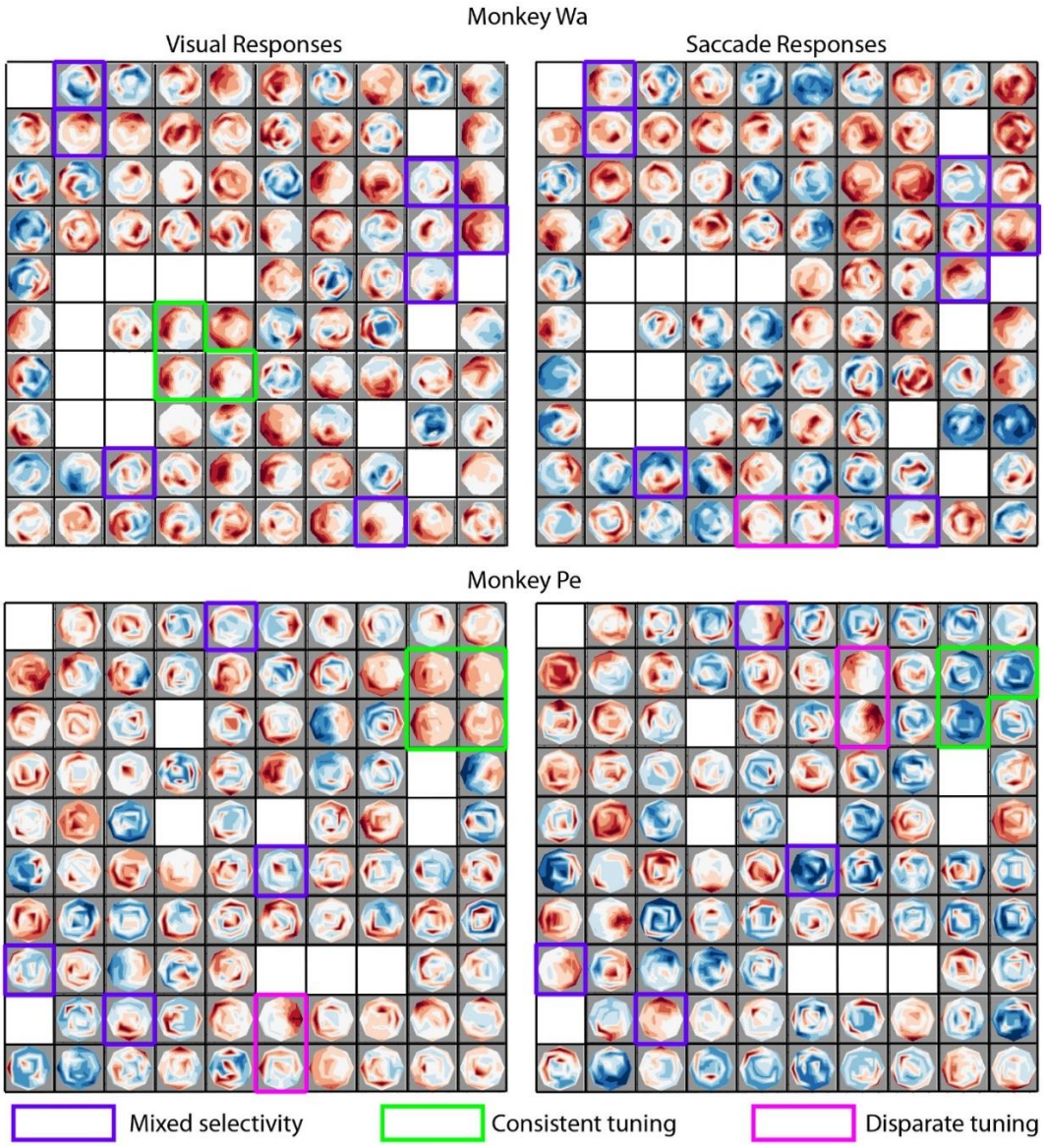

Figure 23: Topography of visual and motor responses in PFC.

Response field heatmaps for one example session in monkey Wa (top) and Pe (bottom) during the visual (left) and saccade (right) epoch. The spatial location of each neuron corresponds to its position on the electrode array (although note, the arrays themselves are not oriented with respect to the brain). If multiple neurons happened to be recorded on the same electrode, the neuron with largest modulation depth (maximum firing rate – minimum firing rate) was used. Colored boxes highlight illustrative examples of neurons near each other with the same tuning (green), neurons near each other with disparate tuning (magenta), and neurons with mixed selectivity across the visual and saccade epochs (purple).

Spatial suppression outside the response field has been previously reported in FEF during natural viewing when saccade target is outside the receptive field (Burman & Segraves 1994) and when a target or distractors are presented in the ipsilateral hemifield (Schall et al 1995a). Suppression had also been reported in PFC for stimuli in a limited portion of the visual field (Kiani et al 2015, Mikami et al 1982), particularly in spatial locations opposite the center of the receptive field and for ipsilateral tuned neurons (Bullock et al 2017), which agrees with our findings. Our results expand upon these findings, by establishing the spatial extent of suppression can vary widely across neurons, from encompassing the entire visual field around the response field to being limited to the opposite hemifield or localized to a specific subregion. Many PFC neurons encode both hemifields, one through excitation and the other through suppression. This suggests the traditional view of a "receptive field", activity above baseline in a spatially localized area and baseline activity everywhere else, may not be the best description of PFC activity.

Other novel findings presented in this report are the direct comparison of FEF and PFC onset latencies, demonstrating PFC neurons have significantly longer latencies, and the comparison between ipsilateral and contralateral tuned PFC neurons, demonstrating ipsilateral tuned neurons have significantly longer latencies. Our findings that a wide variety of latencies exist and that they are uniformly distributed agrees with a previous study from PFC (Mikami et al 1982). We suspected the difference in latency between FEF and PFC could be driven by the ipsilateral tuned population, with the contralateral population resembling the FEF population, however both PFC subpopulations had significantly longer latencies compared to FEF ($p < .001$; paired t-test).

In summary, we characterized the responses of single PFC neurons with respect to spatial distribution, latency, and degree of suppression below baseline and when possible, compared these findings to FEF. Given the wide variety response properties observed, we conclude PFC neurons may be tasked with encoding higher order signals compared to FEF, where signals are more defined within the visual processing and saccade generation network.

3.5.2 Dynamic selectivity

The first studies investigating the neural correlate of working memory signals in PFC observed persistent activity, defined as elevated spiking during the memory period of the task (Fuster & Alexander 1971, Kubota & Niki 1971). Given the timing of this activity coincided with when the memory was being held, this offered a simple explanation for how the memory signal was being encoded. Later studies, however, demonstrated that some neurons during working memory tasks were transiently activated, such as during a vibrotactile discrimination task (Romo et al 1999), a motion discrimination task (Zaksas & Pasternak 2006), and a match to sample task (Warden & Miller 2007). Population analyses added further evidence to the presence of a dynamic code that changes across the delay epoch (Barak et al 2010, Meyers et al 2008, Stokes et al 2013). One theory suggests within this dynamic signal, a stable population code exists that is robust throughout the delay period (Murray et al 2017). Other studies have taken an alternative approach by trying to identify how single neuron properties could lead to a perceived persistent or stable code. Persistent activity, for example, could be the result of sparse coordinated spiking facilitated by gamma oscillations in local networks (Lundqvist et al 2016). Dynamic activity is thought to arise either from a change in encoding task variables or a change in tuning (Parthasarathy et al 2017, Spaak et al 2017), termed mixed selectivity.

Our study examines the latter, leveraging the spatial resolution possible given our task and the large population of neurons recorded, to identify how visual and saccade signals are encoded in single neurons. In agreement with previous studies, we find a subpopulation of PFC neurons which shift their tuning between the visual and saccade epochs. The benefit of our study lies in the ability to precisely identify visual and saccade response fields and determine if there any systematic patterns to how PFC neurons shift their tuning. Ipsilateral and contralateral tuned neurons exhibited similar patterns of shifting, with many of the neurons remaining aligned, however a substantial portion inverted their response fields (shifts greater than 120 degrees) and to a lesser extent rotated them (between 60 and 120 degrees). Comparing the visual and saccade respond field alignment across the trial, the largest disparity occurred between the onset of the visual response and the onset of the saccade. These two pieces of evidence suggest that one feature of PFC (when compared with FEF) is a striking misalignment of the overall code for visual stimuli and saccadic eye movements.

3.5.3 Comparison of PFC and FEF

Given their proximity, it is not surprising PFC and FEF share common attributes. Both areas contain neurons that are responsive to visual stimuli, saccades, or both, in addition to neurons which fire persistently across a memory period. FEF has been shown to contain ipsilateral tuned neurons (Crapse & Sommer 2009) as well as neurons with mixed selectivity (Parthasarathy et al 2017), however for both subpopulations the proportion is larger in PFC. Due to their differences, PFC is thought to be involved in integrating a variety of signals such as reward value, attention, working memory, and sensory stimuli while FEF may be more involved in the saccade generating network (Bullock et al 2017).

Our findings confirm and expand upon these studies, highlighting how visual and saccade signals are represented at the single neuron level and in a population code in FEF and PFC. FEF contained a larger number of neurons tuned to the visual and saccade epochs (or both) and their latencies were more aligned. One explanation is that some of the recorded PFC neurons might have been tuned for other features of the task, such as the reward structure. Our analysis of the most selective neurons in each area revealed a heavy contralateral bias in FEF, yet interestingly the PFC motor population was biased towards ipsilateral tuning.

Through visual inspection of the selective ipsilateral tuned motor neurons, we observed a subset of neurons that clearly shifted their tuning between the visual and saccade epochs but did not pass the visual selectivity or significance test. Having identified differences at the single neuron level between FEF and PFC, we examined what effects this could have on the population readout from each area. One previous study compared the FEF and PFC population readout, observing a dynamic code in PFC while the FEF code was more persistent (Parthasarathy et al 2017). The dynamic nature of the PFC code was thought to stem from the presence of a distractor in the task, which caused the PFC population to morph its activity. Our study is complementary in the sense with the distractor removed, we could determine if the PFC code was still dynamic and how it compared to FEF. Decoding in FEF was substantially more accurate than PFC, even when comparing a small subpopulation of FEF neurons to the entire PFC population. Furthermore, when training and testing on epochs that were temporally separated, the decoder was more accurate for the FEF population. We identified two major neuronal features that contributed to a higher decoding accuracy in FEF: 1) directional selectivity and 2) trial to trial reliability. For both features, the FEF population contained a subset of highly selective and reliable neurons that when grouped together, the decoder had nearly 100%

accuracy. We conclude the population code in PFC is more dynamic than FEF, even without the presence of a distractor, and that PFC lacks a subset of neurons with extremely selective tuning and reliable responses present in FEF.

Our results extend the literature in in three key ways. First, due to the spatial resolution of our task and the sample size of recorded neurons, we were able to with high fidelity map the visual and saccade responses of PFC single neurons. We found a rich pattern of responses in PFC that represent the entire visual field through contralateral and ipsilateral tuning and excitation and suppression. Second, the observed tuning shifted between epochs, quite often to the opposite hemifield, indicating what may be perceived as random dynamics are actually the result of a transition between a visual and motor code. Finally, we compared single neuron and population level responses from PFC and FEF, highlighting the population code in PFC is dynamic even in a simple memory guided saccade paradigm. Furthermore, PFC clearly differed from FEF in all our measures of response properties, although FEF did show hints of the same properties. Taken together, these results demonstrate a richness to the spatial representations in PFC and emphasizes careful consideration of its responses properties should be taken when developing models for spatial working memory.

4.0 GENERAL DISCUSSION

The overarching goal of this dissertation was to investigate how visual and motor signals are processed and integrated in the brain, particularly prefrontal cortex. We recorded from populations of neurons in two prefrontal areas, FEF (Chapters 2 and 3) and PFC (Chapter 3), while subjects performed a simple working memory task, the memory guided saccade task. By using the memory guided saccade task, would could temporally separate responses related to the visual stimulus with those related to the saccade.

The analyses in Chapter 2 focused on correlated variability, the tendency of a pair of neurons to exhibit correlated fluctuations on a trial by trial basis. This provides an index into how FEF neurons, at the population level, communicate when preparing to make an eye movement. We first characterized the structure of correlated variability in FEF with respect to basic response properties (distance, tuning similarity, visual/motor response) and task parameters (time course and task condition). Correlated variability in FEF decreased for pairs of neurons that were spatially far apart or had dissimilar tuning and was larger for visual pairs compared to motor pairs, which is consistent with prior observations from other cortical areas. Across the entire delay epoch, correlated variability was tuned for eye movement direction, indicating a motor preparation signal and not merely a result of the visual stimulus. Finally, we considered the relationship between FEF activity and saccade reaction time. We found two key changes in FEF activity that accompanied fast saccadic reaction times. The first was correlated variability

was lower for trials with fast reaction times, in both preferred and anti-preferred directions. This trend was present across the entire population of FEF neurons but seemed strongest for visual pairs. The second change, present primarily in motor neurons, was a robust increase in firing rate during the time leading up to the saccade.

In Chapter 3, we recorded from populations of PFC neurons during the same task, with the goal of understanding how visual and motor signals are encoded at the single neuron and population level. We first characterized PFC single neuron responses, identifying a rich set of features associated with the response field including ipsilateral tuning, suppression opposite the response field center, and shifts in tuning between the visual and saccade epochs. These shifts in tuning were clearly present at the single neuron level and were not due to a loss of tuning in one of the epochs. Data recorded from FEF was analyzed in a similar way to understand if the shifting phenomena was unique to PFC. While FEF showed evidence of some neurons who shifted their tuning, as a population FEF had a more congruent alignment visual and saccade tuning. The shifts in tuning were particularly intriguing as this feature could greatly affect how the population code is read out. We therefore performed a decoding analysis on the PFC and FEF populations, concluding the FEF population code is more accurate overall, more generalizable temporally, and is driven primarily by a subpopulation of very selective and reliable neurons that are not observed in PFC. In this chapter, we compare our results with previous findings, highlight some limitations in our studies, and discuss future directions

4.1.1 Previous reports of correlated variability in FEF

Previous reports of correlated variability in FEF were observed in three tasks: a visual search task (Cohen et al 2010), a spatial attention task (Astrand et al 2016), and a memory guided saccade task (Dehaqani et al 2018).

Correlated variability during visual search

For the visual search paradigm (Cohen et al 2010), most of the analyses measured correlations in the form of spike synchrony, which relates the spike timing of a pair of neurons on a millisecond by millisecond timescale. Neuronal pairs were more synchronous when the target was in the receptive field of each neuron, compared to when the target was in only one receptive field or neither. Correlated variability, or spike count correlation (r_{sc}), followed the same trend with respect to target location, and additionally, pairs with nonoverlapping receptive fields had negative correlations when the target was in one receptive field but not the other. The authors propose a model by which neurons with spatially overlapping receptive fields excite each other and a population of interneurons that inhibit neurons with nonoverlapping receptive fields (neurons in the other hemisphere for example).

Our findings are consistent with correlations being lower for neurons with disparate tuning, however we observe correlations to be lowest in the preferred direction of a pair of neurons (Figure 9C). The differences observed can be attributed to numerous factors including differences in the task (visual search versus memory guided saccade), the limited sample size in the study (239 versus 7656 pairs in our study), and the inclusion criteria for neurons. For our study, we included all neurons that passed an SNR and firing rate threshold while the previous study included only visual and visuomotor neurons that passed a significance test. Additionally,

the previous study placed targets directly in the receptive field while our study, being a population analysis, chose target locations in an arbitrary manner. It is possible the correlation structure varies across 3 different locations: inside the receptive field, outside the receptive field but within the contralateral hemifield, and in the ipsilateral hemifield. Finally, correlated variability has been shown to increase with firing rate (de la Rocha et al 2007), a potential confound for the Cohen et al (2010) study but not for ours as tuning for correlated variability was opposite that of the firing rate.

Correlated variability and spatial attention

The second study examined correlations during a spatial attention task. Correlated variability decreased when attention was oriented to the preferred location of the neuronal population, in accordance with previous reports in other areas (Cohen & Maunsell 2009, Herrero et al 2013, Mitchell et al 2009, Snyder et al 2016). Additionally, correlated variability varied with trial outcome, being lower on hit trials compared to error trials, irrespective of the spatial specificity of the neural population. This agrees with our findings that correlated variability varied with reaction time even for directions in the ipsilateral hemifield which are less likely to be encoded by the FEF population (Figure 11). Interestingly, 2 observations reveal the relationship between correlated variability and trial outcome may be predictive, the first being differences in correlated variability were seen right after fixation onset before the cue was presented. The second was correlated variability during the intertrial interval before fixation onset varied based on the result of the previous trial (highest when preceded by an incorrect trial, lowest when preceded by a correct trial), although these differences vanished once fixation was achieved.

Correlated variability during visual and motor encoding

The final and most directly comparable analysis of correlated variability in FEF comes from Dehaqani et al (2018), who also analyzed FEF activity during a memory guided saccade task. The primary goal of this study was to understand how single neuron and ensemble activity encodes visual stimuli and saccadic target selection. While in our study we focused on correlated variability in the delay period as a whole, Dehaqani et al (2018) measured correlated variability in the visual and saccade epochs. During the visual epoch, correlated variability was tuned for eye movement direction in a manner consistent with our findings in that it was lowest for the preferred direction. Interestingly, comparing the visual and saccade epochs, tuning inverted such that correlated variability was highest for the preferred direction, and this was driven primarily by decreases at non-preferred spatial locations. As previously stated, our analyses did not include computing correlated variability during the saccade epoch, although it should be noted we observed no difference in correlated variability when calculated separately in the first 200 ms and last 200 ms of the delay period (data not shown) which reinforces our observation that correlated variability remained at a constant low level throughout the delay period (Figure 10). A complementary finding to our results that lower correlations were observed for fast reaction time trials was that smaller changes in correlated variability during the saccade epoch (i.e. less of a decrease in correlated variability compared to the visual epoch) corresponded to longer reaction time trials. From both these findings in can be concluded that high levels of correlated variability in the time leading up to saccade onset correspond to slower reaction times. As a more general point, Dehaqani et al (2018) referred to the shifting of correlated variability levels in non-preferred directions as encoding expansion, or that ensembles of neurons enhance their representation of visual space poorly encoded by single neurons. This interpretation dovetails

nicely with our results that the relationship between correlated variability and reaction time is preserved even for non-preferred directions. As a whole, this indicates the structure of correlated variability in FEF is flexible enough to encode motor plans in directions not typically encoded by single neurons.

4.1.2 Correlated variability in FEF: limitations and future directions

Limitations

The primary limitation in our study was the limited number of spatial locations used as experimental conditions. The limited number of conditions (8) was chosen for two main reasons. First, correlated variability is a trial by trial measure, thus requiring large numbers of repeats per condition to obtain an accurate measurement. As a rule, in our analysis a minimum of 40 repeats per condition were required to calculate correlated variability. This meant the monkey was at a minimum required to complete 320 trials per day (8 conditions x 40 repeats). If we had wanted to tile more of visual space, we could have expanded our condition number to 40, requiring 1600 trials (40 conditions x 40 repeats), which may or may not have been feasible given the satiation of the monkey. Furthermore, as a control to the correlated variability-reaction time analysis, we removed any trials which contained microsaccades to ensure the relationship was not due to the jittering of the visual field. We observed microsaccades on about 30% of trials so taking this into account would require even more repeats to be collected per condition. The second reason was the goal of the study was to analyze how populations of FEF neurons communicated when planning eye movements, so we wanted to choose a consistent set of target conditions to reduce any biases in the subpopulations on a day to day basis. Additionally, while FEF is known to have a medio-lateral topography (large saccades evoked when stimulating medial, small saccades

when stimulating lateral), within a given penetration evoked saccade vectors can vary in direction (Bruce et al 1985). It is therefore uncertain given task condition restraints whether the visual field could be sufficiently tiled to place a stimulus in the receptive field of all recorded neurons in a given subpopulation.

A second limitation in our study was the use of a fixed delay epoch. This decision was primarily made for ease of comparison of the time course of variability across sessions (Figure 10). The fixed duration could affect our results in two ways. First, the correlation between firing rate and reaction time has been thought to depend on whether task conditions can be predicted or remain constant (Heitz & Schall 2012), with the chosen presaccadic analysis window also being a factor (Jantz et al 2013). Second, having a fixed duration could in theory allow the monkey to have an internal estimate of the delay period and prematurely begin their saccade in response to their perceived time in the delay and not in response to the fixation point offset. This could result in faster reaction times and more narrow reaction time distributions.

Future directions

The following paragraphs highlight future directions based on the results and conclusions obtained from Chapter 2. It is divided into future directions based on the analyses and task included in Chapter 2 and novel analyses and tasks that expand upon Chapter 2.

An obvious future direction based on the primary limitation of our study would be to expand the number of target locations to ensure some of the conditions are truly in the receptive field of the neurons. This would potentially allow us to reconcile the differing observations in correlated variability tuning observed in our data (Figure 9) and previously reported in FEF (Cohen et al 2010). Having a better estimation of the receptive fields could also confirm another

aspect of the correlated variability structure is conserved across areas, the relationship between receptive field distance and correlated variability, which we have observed in PFC and V4 (Figure 24). A second experimental manipulation that could be pursued as a future direction is to employ a variable delay epoch. This could be beneficial for two reasons, the first being to disentangle the differing results highlighted above pertaining to the correlation between firing rate and reaction time. The second would be to obtain a wider distribution of reaction times to determine whether correlated variability linearly scales with reaction time (as would be predicted), or whether a nonlinear relationship exists such as in the case of correlated variability and EEG spectral power (Snyder et al 2015). Another future direction based on the current results relies upon a modification to the recording setup to allow for bilateral FEF recordings. It would be interesting to investigate the correlated variability across hemispheres as it pertains to reaction time. Our current results show the relationship between reaction time and correlated variability is independent of saccade direction, meaning FEF at the population level encodes some information about the ipsilateral hemifield. We might then predict a similar relationship with reaction time for interhemispheric pairs, just as the relationship between trial outcome and interhemispheric correlated variability is maintained in FEF (Astrand et al 2016), although there is evidence interhemispheric correlated variability is near zero in V4 (Cohen & Maunsell 2009).

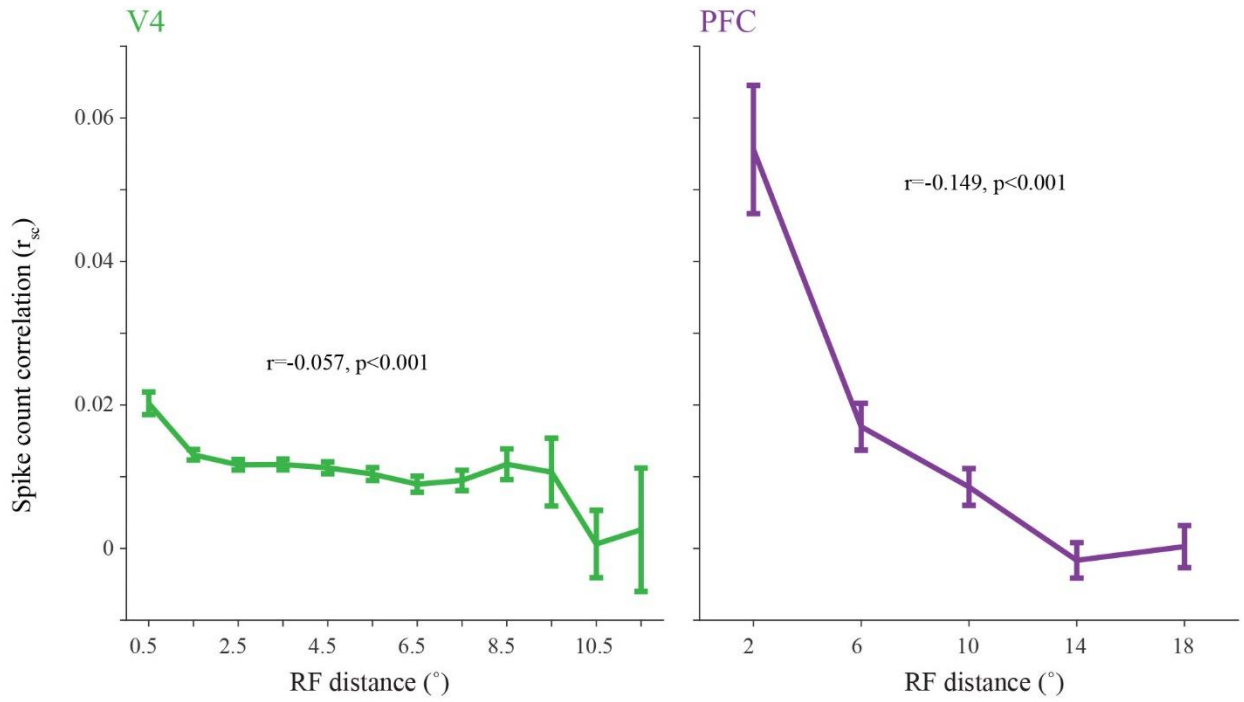

Figure 24: Correlated variability with receptive field distance.

A) V4 correlated variability with receptive field distance. B) PFC correlated variability with receptive field distance. For both PFC and V4 pairs, correlated variability decreased with receptive field distance. Note: Data is from subset of sessions in Chapter 3.

The two novel directions proposed are based on an experimental task which also probes the integration of visual and motor signals, and the application of correlated variability measures to simultaneous multiarea recordings.

A common phenomenon linked to sensorimotor integration is visual stability during saccades. Despite humans making multiple saccades a second, we perceive the visual world around us to be stable. One way to probe visual stability is through a remapping task. During this task, a stimulus is presented briefly before (or during) a saccade at the location where the receptive field will be upon saccade completion. The key observation is that despite the stimulus no longer being present by the time the receptive field arrives at the target's location, the neuron

still increases its activity as if the stimulus was still there, termed receptive field remapping. Sometimes the latency of this increase in activity begins even before the saccade is initiated, which is known as predictive remapping. Receptive field remapping has been observed in many visual and oculomotor areas such as FEF (Joiner et al 2011, Umeno & Goldberg 1997, Zirnsak et al 2014), LIP (Duhamel et al 1992, Kusunoki & Goldberg 2003), SC (Churan et al 2011, Walker et al 1995), MST (Inaba & Kawano 2014), and V4 (Neupane et al 2016), and has been a proposed mechanism for how this stability is achieved. One area of debate among the remapping literature is whether receptive fields shift in parallel to the saccade (termed future field remapping) (Churan et al 2011, Duhamel et al 1992, Inaba & Kawano 2014, Umeno & Goldberg 1997), converge to the eye movement endpoint (Zirnsak et al 2014), or are a combination of both depending on the direction of the saccade vector (Neupane et al 2016).

While remapping has been studied extensively across many different areas, these studies have relied upon measurements of single neuron activity. Because of this, the mechanism for how visual information is transferred during remapping remains an open question. A parsimonious explanation is the neuron whose receptive field is about to be where the stimulus was, receives information about the stimulus from a neuron whose receptive field was at the location of the stimulus while it was flashed. We hypothesize this transfer of information would be observed through a change in correlated variability between the pair of neurons in question. Which pairs of neurons change their correlated variability would be dependent on the location of the stimulus, the neurons' receptive fields, and the saccade vector, such that a third neuron which is neither encoding the stimulus pre-saccade nor will have its receptive field at the location of the stimulus post-saccade would not exhibit changes in correlated variability with the other neurons (Figure 25).

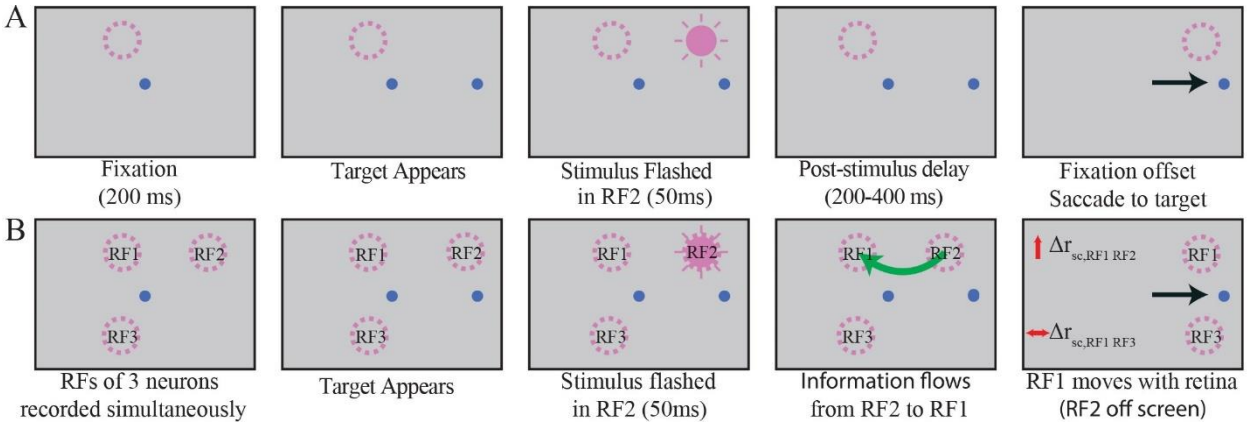

Figure 25: Correlated variability in a remapping paradigm.

A) Remapping paradigm. A dashed pink circle represents a hypothetical receptive field. After fixation, a saccade target appears instructing the monkey to make an eye movement. A stimulus is flashed at the location where the receptive field will be after the saccade is completed. Note the stimulus is extinguished before the receptive field has landed at the location of the target. B) Proposed mechanism for the transfer of information through correlated variability. Neuron 1 (RF1) changes its correlated variability with neuron 2 (RF2) since neuron 2 encodes the stimulus pre-saccade and passes the information to neuron 1. Neuron 1 does not change its correlated variability with neuron 3 since it is not encoding the stimulus.

As the structure or correlated variability is identified in more and more individual areas, a new research direction has emerged, benefiting from the ability to record from multiple brain areas simultaneously. Two studies which examined correlated variability between V1 and MT neurons found that the stimulus (Ruff & Cohen 2016b) and attention (Ruff & Cohen 2016a) have opposite effects on correlated variability within and between areas. On a subset of sessions in Chapter 3, in addition to recording PFC neurons, we were able record from a population of V4 neurons in the same hemisphere. As a first step, we were interested in how correlated variability differed between V4 and PFC based on the tuning properties of PFC neurons. Having identified both contralateral and ipsilateral tuned neurons in chapter 3, we predicted correlated variability would be lower between V4 and ipsilateral tuned PFC neurons. Since most early visual areas have a large contralateral bias, we would expect ipsilateral tuned PFC neurons to receive visual input from the opposite hemisphere, not the same (where our recorded population was). In agreement with our prediction, correlated variability between ipsilateral tuned PFC neurons and V4 neurons was significantly lower than contralateral tuned PFC neurons and V4 neurons (Figure 26). A previous study has highlighted firing rate and correlated variability in PFC neurons may be biased to quadrants of visual space (Leavitt et al 2017), however we saw no difference in correlated variability between pairs in the same hemifield but different quadrants compared to in the same quadrant. Some remaining questions included whether the correlation structure is different for neurons with mixed selectivity, or whether the relationship between correlated variability and reaction time observed in Chapter 2 extends to within and between area interactions in PFC and V4.

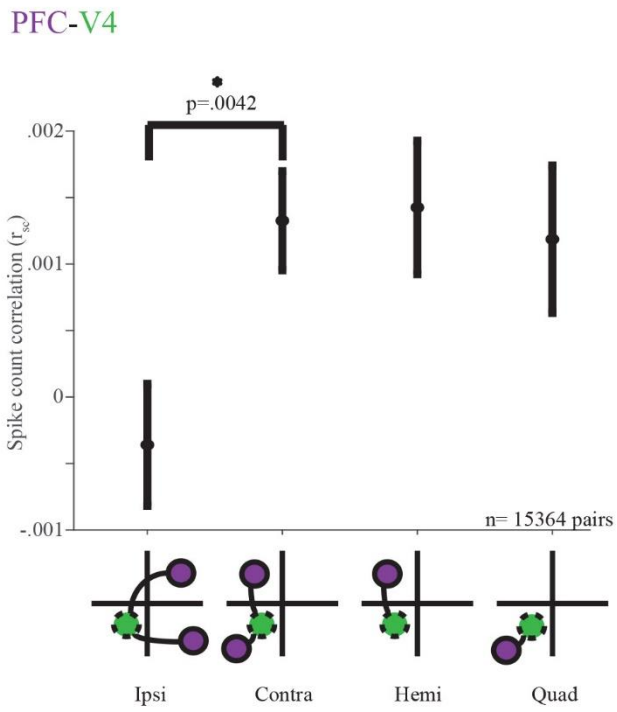

Figure 26: Correlated variability between V4 and PFC.

Correlated variability of V4 neurons with ipsilateral and contralateral tuned neurons. Ipsilateral tuned neurons have significantly lower correlated variability with V4 when compared to contralateral tuned neurons. The contralateral population was also divided into pairs where both neurons were in the same hemifield but not same quadrant ("Hemi") or in the same quadrant ("Quad") but no difference was observed.

4.1.3 Previous reports of dynamic selectivity in PFC

As highlighted in the introduction, research into the neural correlates of working memory has been pursued for decades. In this section, we will highlight studies that directly relate to our findings in Chapter 3, focusing primarily on recent studies involving visual and presaccadic response properties in PFC (Bullock et al 2017), mixed selectivity in PFC (Spaak et al 2017), and a comparison between PFC and FEF encoding in working memory (Parthasarathy et al 2017).

Visual and saccade responses in PFC

The study by Bullock et al (2017) provides the best comparison to our response field findings, given the task is nearly identical and similar analyses were performed. In their study, a memory guided saccade task was also employed albeit with a longer stimulus duration (650 ms compared to 50 ms in ours) and a longer memory period (1300 ms compared to 500 ms). The authors report the distribution of visual, visuomotor, and motor neurons was 32%, 56%, and 12% respectively. Additionally, they found all groups (visual, visuomotor, and motor) had strong contralateral biases, however neurons that exhibited suppression were more likely to be ipsilateral tuned. The authors also examined visual and motor response alignment, calculating the Euclidean distance between the center of the visual and saccade response fields, and concluded they largely overlap. They do note, however, that a small subset (~5 neurons) had large shifts. Finally, the authors highlight evidence of spatial topography within PFC using a measure of spatial autocorrelation, Moran's I.

In our study, PFC neurons were most likely to be visual (56%), followed by motor (30%), and visuomotor (19%). One possibility for the observed differences between studies is there

exists a visual/motor/visuomotor topography within PFC, such that neurons with similar response properties are more likely to be clustered together. This was not examined in our study and to our knowledge has not been reported previously in PFC. A small amount of evidence points to segregation of visual and motor neurons across laminar layers in FEF (Bruce et al 1985), perhaps this trend extends to PFC as well. Additionally, while both findings report suppressive cells to be ipsilaterally biased, our findings also show motor neurons are ipsilaterally biased (particularly for selective neurons, Figure 20). Given the sampling of visual space was consistent across studies (equal number of stimuli presented in each hemifield, maximum target eccentricity 15 degrees), we suspect the observed differences might be due to the limited sample size in the previous study (14 motor neurons vs 236 in our study). The smaller number (compared to our study) of neurons Bullock et al (2017) observed with mixed selectivity could be due to a limited sample size as well. This is where our study is most beneficial, as having nearly 10 times the number of neurons (68 visuomotor vs 629 in our study) allowed us to determine with confidence that neurons with shifting response fields are a legitimate subpopulation. With respect to topographic clustering in PFC, as highlighted in Chapter 3, visual inspection of response field heatmaps with respect to electrode array location did not reveal any appreciable topography, however a more systematic investigation should be performed. Bullock et al (2017) reported evidence of clustering, however this analysis was done on threshold crossings which could be biased if nearby electrodes had localized common noise. Given both results, we believe a conclusion cannot be made either way, and clearly more refined analyses are needed. In summary, the findings in our study and that of Bullock et al (2017) largely agree, with some of the differences most likely arising from a limited sample of neurons or subtle differences between task or analysis methods.

Dynamic selectivity in PFC

Much of the early evidence of dynamic selectivity in PFC was found in the context of some form of a match to sample task. This included matching stimulation frequencies in a vibrotactile task (Barak et al 2010), matching categories (Meyers et al 2008), and a delayed paired associate task (Stokes et al 2013). The contribution of the Spaak et al (2017) study was to demonstrate dynamic coding exists even in one of the simplest working memory paradigms: the memory guided saccade task. The authors used a discriminability measure which was based on the correlation of population activity differences across conditions between 2 independent data sets (Stokes et al 2013). They found the code to be generalizable, meaning discriminability was above chance even when training and testing epochs were not temporally aligned, but also dynamic, meaning cross-temporal discriminability was significantly lower than discriminability when the training and testing epochs were aligned. The authors posited two mechanisms at the single neuron level which could contribute to the dynamic population code. The first was neurons with mixed selectivity throughout the trial, which they found in the range of 26% to 37% of location selective neurons. The second was variability in single neuron latencies, which could affect the population code in conjunction with mixed selectivity or on its own. Using a simulation analysis, the authors concluded both factors underlie the dynamic nature of the population code.

Our results are largely in agreement with that of Spaak et al (2017). We also observed evidence of a dynamic population code in that decoding accuracy decreased when training and testing epochs were not aligned temporally. The extent of how generalizable/dynamic the population code was is difficult to interpret across studies given the different measures used (discriminability vs decoding accuracy). For both, it is clear the discriminability/decoding accuracy is highest when training and testing in the same epoch but can remain high even when

training/testing are temporally separated (generalizable coding). However, larger temporal separations can result in substantial drops in discriminability/decoding accuracy. The authors conclude the primary drivers of the dynamic code are neurons shifting their tuning (mixed selectivity) and temporally changing when they are encoding the task (dynamic subpopulations), which our analyses confirm. Evidence of dynamic subpopulations in our results stem from the latency distribution of PFC neurons being relatively uniform, specifically within the population of ipsilateral tuned neurons (Figure 16). For mixed selectivity, one benefit of our study is the ability to visualize activity in two dimensions, while Spaak et al (2017) only used stimuli at one amplitude, which allowed us to know with confidence we were truly observing the response field of each neuron. The single neuron examples of mixed selectivity from Spaak et al (2017) demonstrate rotations (shifts of 90 degrees) and inversions (shifts of 180 degrees), however no population summary is identified, highlighting another benefit of our study (Figure 19). Finally, although our analysis did not include a simulation demonstrating the dynamics of the population code decrease with the removal of mixed selectivity, it would seem obvious decoding would become more generalizable if we removed neurons from our analysis that shifted their tuning. Nevertheless, this presents a future direction or additional analysis that could be done. In summary, many of the same observations made by Spaak et al (2017) are confirmed in our study with greater spatial resolution and a larger sample of neurons. One novel aspect of our analysis was the comparison with FEF which will be discussed below.

PFC and FEF decoding of working memory

To our knowledge, the only direct comparison of dynamic selectivity between PFC and FEF was done by Parthasarathy et al (2017) during a memory guided saccade task with the addition of a

distractor. The authors employed a pseudo-population analysis within a decoding framework, however it should be noted the recorded PFC neurons were much more anterior than our study (Figure 27 compared to Figure 13). The authors report decoding performance was similar between PFC and FEF after stimulus onset, however for most other time points the PFC population was more accurate. This was particularly evident for decoding during the epoch after distractor presentation, where PFC maintained information about the target while information degraded in FEF. Despite this maintenance of target information when training and testing in the same epoch after the distractor, PFC decoding accuracy dropped significantly when training pre-distractor and testing post-distractor, or vice versa. A much smaller drop in accuracy was observed in FEF, which lead the authors to conclude the PFC population dynamically morphs its code between the target and distractor epochs but maintains information about the target, while the FEF code is stable throughout the trial and loses information after the presentation of the distractor. The authors then identify a subpopulation of neurons in PFC and FEF (25% and 19% respectively) which exhibit nonlinear mixed selectivity, defined as neurons with a significant main effect of spatial location and task epoch, and a significant interaction term using a two-way ANOVA. After removing these nonlinear mixed selectivity neurons from the decoder, the PFC population code became less dynamic. Finally, equilibrating the PFC and FEF populations through adding nonlinear mixed selectivity neurons to FEF or subtracting nonlinear mixed selectivity neurons from PFC made the population code resemble the other area.

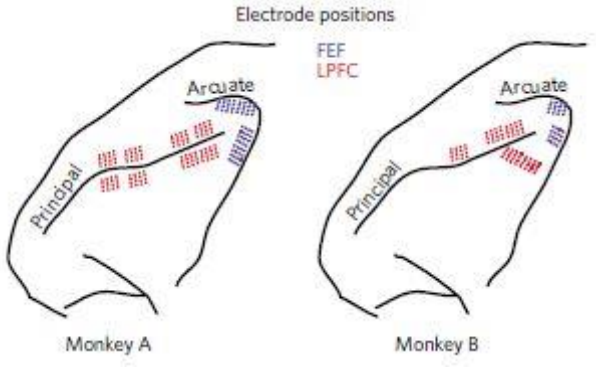

Figure 27: Electrode locations in PFC and FEF.

Note Parthasarathy et al (2017) PFC electrode locations are much more anterior.

In a similar fashion to the comparisons made between our study and Bullock et al (2017), our results are largely consistent with Parthasarathy et al (2017) with some differences that may be meaningful or may be a result of task and analysis differences. Perhaps the most striking difference is between the decoding accuracies in the PFC and FEF populations. Parthasarathy et al (2017) report decoding accuracies in the range of 50% to 65% during the target epoch and ensuing delay period, while our decoding accuracy was between 40% and 50% even with nearly 3 times the number of neurons (256 compared to 770 for our study, Figure 21). Stated differently, for a comparable population size (300 neurons) we observed a decoding accuracy less than 40% during the visual epoch, while in the Parthasarathy et al (2017) reported an accuracy around 65%. For FEF, the opposite trend was observed, where decoding was higher in our analysis (particularly in the delay period, Figure 28). Within PFC, the disparity in findings may be due the recording location of each study, however the opposite trend might be expected as more posterior neurons in PFC tend to have more spatial stimulus properties (Riley et al 2017). Another possible explanation is the target locations were more aligned to PFC response fields in Parthasarathy et al (2017). This may also explain why FEF decoding between studies is

the opposite trend, perhaps our study was more aligned to the FEF population while the Parthasarathy et al (2017) was more aligned to the PFC population. Further evidence this may be the case is our analysis yielded more selective neurons in FEF compared to PFC (Figure 20) while Parthasarathy et al (2017) report the opposite (48% selective neurons in PFC, 27% selective neurons in FEF). A final explanation might be the decoder used (Linear Discriminant Analysis vs Naïve Bayes) although the differences between PFC and FEF make this seem unlikely. If true (LDA better describes PFC, Naïve Bayes better describes FEF) however, this would provide an intriguing result to base future analyses on. The second major difference between the studies was the number of mixed selectivity neurons reported. Of selective neurons, Parthasarathy et al (2017) determined about 50% showed mixed selectivity in PFC and nearly 80% in FEF. It should be noted we didn't explicitly classify neurons as having mixed selectivity or not, but setting a generous criterion that any neuron with an angular difference greater than 30 degrees (45 degrees being the separation between each target location) would result in about 70% of PFC neurons and 50% of FEF neurons having mixed selectivity. One factor which could explain the difference is the lack of a distractor in our task, however we would expect the distractor to increase mixed selectivity in PFC, not decrease it if that is indeed what is driving the population code to morph. Parthasarathy et al (2017) show only one example of a mixed selectivity neuron, which appears to invert its tuning (shift of ~180 degrees) however no population summary is given. Ultimately, this leads us to question whether the ANOVA analysis, whose advantage is it offer a systematic way of labeling neurons as mixed selective or not, is the most accurate method of determining mixed selectivity. In summary, the general findings that mixed selectivity neurons exist in both PFC and FEF, and that PFC contains a more dynamic code is concurrent across studies. Disparate findings are most likely due to subtle task and

analysis differences. Our findings improve upon those of Parthasarathy et al (2017) by identifying single neuron factors which might be responsible for decoding accuracy differences across the regions (direction selectivity and reliability, Figure 22) in addition to providing a more parsimonious method of quantifying mixed selectivity in single neurons.

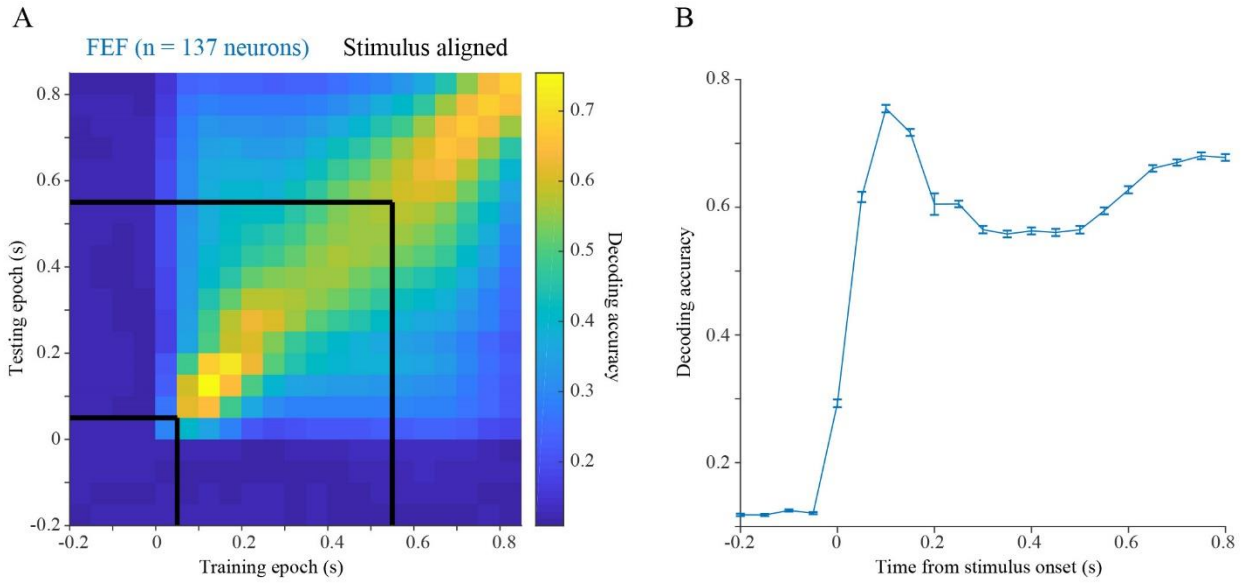

Figure 28: Decoding in FEF.

Decoding accuracy for FEF subpopulations matched to Parthasarathy et al (2017). 137 neurons were randomly selected from the available population (770 neurons) 100 times. A) Decoding accuracy is the average across the 100 iterations from all training and testing time points. B) Decoding accuracy for temporally aligned training and testing epochs (the diagonal of the heatmap). Even with matched number of neurons, decoding accuracy was higher in our study compared to Parthasarathy et al (2017).

4.1.4 Dynamic selectivity in PFC and FEF: limitations and future directions

Limitations

The primary limitation in our study was the lack of spatial conditions in the FEF dataset compared to the PFC dataset. This required us to down sample the number of PFC conditions from 40 to 8 to allow for an equal comparison. To further balance the FEF and PFC datasets, we selected the target amplitude in the PFC conditions that most closely matched the amplitude in the FEF task. When visually inspecting the PFC response field heatmaps, there were clearly neurons which were tuned for more eccentric locations than this amplitude, which would've increased the decoding accuracy had all conditions been used. One piece of evidence supporting this is the number of neurons significantly tuned in the visual and motor epochs (criteria used for the angular difference plots) across all 40 conditions was much larger compared to the subset that was tuned for the FEF matched conditions (Figure 19; 40 conditions = 629 neurons, matched FEF = 152 neurons). A second limitation was given the proximity of FEF and PFC, it is possible some neurons were classified as one area when in reality they were in the another. As mentioned in Chapter 3, stimulation of the PFC electrode array did not evoke saccades, so it seems unlikely FEF neurons were recorded on the PFC array. For the FEF recordings however, penetrations were not necessarily completely normal to cortex and not all grid locations were stimulated to determine if they evoked saccades (any grid location that was directly next to a successful stimulation site was considered FEF). If PFC neurons were in fact recorded in the FEF dataset, this could inflate the number of mixed selectivity neurons observed in FEF and those with ipsilateral tuning. A third limitation was the use of a pseudo-population. We used a pseudo-population primarily to increase the neuron set size for the FEF dataset, where using a session by

session approach would limit our decoding populations to tens of neurons. The use of a pseudo-population removes the ability to analyze any trial by trial measures and their effects on decoding.

Future directions

An obvious expansion upon our current findings would be to perform the PFC analysis on FEF data using the full 40 condition dataset. This would be beneficial for 3 reasons. First, we could be more confident mixed selectivity and ipsilateral tuning exists in FEF with the ability to visualize response field heatmaps in 2 dimensions. Second, we could examine whether any systematic differences occur in response field eccentricity between PFC and FEF, which may be the cause of the large difference in decoding accuracies between the two areas. Finally, we could directly compare whether FEF possesses some of the rich spatial responses observed in PFC, specifically the suppression below baseline.

A second future direction would be to perform the decoding analysis on a session by session basis. This would dovetail nicely with the findings in Chapter 2, as we could determine whether correlated variability influences decoding performance by decoding when the trial structure was preserved and then when it was shuffled randomly. With correlated variability removed, a previous study reported a 6% increase in decoding accuracy for visual and delay activity, but not for saccade (Dehaqani et al 2018).

Expanding upon this finding, it would be interesting to examine how correlated variability, reaction time, and decoding accuracy are all intertwined. The recent advances in electrode array technologies such as the Matrix Array (Neuronexus), which allows for chronic

implantation of linear microelectrode arrays, should increase the yield of simultaneously recorded FEF neurons, making it easier to apply decoding analyses on a session by session basis.

A third direction would be to examine dynamic selectivity in the context of a more complicated working memory task. There is a benefit to the simplicity of the memory guided saccade task in that visual and motor signals are more easily differentiable, however if the goal is to truly understand how working memory is signaled in the brain, more complicated tasks with distractors are necessary. Indeed, one of the main limitations of the persistent activity model is the lack of evidence in tasks with distractors (Lundqvist et al 2018). An intriguing question stemming from this is can neurons shift their tuning more than once in the presence of multiple distractors.

A final future direction involves consideration of neural rhythms and their impact on working memory. Highlighted in the introduction, many previous reports have shown oscillations at the level of the local field potential are modulated during working memory and could in turn modulate spiking activity. Our results remain largely agnostic to this idea, however an analysis which shows shifts in local field potential tuning could further cement the existence of dynamic coding.

4.1.5 Final thoughts: Sensorimotor encoding and dynamic selectivity

Dating as far back as the 19th century and the rise of phrenology, scientists have sought to map cortical areas to specific functions. More recently, the accepted view was different sets of neurons encode different features such as space, motion, objects, and salience. Traditionally, single neurons were thought to increase their activity for a small portion of stimulus space and remain at baseline for all other stimuli, termed the receptive field. While cortex can indeed be

grossly separated into areas that are more sensory or motor, and many cortical areas contain some form of topography, the strict specialization of cortical areas to one feature seems to be the exception more than the rule. Prefrontal cortex is a perfect example, with wide variety of visual, motor, and more abstract signals such as reward, categorization, and rule definition all being encoded in the same cortical space. In particular, how working memory signals are multiplexed within PFC has been a central question in recent years.

One proposal for how this encoding is accomplished is through dynamic selectivity. Indeed, numerous neurophysiological studies have confirmed non-stationary activity during a memory epoch, but how then is the memory stored if there is little to no spiking activity? One model postulates the "activity silent" memory signal is encoded at the level of synaptic weights, termed functional connectivity (Stokes 2015). One study that reinforces this notion found the pattern of synaptic connections was dynamically modulated during a working memory dependent maze task in rodents (Fujisawa et al 2008).

At the level of single neurons, dynamic selectivity is thought to manifest as transient spiking from different subpopulations of neurons (dynamic subpopulations) and shifts in tuning selectivity of individual neurons throughout the memory period (mixed selectivity). Both these phenomena are thought to add additional dimensionality to the network (Stokes 2015), where high dimensional neural representations have the benefit of allowing simple linear readouts such as linear classifiers to discriminate a large set of input-output relations (Rigotti et al 2013). A high dimensional representation may be beneficial in complex tasks such as a match to sample or categorization task, but is it necessary for the memory guided saccade task? Within the arm reaching literature, preparatory activity transitions from a high dimensional "null" subspace to a "potent" subspace, ensuring the reach is made at the appropriate time (Kaufman et al 2014).

Whether working memory is stored as persistent (but perhaps not stationary) activity or transient dynamic activity still remains an open question. It is clear in some working memory tasks a subspace can be defined where stimulus and memory representations are stable (Murray et al 2017), presumably relying on neurons that have high persistent firing that may vary temporally. However, other studies have shown when removing neurons with persistent firing, it is still possible to decode the memory trace (Baeg et al 2003, Meyers et al 2008). One review notes stationary codes seem present when simple stimulus attributes need to be remembered while dynamic codes are present when more complex transformations are necessary, and that persistent activity tends to be observed in the anterior-dorsal region of PFC while posterior-dorsal regions exhibit more dynamic representations (Meyers 2018). Furthermore, rodent studies have shown neurons remain active in short transient bursts (Bolkan et al 2017, Runyan et al 2017), while persistent activity has only been observed in primates, suggesting perhaps an evolutionary component to persistent activity. Ultimately, further studies are needed, such as whether the stable subspace model functions in the presence of a distractor and whether the "activity silent" synaptic changes are observed in primates.

In this dissertation, we studied two prefrontal areas, PFC and FEF, and investigated how visual and motor signals are parsed in a simple memory guided saccade task. We first highlight visual and motor encoding can occur at distinct levels acting through increases in firing rate and changes in correlated variability. While correlated variability is not as direct a measurement of functional connectivity as synaptic changes are, it nonetheless influences eye movement planning, and could be another means by which to measure the "activity silent" state. Secondly, the richness in response dynamics at both the spatial and temporal level in PFC neurons expand upon the notion of the traditional receptive field. These responses result in a dynamic population

code and could signal the transition between “null” and “potent” subspaces. While both these notions need further examination, our results add novel findings at the single neuron, pairwise, and population level that should be considered when forming models of sensorimotor encoding and working memory.

BIBLIOGRAPHY

Abbott LF, Dayan P. 1999. The effect of correlated variability on the accuracy of a population code. *Neural Comput* 11: 91-101

Adibi M, McDonald JS, Clifford CW, Arabzadeh E. 2014. Population decoding in rat barrel cortex: optimizing the linear readout of correlated population responses. *PLoS Comput Biol* 10: e1003415

Anderson JC, Kennedy H, Martin KA. 2011. Pathways of attention: synaptic relationships of frontal eye field to V4, lateral intraparietal cortex, and area 46 in macaque monkey. *J Neurosci* 31: 10872-81

Asaad WF, Rainer G, Miller EK. 1998. Neural activity in the primate prefrontal cortex during associative learning. *Neuron* 21: 1399-407

Astrand E, Wardak C, Baraduc P, Ben Hamed S. 2016. Direct Two-Dimensional Access to the Spatial Location of Covert Attention in Macaque Prefrontal Cortex. *Curr Biol* 26: 1699-704

Averbeck BB, Latham PE, Pouget A. 2006. Neural correlations, population coding and computation. *Nat Rev Neurosci* 7: 358-66

Averbeck BB, Lee D. 2003. Neural noise and movement-related codes in the macaque supplementary motor area. *J Neurosci* 23: 7630-41

Baeg EH, Kim YB, Huh K, Mook-Jung I, Kim HT, Jung MW. 2003. Dynamics of population code for working memory in the prefrontal cortex. *Neuron* 40: 177-88

Bahill AT, Clark MR, Stark L. 1975. The main sequence, a tool for studying human eye movements. *Mathematical Biosciences* 24: 191-204

Bair W, Zohary E, Newsome WT. 2001. Correlated firing in macaque visual area MT: time scales and relationship to behavior. *J Neurosci* 21: 1676-97

Barak O, Sussillo D, Romo R, Tsodyks M, Abbott LF. 2013. From fixed points to chaos: three models of delayed discrimination. *Prog Neurobiol* 103: 214-22

Barak O, Tsodyks M, Romo R. 2010. Neuronal population coding of parametric working memory. *J Neurosci* 30: 9424-30

Barbas H, Pandya DN. 1989. Architecture and intrinsic connections of the prefrontal cortex in the rhesus monkey. *J Comp Neurol* 286: 353-75

Barone P, Joseph JP. 1989. Prefrontal cortex and spatial sequencing in macaque monkey. *Exp Brain Res* 78: 447-64

Batuev AS. 1994. Two neuronal systems involved in short-term spatial memory in monkeys. *Acta Neurobiol Exp (Wars)* 54: 335-44

Ben Hamed S, Duhamel JR, Bremmer F, Graf W. 2001. Representation of the visual field in the lateral intraparietal area of macaque monkeys: a quantitative receptive field analysis. *Exp Brain Res* 140: 127-44

Blatt GJ, Andersen RA, Stoner GR. 1990. Visual receptive field organization and cortico-cortical connections of the lateral intraparietal area (area LIP) in the macaque. *J Comp Neurol* 299: 421-45

Boch RA, Goldberg ME. 1989. Participation of prefrontal neurons in the preparation of visually guided eye movements in the rhesus monkey. *J Neurophysiol* 61: 1064-84

Bolkan SS, Stujenske JM, Parnaudeau S, Spellman TJ, Rauffenbart C, et al. 2017. Thalamic projections sustain prefrontal activity during working memory maintenance. *Nat Neurosci* 20: 987-96

Brainard DH. 1997. The Psychophysics Toolbox. *Spat Vis* 10: 433-6

Brody CD, Hernandez A, Zainos A, Romo R. 2003. Timing and neural encoding of somatosensory parametric working memory in macaque prefrontal cortex. *Cereb Cortex* 13: 1196-207

Brown JW, Hanes DP, Schall JD, Stuphorn V. 2008. Relation of frontal eye field activity to saccade initiation during a countermanding task. *Exp Brain Res* 190: 135-51

Bruce CJ, Goldberg ME. 1985. Primate frontal eye fields. I. Single neurons discharging before saccades. *J Neurophysiol* 53: 603-35

Bruce CJ, Goldberg ME, Bushnell MC, Stanton GB. 1985. Primate frontal eye fields. II. Physiological and anatomical correlates of electrically evoked eye movements. *J Neurophysiol* 54: 714-34

Bullock KR, Pieper F, Sachs AJ, Martinez-Trujillo JC. 2017. Visual and presaccadic activity in area 8Ar of the macaque monkey lateral prefrontal cortex. *J Neurophysiol* 118: 15-28

Burman DD, Segraves MA. 1994. Primate frontal eye field activity during natural scanning eye movements. *J Neurophysiol* 71: 1266-71

Butters N, Pandya D. 1969. Retention of delayed-alternation: effect of selective lesions of sulcus principalis. *Science* 165: 1271-3

Chafee MV, Goldman-Rakic PS. 1998. Matching patterns of activity in primate prefrontal area 8a and parietal area 7ip neurons during a spatial working memory task. *J Neurophysiol* 79: 2919-40

Chafee MV, Goldman-Rakic PS. 2000. Inactivation of parietal and prefrontal cortex reveals interdependence of neural activity during memory-guided saccades. *J Neurophysiol* 83: 1550-66

Chang MH, Armstrong KM, Moore T. 2012. Dissociation of response variability from firing rate effects in frontal eye field neurons during visual stimulation, working memory, and attention. *J Neurosci* 32: 2204-16

Churan J, Guitton D, Pack CC. 2011. Context dependence of receptive field remapping in superior colliculus. *J Neurophysiol* 106: 1862-74

Churchland MM, Shenoy KV. 2007. Temporal complexity and heterogeneity of single-neuron activity in premotor and motor cortex. *J Neurophysiol* 97: 4235-57

Churchland MM, Yu BM, Cunningham JP, Sugrue LP, Cohen MR, et al. 2010. Stimulus onset quenches neural variability: a widespread cortical phenomenon. *Nat Neurosci* 13: 369-78

Clark KL, Noudoost B, Moore T. 2012. Persistent spatial information in the frontal eye field during object-based short-term memory. *J Neurosci* 32: 10907-14

Cohen JY, Crowder EA, Heitz RP, Subraveti CR, Thompson KG, et al. 2010. Cooperation and competition among frontal eye field neurons during visual target selection. *J Neurosci* 30: 3227-38

Cohen MR, Kohn A. 2011. Measuring and interpreting neuronal correlations. *Nat Neurosci* 14: 811-9

Cohen MR, Maunsell JH. 2009. Attention improves performance primarily by reducing interneuronal correlations. *Nat Neurosci* 12: 1594-600

Compte A, Brunel N, Goldman-Rakic PS, Wang XJ. 2000. Synaptic mechanisms and network dynamics underlying spatial working memory in a cortical network model. *Cereb Cortex* 10: 910-23

Constantinidis C, Franowicz MN, Goldman-Rakic PS. 2001a. Coding specificity in cortical microcircuits: a multiple-electrode analysis of primate prefrontal cortex. *J Neurosci* 21: 3646-55

Constantinidis C, Franowicz MN, Goldman-Rakic PS. 2001b. The sensory nature of mnemonic representation in the primate prefrontal cortex. *Nat Neurosci* 4: 311-6

Crapse TB, Sommer MA. 2009. Frontal eye field neurons with spatial representations predicted by their subcortical input. *J Neurosci* 29: 5308-18

Crapse TB, Sommer MA. 2012. Frontal eye field neurons assess visual stability across saccades. *J Neurosci* 32: 2835-45

Curtis CE, D'Esposito M. 2003. Persistent activity in the prefrontal cortex during working memory. *Trends Cogn Sci* 7: 415-23

Cynader M, Berman N. 1972. Receptive-field organization of monkey superior colliculus. *J Neurophysiol* 35: 187-201

de la Rocha J, Doiron B, Shea-Brown E, Josic K, Reyes A. 2007. Correlation between neural spike trains increases with firing rate. *Nature* 448: 802-6

Dehaqani MA, Vahabie AH, Parsa M, Noudoost B, Soltani A. 2018. Selective Changes in Noise Correlations Contribute to an Enhanced Representation of Saccadic Targets in Prefrontal Neuronal Ensembles. *Cereb Cortex* 28: 3046-63

Desimone R, Ungerleider LG. 1986. Multiple visual areas in the caudal superior temporal sulcus of the macaque. *J Comp Neurol* 248: 164-89

Dias EC, Kiesau M, Segraves MA. 1995. Acute activation and inactivation of macaque frontal eye field with GABA-related drugs. *J Neurophysiol* 74: 2744-8

Dias EC, Segraves MA. 1999. Muscimol-induced inactivation of monkey frontal eye field: effects on visually and memory-guided saccades. *J Neurophysiol* 81: 2191-214

Ding L, Gold JI. 2012. Neural correlates of perceptual decision making before, during, and after decision commitment in monkey frontal eye field. *Cereb Cortex* 22: 1052-67

Donahue CH, Lee D. 2015. Dynamic routing of task-relevant signals for decision making in dorsolateral prefrontal cortex. *Nat Neurosci* 18: 295-301

Dorris MC, Pare M, Munoz DP. 1997. Neuronal activity in monkey superior colliculus related to the initiation of saccadic eye movements. *J Neurosci* 17: 8566-79

Duhamel JR, Colby CL, Goldberg ME. 1992. The updating of the representation of visual space in parietal cortex by intended eye movements. *Science* 255: 90-2

Ecker AS, Berens P, Keliris GA, Bethge M, Logothetis NK, Tolias AS. 2010. Decorrelated neuronal firing in cortical microcircuits. *Science* 327: 584-7

Ekstrom LB, Roelfsema PR, Arsenault JT, Bonmassar G, Vanduffel W. 2008. Bottom-up dependent gating of frontal signals in early visual cortex. *Science* 321: 414-7

Elsayed GF, Lara AH, Kaufman MT, Churchland MM, Cunningham JP. 2016. Reorganization between preparatory and movement population responses in motor cortex. *Nat Commun* 7: 13239

Engbert R, Kliegl R. 2003. Microsaccades uncover the orientation of covert attention. *Vision Res* 43: 1035-45

Everling S, Dorris MC, Munoz DP. 1998. Reflex suppression in the anti-saccade task is dependent on prestimulus neural processes. *J Neurophysiol* 80: 1584-9

Everling S, Munoz DP. 2000. Neuronal correlates for preparatory set associated with pro-saccades and anti-saccades in the primate frontal eye field. *J Neurosci* 20: 387-400

Felleman DJ, Van Essen DC. 1991. Distributed hierarchical processing in the primate cerebral cortex. *Cereb Cortex* 1: 1-47

Ferrier D. 1874. On the Localisation of the Functions of the Brain. *Br Med J* 2: 766-7

Fries P, Womelsdorf T, Oostenveld R, Desimone R. 2008. The effects of visual stimulation and selective visual attention on rhythmic neuronal synchronization in macaque area V4. *J Neurosci* 28: 4823-35

Fujisawa S, Amarasingham A, Harrison MT, Buzsaki G. 2008. Behavior-dependent short-term assembly dynamics in the medial prefrontal cortex. *Nat Neurosci* 11: 823-33

Fukushima J, Fukushima K, Miyasaka K, Yamashita I. 1994. Voluntary control of saccadic eye movement in patients with frontal cortical lesions and parkinsonian patients in comparison with that in schizophrenics. *Biol Psychiatry* 36: 21-30

Funahashi S. 2014. Saccade-related activity in the prefrontal cortex: its role in eye movement control and cognitive functions. *Front Integr Neurosci* 8: 54

Funahashi S. 2015. Functions of delay-period activity in the prefrontal cortex and mnemonic scotomas revisited. *Front Syst Neurosci* 9: 2

Funahashi S, Bruce CJ, Goldman-Rakic PS. 1989. Mnemonic coding of visual space in the monkey's dorsolateral prefrontal cortex. *J Neurophysiol* 61: 331-49

Funahashi S, Bruce CJ, Goldman-Rakic PS. 1990. Visuospatial coding in primate prefrontal neurons revealed by oculomotor paradigms. *J Neurophysiol* 63: 814-31

Funahashi S, Bruce CJ, Goldman-Rakic PS. 1991. Neuronal activity related to saccadic eye movements in the monkey's dorsolateral prefrontal cortex. *J Neurophysiol* 65: 1464-83

Fuster JM. 1973. Unit activity in prefrontal cortex during delayed-response performance: neuronal correlates of transient memory. *J Neurophysiol* 36: 61-78

Fuster JM, Alexander GE. 1971. Neuron activity related to short-term memory. *Science* 173: 652-4

Gattass R, Gross CG. 1981. Visual topography of striate projection zone (MT) in posterior superior temporal sulcus of the macaque. *J Neurophysiol* 46: 621-38

Gattass R, Gross CG, Sandell JH. 1981. Visual topography of V2 in the macaque. *J Comp Neurol* 201: 519-39

Gattass R, Sousa AP, Gross CG. 1988. Visuotopic organization and extent of V3 and V4 of the macaque. *J Neurosci* 8: 1831-45

Goldberg ME, Bruce CJ. 1990. Primate frontal eye fields. III. Maintenance of a spatially accurate saccade signal. *J Neurophysiol* 64: 489-508

Goldberg ME, Wurtz RH. 1972. Activity of superior colliculus in behaving monkey. I. Visual receptive fields of single neurons. *J Neurophysiol* 35: 542-59

Goldman-Rakic PS. 1995. Cellular basis of working memory. *Neuron* 14: 477-85

Gray CM, Singer W. 1989. Stimulus-specific neuronal oscillations in orientation columns of cat visual cortex. *Proc Natl Acad Sci U S A* 86: 1698-702

Gregoriou GG, Gotts SJ, Desimone R. 2012. Cell-type-specific synchronization of neural activity in FEF with V4 during attention. *Neuron* 73: 581-94

Gutnisky DA, Dragoi V. 2008. Adaptive coding of visual information in neural populations. *Nature* 452: 220-4

Hall WC, Moschovakis AK. 2003. *The superior colliculus: new approaches for studying sensorimotor integration*. CRC Press.

Hanes DP, Patterson WF, 2nd, Schall JD. 1998. Role of frontal eye fields in countermanding saccades: visual, movement, and fixation activity. *J Neurophysiol* 79: 817-34

Hanes DP, Schall JD. 1996. Neural control of voluntary movement initiation. *Science* 274: 427-30

Hauser CK, Zhu D, Stanford TR, Salinas E. 2018. Motor selection dynamics in FEF explain the reaction time variance of saccades to single targets. *Elife* 7

Heitz RP, Schall JD. 2012. Neural mechanisms of speed-accuracy tradeoff. *Neuron* 76: 616-28

Heitz RP, Schall JD. 2013. Neural chronometry and coherency across speed-accuracy demands reveal lack of homomorphism between computational and neural mechanisms of evidence accumulation. *Philos Trans R Soc Lond B Biol Sci* 368: 20130071

Helminski JO, Segraves MA. 2003. Macaque frontal eye field input to saccade-related neurons in the superior colliculus. *J Neurophysiol* 90: 1046-62

Herrero JL, Gieselmann MA, Sanayei M, Thiele A. 2013. Attention-induced variance and noise correlation reduction in macaque V1 is mediated by NMDA receptors. *Neuron* 78: 729-39

Hikosaka O, Wurtz RH. 1983. Visual and oculomotor functions of monkey substantia nigra pars reticulata. III. Memory-contingent visual and saccade responses. *J Neurophysiol* 49: 1268-84

Hoshi E, Shima K, Tanji J. 1998. Task-dependent selectivity of movement-related neuronal activity in the primate prefrontal cortex. *J Neurophysiol* 80: 3392-7

Howard MW, Rizzuto DS, Caplan JB, Madsen JR, Lisman J, et al. 2003. Gamma oscillations correlate with working memory load in humans. *Cereb Cortex* 13: 1369-74

Huang X, Lisberger SG. 2009. Noise correlations in cortical area MT and their potential impact on trial-by-trial variation in the direction and speed of smooth-pursuit eye movements. *J Neurophysiol* 101: 3012-30

Hussar C, Pasternak T. 2010. Trial-to-trial variability of the prefrontal neurons reveals the nature of their engagement in a motion discrimination task. *Proc Natl Acad Sci U S A* 107: 21842-7

Iba M, Sawaguchi T. 2002. Neuronal activity representing visuospatial mnemonic processes associated with target selection in the monkey dorsolateral prefrontal cortex. *Neurosci Res* 43: 9-22

Inaba N, Kawano K. 2014. Neurons in cortical area MST remap the memory trace of visual motion across saccadic eye movements. *Proc Natl Acad Sci U S A* 111: 7825-30

Izawa Y, Suzuki H, Shinoda Y. 2005. Initiation and suppression of saccades by the frontal eye field in the monkey. *Ann N Y Acad Sci* 1039: 220-31

Jagadisan UK, Gandhi NJ. 2017. Removal of inhibition uncovers latent movement potential during preparation. *Elife* 6

Jagadisan UK, Gandhi NJ. 2018. Population Temporal Structure Supplements The Rate Code During Sensorimotor Transformations. *bioRxiv*

Jantz JJ, Watanabe M, Everling S, Munoz DP. 2013. Threshold mechanism for saccade initiation in frontal eye field and superior colliculus. *J Neurophysiol* 109: 2767-80

Joiner WM, Cavanaugh J, Wurtz RH. 2011. Modulation of shifting receptive field activity in frontal eye field by visual salience. *J Neurophysiol* 106: 1179-90

Jun JK, Miller P, Hernandez A, Zainos A, Lemus L, et al. 2010. Heterogenous population coding of a short-term memory and decision task. *J Neurosci* 30: 916-29

Kaufman MT, Churchland MM, Ryu SI, Shenoy KV. 2014. Cortical activity in the null space: permitting preparation without movement. *Nat Neurosci* 17: 440-8

Kelly RC, Smith MA, Samonds JM, Kohn A, Bonds AB, et al. 2007. Comparison of recordings from microelectrode arrays and single electrodes in the visual cortex. *J Neurosci* 27: 261-4

Kiani R, Cueva CJ, Reppas JB, Peixoto D, Ryu SI, Newsome WT. 2015. Natural grouping of neural responses reveals spatially segregated clusters in prearcuate cortex. *Neuron* 85: 1359-73

Kleiner M, Brainard D, Pelli D, Ingling A, Murray R, Broussard C. 2007. What's new in Psychtoolbox-3. *Perception* 36: 1

Knight TA, Fuchs AF. 2007. Contribution of the frontal eye field to gaze shifts in the head-unrestrained monkey: effects of microstimulation. *J Neurophysiol* 97: 618-34

Kohn A, Smith MA. 2005. Stimulus dependence of neuronal correlation in primary visual cortex of the macaque. *J Neurosci* 25: 3661-73

Kojima S. 1980. Prefrontal unit activity in the monkey: relation to visual stimuli and movements. *Exp Neurol* 69: 110-23

Kritzer MF, Goldman-Rakic PS. 1995. Intrinsic circuit organization of the major layers and sublayers of the dorsolateral prefrontal cortex in the rhesus monkey. *J Comp Neurol* 359: 131-43

Kubota K, Niki H. 1971. Prefrontal cortical unit activity and delayed alternation performance in monkeys. *J Neurophysiol* 34: 337-47

Kusunoki M, Goldberg ME. 2003. The time course of perisaccadic receptive field shifts in the lateral intraparietal area of the monkey. *J Neurophysiol* 89: 1519-27

Lawrence BM, White RL, 3rd, Snyder LH. 2005. Delay-period activity in visual, visuomovement, and movement neurons in the frontal eye field. *J Neurophysiol* 94: 1498-508

Leavitt ML, Pieper F, Sachs A, Joober R, Martinez-Trujillo JC. 2013. Structure of spike count correlations reveals functional interactions between neurons in dorsolateral prefrontal cortex area 8a of behaving primates. *PLoS One* 8: e61503

Leavitt ML, Pieper F, Sachs AJ, Martinez-Trujillo JC. 2017. A Quadrantic Bias in Prefrontal Representation of Visual-Mnemonic Space. *Cereb Cortex*: 1-17

Lee D, Port NL, Kruse W, Georgopoulos AP. 1998. Variability and correlated noise in the discharge of neurons in motor and parietal areas of the primate cortex. *J Neurosci* 18: 1161-70

Leigh RJ, Zee DS. 2015. *The Neurology of Eye Movements*.

Lennert T, Martinez-Trujillo JC. 2013. Prefrontal neurons of opposite spatial preference display distinct target selection dynamics. *J Neurosci* 33: 9520-9

Leon MI, Shadlen MN. 1999. Effect of expected reward magnitude on the response of neurons in the dorsolateral prefrontal cortex of the macaque. *Neuron* 24: 415-25

Lim S, Goldman MS. 2013. Balanced cortical microcircuitry for maintaining information in working memory. *Nat Neurosci* 16: 1306-14

Lundqvist M, Herman P, Miller EK. 2018. Working Memory: Delay Activity, Yes! Persistent Activity? Maybe Not. *J Neurosci* 38: 7013-19

Lundqvist M, Rose J, Herman P, Brincat SL, Buschman TJ, Miller EK. 2016. Gamma and Beta Bursts Underlie Working Memory. *Neuron* 90: 152-64

Marino RA, Munoz DP. 2009. The effects of bottom-up target luminance and top-down spatial target predictability on saccadic reaction times. *Exp Brain Res* 197: 321-35

Meyers EM. 2018. Dynamic population coding and its relationship to working memory. *J Neurophysiol*

Meyers EM, Freedman DJ, Kreiman G, Miller EK, Poggio T. 2008. Dynamic population coding of category information in inferior temporal and prefrontal cortex. *J Neurophysiol* 100: 1407-19

Mikami A, Ito S, Kubota K. 1982. Visual response properties of dorsolateral prefrontal neurons during visual fixation task. *J Neurophysiol* 47: 593-605

Miller EK. 2000. The prefrontal cortex and cognitive control. *Nat Rev Neurosci* 1: 59-65

Miller EK, Cohen JD. 2001. An integrative theory of prefrontal cortex function. *Annu Rev Neurosci* 24: 167-202

Mitchell JF, Sundberg KA, Reynolds JH. 2009. Spatial attention decorrelates intrinsic activity fluctuations in macaque area V4. *Neuron* 63: 879-88

Moore T, Armstrong KM. 2003. Selective gating of visual signals by microstimulation of frontal cortex. *Nature* 421: 370-3

Moore T, Fallah M. 2004. Microstimulation of the frontal eye field and its effects on covert spatial attention. *J Neurophysiol* 91: 152-62

Munoz DP, Everling S. 2004. Look away: the anti-saccade task and the voluntary control of eye movement. *Nat Rev Neurosci* 5: 218-28

Murray JD, Bernacchia A, Roy NA, Constantinidis C, Romo R, Wang XJ. 2017. Stable population coding for working memory coexists with heterogeneous neural dynamics in prefrontal cortex. *Proc Natl Acad Sci U S A* 114: 394-99

Neupane S, Guitton D, Pack CC. 2016. Two distinct types of remapping in primate cortical area V4. *Nat Commun* 7: 10402

Ni AM, Ruff DA, Alberts JJ, Symmonds J, Cohen MR. 2018. Learning and attention reveal a general relationship between population activity and behavior. *Science* 359: 463-65

Nirenberg S, Latham PE. 2003. Decoding neuronal spike trains: how important are correlations? *Proc Natl Acad Sci U S A* 100: 7348-53

Pare M, Hanes DP. 2003. Controlled movement processing: superior colliculus activity associated with countermanded saccades. *J Neurosci* 23: 6480-9

Parthasarathy A, Herikstad R, Bong JH, Medina FS, Libedinsky C, Yen SC. 2017. Mixed selectivity morphs population codes in prefrontal cortex. *Nat Neurosci* 20: 1770-79

Patel GH, Shulman GL, Baker JT, Akbudak E, Snyder AZ, et al. 2010. Topographic organization of macaque area LIP. *Proc Natl Acad Sci U S A* 107: 4728-33

Pelli DG. 1997. The VideoToolbox software for visual psychophysics: transforming numbers into movies. *Spat Vis* 10: 437-42

Pesaran B, Pezaris JS, Sahani M, Mitra PP, Andersen RA. 2002. Temporal structure in neuronal activity during working memory in macaque parietal cortex. *Nat Neurosci* 5: 805-11

Pierrot-Deseilligny C, Rivaud S, Gaymard B, Agid Y. 1991. Cortical control of memory-guided saccades in man. *Exp Brain Res* 83: 607-17

Ploner CJ, Gaymard BM, Rivaud-Pechoux S, Pierrot-Deseilligny C. 2005. The prefrontal substrate of reflexive saccade inhibition in humans. *Biol Psychiatry* 57: 1159-65

Pouget P, Stepniewska I, Crowder EA, Leslie MW, Emeric EE, et al. 2009. Visual and motor connectivity and the distribution of calcium-binding proteins in macaque frontal eye field: implications for saccade target selection. *Front Neuroanat* 3: 2

Purcell BA, Heitz RP, Cohen JY, Schall JD. 2012. Response variability of frontal eye field neurons modulates with sensory input and saccade preparation but not visual search salience. *J Neurophysiol* 108: 2737-50

Qi XL, Meyer T, Stanford TR, Constantinidis C. 2011. Changes in prefrontal neuronal activity after learning to perform a spatial working memory task. *Cereb Cortex* 21: 2722-32

Rainer G, Asaad WF, Miller EK. 1998. Memory fields of neurons in the primate prefrontal cortex. *Proc Natl Acad Sci U S A* 95: 15008-13

Rainer G, Miller EK. 2002. Timecourse of object-related neural activity in the primate prefrontal cortex during a short-term memory task. *Eur J Neurosci* 15: 1244-54

Ray S, Pouget P, Schall JD. 2009. Functional distinction between visuomovement and movement neurons in macaque frontal eye field during saccade countermanding. *J Neurophysiol* 102: 3091-100

Rigotti M, Barak O, Warden MR, Wang XJ, Daw ND, et al. 2013. The importance of mixed selectivity in complex cognitive tasks. *Nature* 497: 585-90

Riley MR, Constantinidis C. 2015. Role of Prefrontal Persistent Activity in Working Memory. *Front Syst Neurosci* 9: 181

Riley MR, Qi XL, Constantinidis C. 2017. Functional specialization of areas along the anterior-posterior axis of the primate prefrontal cortex. *Cereb Cortex* 27: 3683-97

Robinson DA, Fuchs AF. 1969. Eye movements evoked by stimulation of frontal eye fields. *J Neurophysiol* 32: 637-48

Romo R, Brody CD, Hernandez A, Lemus L. 1999. Neuronal correlates of parametric working memory in the prefrontal cortex. *Nature* 399: 470-3

Ruff DA, Cohen MR. 2014a. Attention can either increase or decrease spike count correlations in visual cortex. *Nat Neurosci* 17: 1591-7

Ruff DA, Cohen MR. 2014b. Global cognitive factors modulate correlated response variability between V4 neurons. *J Neurosci* 34: 16408-16

Ruff DA, Cohen MR. 2016a. Attention Increases Spike Count Correlations between Visual Cortical Areas. *J Neurosci* 36: 7523-34

Ruff DA, Cohen MR. 2016b. Stimulus Dependence of Correlated Variability across Cortical Areas. *J Neurosci* 36: 7546-56

Runyan CA, Piasini E, Panzeri S, Harvey CD. 2017. Distinct timescales of population coding across cortex. *Nature* 548: 92-96

Sajad A, Sadeh M, Keith GP, Yan X, Wang H, Crawford JD. 2015. Visual-Motor Transformations Within Frontal Eye Fields During Head-Unrestrained Gaze Shifts in the Monkey. *Cereb Cortex* 25: 3932-52

Saslow MG. 1967. Latency for saccadic eye movement. *J Opt Soc Am* 57: 1030-3

Sato TR, Schall JD. 2003. Effects of stimulus-response compatibility on neural selection in frontal eye field. *Neuron* 38: 637-48

Sawaguchi T, Yamane I. 1999. Properties of delay-period neuronal activity in the monkey dorsolateral prefrontal cortex during a spatial delayed matching-to-sample task. *J Neurophysiol* 82: 2070-80

Schall JD. 2002. The neural selection and control of saccades by the frontal eye field. *Philos Trans R Soc Lond B Biol Sci* 357: 1073-82

Schall JD, Hanes DP, Thompson KG, King DJ. 1995a. Saccade target selection in frontal eye field of macaque. I. Visual and premovement activation. *J Neurosci* 15: 6905-18

Schall JD, Morel A, King DJ, Bullier J. 1995b. Topography of visual cortex connections with frontal eye field in macaque: convergence and segregation of processing streams. *J Neurosci* 15: 4464-87

Schiller PH, Chou IH. 1998. The effects of frontal eye field and dorsomedial frontal cortex lesions on visually guided eye movements. *Nat Neurosci* 1: 248-53

Schiller PH, Koerner F. 1971. Discharge characteristics of single units in superior colliculus of the alert rhesus monkey. *J Neurophysiol* 34: 920-36

Schiller PH, Sandell JH, Maunsell JH. 1987. The effect of frontal eye field and superior colliculus lesions on saccadic latencies in the rhesus monkey. *J Neurophysiol* 57: 1033-49

Schiller PH, True SD, Conway JL. 1980. Deficits in eye movements following frontal eye-field and superior colliculus ablations. *J Neurophysiol* 44: 1175-89

Schlag J, Schlag-Rey M. 1987. Evidence for a supplementary eye field. *J Neurophysiol* 57: 179-200

Shadlen MN, Newsome WT. 1998. The variable discharge of cortical neurons: implications for connectivity, computation, and information coding. *J Neurosci* 18: 3870-96

Shoham S, Fellows MR, Normann RA. 2003. Robust, automatic spike sorting using mixtures of multivariate t-distributions. *J Neurosci Methods* 127: 111-22

Smith MA, Bair W, Movshon JA. 2002. Signals in macaque striate cortical neurons that support the perception of glass patterns. *J Neurosci* 22: 8334-45

Smith MA, Kohn A. 2008. Spatial and temporal scales of neuronal correlation in primary visual cortex. *J Neurosci* 28: 12591-603

Smith MA, Majaj NJ, Movshon JA. 2005. Dynamics of motion signaling by neurons in macaque area MT. *Nat Neurosci* 8: 220-8

Smith MA, Sommer MA. 2013. Spatial and temporal scales of neuronal correlation in visual area V4. *J Neurosci* 33: 5422-32

Snyder AC, Issar D, Smith MA. 2018. What does scalp electroencephalogram coherence tell us about long-range cortical networks? *Eur J Neurosci*

Snyder AC, Morais MJ, Kohn A, Smith MA. 2014. Correlations in V1 are reduced by stimulation outside the receptive field. *J Neurosci* 34: 11222-7

Snyder AC, Morais MJ, Smith MA. 2016. Dynamics of excitatory and inhibitory networks are differentially altered by selective attention. *J Neurophysiol* 116: 1807-20

Snyder AC, Morais MJ, Willis CM, Smith MA. 2015. Global network influences on local functional connectivity. *Nat Neurosci* 18: 736-43

Sommer MA, Tehovnik EJ. 1997. Reversible inactivation of macaque frontal eye field. *Exp Brain Res* 116: 229-49

Sommer MA, Wurtz RH. 1998. Frontal eye field neurons orthodromically activated from the superior colliculus. *J Neurophysiol* 80: 3331-5

Sommer MA, Wurtz RH. 2000. Composition and topographic organization of signals sent from the frontal eye field to the superior colliculus. *J Neurophysiol* 83: 1979-2001

Sommer MA, Wurtz RH. 2006. Influence of the thalamus on spatial visual processing in frontal cortex. *Nature* 444: 374-7

Spaak E, Watanabe K, Funahashi S, Stokes MG. 2017. Stable and Dynamic Coding for Working Memory in Primate Prefrontal Cortex. *J Neurosci* 37: 6503-16

Stanton GB, Deng SY, Goldberg ME, McMullen NT. 1989. Cytoarchitectural characteristic of the frontal eye fields in macaque monkeys. *J Comp Neurol* 282: 415-27

Stanton GB, Goldberg ME, Bruce CJ. 1988. Frontal eye field efferents in the macaque monkey: II. Topography of terminal fields in midbrain and pons. *J Comp Neurol* 271: 493-506

Stokes MG. 2015. 'Activity-silent' working memory in prefrontal cortex: a dynamic coding framework. *Trends Cogn Sci* 19: 394-405

Stokes MG, Kusunoki M, Sigala N, Nili H, Gaffan D, Duncan J. 2013. Dynamic coding for cognitive control in prefrontal cortex. *Neuron* 78: 364-75

Suzuki H, Azuma M. 1983. Topographic studies on visual neurons in the dorsolateral prefrontal cortex of the monkey. *Exp Brain Res* 53: 47-58

Tanji J, Hoshi E. 2008. Role of the lateral prefrontal cortex in executive behavioral control. *Physiol Rev* 88: 37-57

Thomas JG. 1969. The dynamics of small saccadic eye movements. *J Physiol* 200: 109-27

Thompson KG, Biscoe KL, Sato TR. 2005. Neuronal basis of covert spatial attention in the frontal eye field. *J Neurosci* 25: 9479-87

Thompson KG, Hanes DP, Bichot NP, Schall JD. 1996. Perceptual and motor processing stages identified in the activity of macaque frontal eye field neurons during visual search. *J Neurophysiol* 76: 4040-55

Ueda H, Takahashi K, Watanabe K. 2014. Effects of direct and averted gaze on the subsequent saccadic response. *Atten Percept Psychophys* 76: 1085-92

Umeno MM, Goldberg ME. 1997. Spatial processing in the monkey frontal eye field. I. Predictive visual responses. *J Neurophysiol* 78: 1373-83

Umeno MM, Goldberg ME. 2001. Spatial processing in the monkey frontal eye field. II. Memory responses. *J Neurophysiol* 86: 2344-52

Ungerleider LG. 1983. Cortical Sensory Organization, Vol. 2: Multiple Visual Areas: edited by Clinton N. Woolsey, The Humana Press, Inc., 1981. $34.50 (USA and Canada) $44.50 (elsewhere) (xv + 222 pages) ISBN 0 896 03031 8. *Trends in Neurosciences* 6: 434

Van Essen DC, Maunsell JH, Bixby JL. 1981. The middle temporal visual area in the macaque: myeloarchitecture, connections, functional properties and topographic organization. *J Comp Neurol* 199: 293-326

Wagman IH, Krieger HP, Papatheodorou CA, Bender MB. 1961. Eye movements elicited by surface and depth stimulation of the frontal lobe of Macaque mulatta. *J Comp Neurol* 117: 179-88

Walker MF, Fitzgibbon EJ, Goldberg ME. 1995. Neurons in the monkey superior colliculus predict the visual result of impending saccadic eye movements. *J Neurophysiol* 73: 1988-2003

Wallis JD, Anderson KC, Miller EK. 2001. Single neurons in prefrontal cortex encode abstract rules. *Nature* 411: 953-6

Warden MR, Miller EK. 2007. The representation of multiple objects in prefrontal neuronal delay activity. *Cereb Cortex* 17 Suppl 1: i41-50

Warden MR, Miller EK. 2010. Task-dependent changes in short-term memory in the prefrontal cortex. *J Neurosci* 30: 15801-10

Watanabe K, Funahashi S. 2007. Prefrontal delay-period activity reflects the decision process of a saccade direction during a free-choice ODR task. *Cereb Cortex* 17 Suppl 1: i88-100

Watanabe M. 1990. Prefrontal unit activity during associative learning in the monkey. *Exp Brain Res* 80: 296-309

Watanabe M. 1996. Reward expectancy in primate prefrontal neurons. *Nature* 382: 629-32

Wimmer K, Nykamp DQ, Constantinidis C, Compte A. 2014. Bump attractor dynamics in prefrontal cortex explains behavioral precision in spatial working memory. *Nat Neurosci* 17: 431-9

Wolff MJ, Jochim J, Akyurek EG, Stokes MG. 2017. Dynamic hidden states underlying working-memory-guided behavior. *Nat Neurosci* 20: 864-71

Wurtz RH. 2008. Neuronal mechanisms of visual stability. *Vision Res* 48: 2070-89

Zaksas D, Pasternak T. 2006. Directional signals in the prefrontal cortex and in area MT during a working memory for visual motion task. *J Neurosci* 26: 11726-42

Zirnsak M, Steinmetz NA, Noudoost B, Xu KZ, Moore T. 2014. Visual space is compressed in prefrontal cortex before eye movements. *Nature* 507: 504-7

Zohary E, Shadlen MN, Newsome WT. 1994. Correlated neuronal discharge rate and its implications for psychophysical performance. *Nature* 370: 140-3